



Annemarie SOMMITSCH, BSc.

Validation and optimization of a continuous flow calorimeter

MASTER'S THESIS

to achieve the university degree of

Diplom-Ingenieurin

Masters's degree programme: Chemical and Process Engineering

submitted to

Graz University of Technology

Supervisor

Assoc.-Prof. Dipl.-Ing. Dr.techn. Heidrun Gruber-Wölfler

Advisor

Dipl.-Ing. Dr.techn. Sebastian Soritz

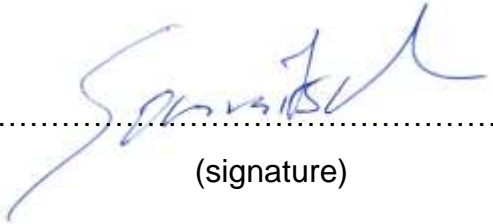
Institute of Process and Particle Engineering

Graz, September 2024

STATUTORY DECLARATION

I declare that I have authored this thesis independently, that I have not used other than the declared sources / resources, and that I have explicitly marked all material which has been quoted either literally or by content from the used sources.

Graz, 30.09.2024
date


(signature)

Abstract

Thermokinetic data of various chemical reactions are important parameters with regard to safety in the industrial use of chemical substances. Accordingly, there is a growing interest in research into microreactor systems and continuous calorimeters in order to be able to carry out fast and aggressive chemical reactions safely.

The main focus of the work was the validation and optimization of a continuous and isothermal heat flow calorimeter. Various measurements were carried out to characterize different 3D printed microreactor plates in different sizes made of ceramic or stainless steel.

The backmixing and flow behavior within different microreactor plates was defined by measuring the residence time distribution (RTD).

By comparison with the respective literature values, the calorimeter investigated was validated using the Bourne reaction, a solvent system (methanol-water), a standardized neutralization reaction (1 M sodium hydroxide and 1 M acetic acid), an aggressive nitration reaction (toluene with nitric acid and sulphuric acid) and a metal-sensitive nitrosylation reaction (tert-butyl nitrite, acetone and hydrochloric acid). Different temperatures and flow rates were examined in order to investigate the accuracy of the calorimeter under different operating modes.

Furthermore, mixing enthalpies were measured for the mixing of high viscosity triethylene glycol (TEG) and water and for the mixing of TEG and 1-propanol at different temperatures and flow rates.

Kurzfassung

Thermokinetische Daten verschiedenster chemischer Reaktionen sind wichtige Parameter in Bezug auf die Sicherheit in der industriellen Verwendung chemischer Substanzen. Dementsprechend ist das Interesse an der Forschung zum Thema Mikroreaktorsysteme und kontinuierlichen Kalorimeter steigend, um schnell ablaufende und aggressive chemische Reaktionen sicher durchführen zu können.

Der Hauptfokus dieser Arbeit lag in der Validierung und der Optimierung eines kontinuierlichen und isothermen Wärmestromkalorimeters. Zur Charakterisierung verschiedener 3D gedruckter Mikroreaktorplatten in verschiedenen Größen aus Keramik oder Metall wurden diverse Messungen durchgeführt.

Die Rückvermischung und das Strömungsverhalten innerhalb verschiedener Mikroreaktorplatten wurde mithilfe der Messung der Verweilzeitverteilung (RTD) definiert.

Durch den Vergleich mit den jeweiligen Literaturwerten konnte das untersuchte Kalorimeter mithilfe der Bourne Reaktion, einem Mischungssystem (Methanol-Wasser), einer standardisierten Neutralisationsreaktion (1 M Natriumhydroxid und 1 M Essigsäure), einer aggressiven Nitrationsreaktion (Toluol mit Salpetersäure und Schwefelsäure) und einer metall-sensiblen Nitrosylationsreaktion (Tert-Butylnitrit, Aceton und Salzsäure) validiert werden. Hierbei wurden verschiedene Temperaturen und Fließgeschwindigkeiten untersucht, um die Genauigkeit des Kalorimeters bei unterschiedlichen Betriebsmodi zu untersuchen.

Weiters wurden Mischungsenthalpien für das Mischen von hoch viskosem Triethylenglycol (TEG) und Wasser und für das Mischen von TEG und 1-Propanol bei verschiedenen Temperaturen und Fließgeschwindigkeiten gemessen.

Danksagung

„Alle Dinge sind möglich dem, der da glaubt.“

Markus 9,23

Dieses Bibelzitat ist nicht einfach nur mein Taufspruch, sondern hat mich auch mein ganzes Leben lang begleitet. Ich bin in meinem Leben und vor allem auch während dem Studium immer wieder auf Hürden und Aufgaben gestoßen, die im ersten Moment unbezwingbar wirkten und mich gebremst haben. Um wieder in Schwung zu kommen und neue Motivation zu erlangen, haben mir zusätzlich zu diesem Spruch auch diverse Menschen aus meinem Studium, aus unterschiedlichen Jobs und aus meinem privaten Leben den nötigen Schubs gegeben. Dafür möchte ich mich an dieser Stelle hier bedanken. Ohne euch hätten die Prüfungsvorbereitungen, sowie die allgemeine organisatorische Zeiteinteilung sicherlich mehr Zeit in Anspruch genommen. Ihr habt meinen Alltag bereichert, mich unterstützt bei meinem Streben nach vorne und habt mir geholfen erwachsen zu werden. Durch euch habe ich auch gelernt wie viel Spaß man haben kann und worauf es im Leben wirklich ankommt. Durch euch bin ich der Mensch geworden, der ich jetzt sein kann.

Bedanken möchte ich mich außerdem bei Heidrun Gruber-Wölfler und Sebastian Soritz für die Unterstützung während der Arbeit, der lehrreiche Zeit im Labor und für die Beantwortung jeglicher (möglicherweise nicht immer von vorne bis hinten durchdachten) Fragen. Außerdem möchte ich dem ganzen Team für die unterhaltsame Zeit im Labor und in den Mittagspausen danken. Zusätzlich möchte ich mich beim RCPE für die Möglichkeit dieser Masterarbeit bedanken.

Abschließend möchte ich mich noch einmal hervorgehoben bei meiner Familie bedanken, die mich immer unterstützt hat und mir zur Seite gestanden ist, wenn ich einmal eine gut gemeinte Richtungsweisung oder aber auch einfach einmal eine Ablenkung gebraucht habe.

Content

1	<i>Introduction and objective</i>	1
2	<i>Theoretical background</i>	2
2.1	Flow calorimeter	2
2.2	Microreactor plates	4
2.2.1	Selective laser melting (SLM)	6
2.2.2	Stereolithography (SLA)	8
2.3	General calculations	10
2.4	Experimental overview	11
2.4.1	Residence time distribution (RTD)	11
2.4.2	Bourne reaction	16
2.4.3	Solvent mixtures	19
2.4.4	Neutralization reaction	19
2.4.5	Nitration reaction	21
2.4.6	Nitrosylation reaction	22
3	<i>Results and discussion</i>	24
3.1	Selection of data	24
3.2	Residence time distribution (RTD)	27
3.3	Bourne reaction	32
3.4	Solvent mixtures	37
3.4.1	Methanol-water	37
3.4.2	Triethylene glycol (TEG)-water and Triethylene glycol (TEG)-1-propanol	41
3.5	Neutralization reaction	43
3.5.1	Neutralization in ceramic reactor plate (C3E)	43
3.5.2	Neutralization in stainless steel reactor plate (M6E)	46
3.6	Nitration reaction	47
3.7	Nitrosylation reaction	49

4	Conclusion and outlook	55
5	Experimental	59
5.1	Reactor plates	59
5.2	Experimental set-up	60
5.2.1	Overall set-up	60
5.3	Calibration of the calorimeter	61
5.4	Methods for analyses	63
5.4.1	UV-Vis spectroscopy	64
5.4.2	HPLC analysis	66
5.5	Residence time distribution (RTD)	67
5.6	Bourne reaction	69
5.6.1	Evaluation of Bourne reaction	70
5.7	Solvent mixtures	71
5.7.1	Methanol-water	71
5.7.2	Triethylene glycol (TEG)-water and Triethylene glycol (TEG)-1-propanol	72
5.8	Neutralization reaction	72
5.9	Nitration reaction	73
5.10	Nitrosylation reaction	74
6	References	76
7	List of figures	80
8	List of tables	84
9	Appendix	88
9.1	Abbreviations and symbols	88
9.2	List of chemicals	92
9.3	Reactor plates	94
9.4	Calibration	95
9.4.1	SOP-calibration	95
9.4.2	Calibration values for the Seebeck elements of the flow calorimeter	96

9.5	Residence time distribution (RTD)	100
9.5.1	SOP-RTD	100
9.5.2	RTD experimental results	101
9.6	Bourne reaction	104
9.6.1	Preparation of reagents for Bourne reaction [10]	104
9.6.2	Laboratory checklist for Bourne reaction	105
9.6.3	SOP-Bourne reaction	105
9.6.4	MATLAB code for calculations Bourne reaction	107
9.6.5	Extinction coefficients for Bourne reaction	109
9.7	Mixing enthalpy	110
9.7.1	Methanol-water experimental results	110
9.7.2	methanol-water literature values	112
9.7.3	TEG-water experimental results	115
9.7.4	TEG-1-propanol experimental results	116
9.8	Neutralization reaction results	118

1 Introduction and objective

Especially in recent years, calorimetric measurements have become increasingly interesting for research. This is becoming more and more relevant for safety reasons, especially in the chemical industry, in order to be able to build large plants and guarantee a safe scale-up. [1], [2] Mixing and/or reaction enthalpy are important parameters for the safe handling and construction of chemical reactors. [3]

In order to be able to investigate highly exothermic and fast reactions in particular, the possibility of investigating them in a microreactor and researching them is of great relevance. [3]

The goal of this project is to validate and optimize the design of an already established calorimeter available at the RCPE GmbH. using a microreactor plate for reactions on continuous flow. [2] This is done to broaden the scope of possible reactions that can be investigated with this device. The work touches upon the topics of sensor technology, Arduino microcontrollers and -electronics, as well as flow chemistry.

Previously to this thesis, various microreactor plates of different materials and sizes were designed and 3D printed and, in some cases, already investigated, but the aim of this work is to deepen this investigation and to further test the calorimeters with these microreactor plates.

In order to cover as many different chemical reactions with different properties as possible, six different reactions were investigated. First, the reactor plates were tested for their mixing behavior using a residence time distribution analyses and a Bourne reaction [4]. Furthermore, solvent mixing systems with low mixing enthalpies were tested and last, nitration reactions and nitrosylation reactions were investigated in order to examine chemical reactions with a high reaction enthalpy and fast reaction process.

2 Theoretical background

Calorimetry, and in particular the calorimeter used for it, has several applications. The most common are the investigation of the reaction enthalpy, the activation energy, the heat capacity and the reaction rate. [5]

The reason why it is so important to know about such data, especially for highly exothermic reactions, is to be able to guarantee a safe handling of chemical reactions. In the past, a batch process was often used to investigate this, but a continuous flow process also has many advantages and is being used more and more frequently.

To be able to investigate different reactions in more detail, a microreactor can be used when studying a reaction in a calorimeter. The high surface area compared to the volume generates rapid mixing and therefore high mass and heat transfer. [1]

2.1 Flow calorimeter

Spatial and temporal progressions in reactions can be analyzed more accurately in continuous reactors than in batch calorimeters. Fast reactions in particular pose a challenge when analyzed using a batch calorimeter, which is why continuous calorimeters are increasingly being investigated and used. [2] A list of the calorimeters currently often used can be found in the literature [1].

In this chapter, the calorimeter used in this work is explained in more detail. The calorimeter was built in previous projects and has already been tested with various reactions. [1], [2], [5], [6]

The following diagram (Figure 2-1) shows one of the used calorimeters (reactor plate with a total of three segments). Two different sizes of reactor plates are used in this work, which are explained in more detail in the next chapter (Chapter 2.2). As the basic principle of both is the same, only the smaller one with a total of three segments will be discussed in more detail here (Figure 2-1).

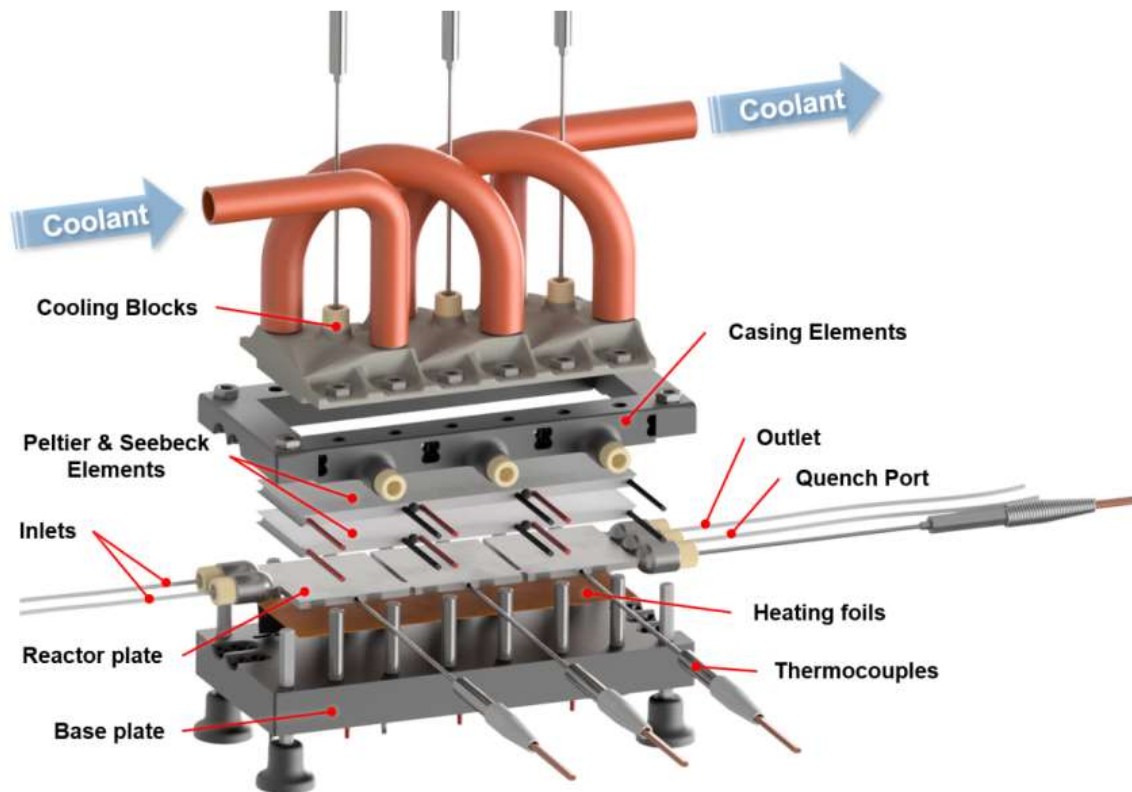


Figure 2-1: Structure of the calorimeter using a reactor plate with 3 segments. From the bottom up: base plate, heating foils, reactor plate, Seebeck elements, Peltier elements, casing elements to secure everything together, metal cooling blocks. [2], [5], [6]

As can be seen in Figure 2-1, there is a reactor plate in the middle of the calorimeter with two inlets and one outlet, and there is also an additional option for a quench. Temperature sensors are fitted in each segment of the reactor plate and one at the outlet. There are heating foils on the underside of the reactor plate and Peltier and Seebeck elements on the top of the reactor plate. The top component of the calorimeter is a cooling block, which is cooled using a thermostat [7].

One of the great advantages of this calorimeter is that the individual parts are modular and easy to replace. This makes the exchange of defective parts simple and modulations/optimizations possible. [6]

The calorimeter is isothermal, which enables the calorimeter to perform the measurements as described in the following. The output of the Seebeck element during an experiment is the amount of volts, which correlates to a temperature rise in the calorimeter. The heat flux can therefore be measured directly. The exact functionality of a Seebeck element is described in full detail by Manuel Maier et al. [5]. Briefly summarized, heat transfer from one side of the Seebeck element to the

other side, i.e. from the reactor plate to the Peltier elements, can be measured using electrical volts. The Peltier elements have the task of tempering the calorimeter to a desired temperature. If the temperature in the reactor plate rises, the Seebeck element detects this heat difference and indicates this with registered volts. The exact heat flux can be calculated from the data of the Seebeck elements with the help of a previously performed calibration, which needs the use of the heating foils. The calibration is described in more detail in Chapter 5.3. [2], [5]

2.2 Microreactor plates

The reaction time is greatly minimized for reactions in microreactors, as there is generally better mixing. As a result, the yield is also higher. [8] Reactors are normally referred to as microreactors if they are scaled on a micro-scale, thus the channel diameter is less than 1 mm. [3], [9], [10] Microreactors are generally well suited for very high heat transfer rates due to the high surface area in relation to the volume. [11], [12] However, the process is often assumed to be isothermal precisely for this reason, but this can be a possible source of error in the results, as ideal isothermal behavior is usually not given. [5]

However, the small reactor volume also has many advantages. For example, smaller quantities of hazardous chemicals are used and there is less waste due to the generally smaller quantity of chemicals used. [5], [8], [12]

Furthermore, highly exothermic reactions, which have an explosive potential on a larger scale, can be carried out on a laboratory scale in a controlled manner. Here, the heat released and the possible need for cooling can be controlled and carried out. [8]

In this thesis, calorimeters with different reactor plates were investigated. In general, two different materials were used and different sizes, diameters and lengths of the channels were investigated. The two materials used are either ceramic or stainless steel. The reactor plates were each printed using a 3D printer, which is described in more detail in Chapter 2.2.1 and Chapter 2.2.2.

The stainless steel reactor plates were produced using Selective laser melting (SLM) by Anton Paar GmbH, while the ceramic plates were manufactured by Lithoz using SLA. The models for the various plates were designed and optimized in advance as part of several other projects. [5], [6] The plates used in this work are shown in the following figures (Figure 2-2, Figure 2-3).

The reaction plate seen in Figure 2-2 was printed in ceramic (C3E) or in stainless steel with two different diameters (M3E, M3Ebd). Figure 2-2 shows that the reactor plate is roughly divided into three different compartments. There are two inlets in front of the first segment so that two reactants can be fed into the reactor separately. The first section is used to temper the liquids before they meet. This section is referred to as “pre”. The two subsequent segments are intended for the reaction and are interspersed with so-called split-and-recombine elements (SAR). These are declared as “r1” and “r2”. The SAR element is intended for better mixing of the liquids. Here, the stream is first split into two streams and then recombined again. At the outlet of the reactor plate there is an option for measuring the temperature and an option for a quench. [3]

The plate has a total length of 150 mm, a thickness of 2.4 mm and a width of 40 mm. Each segment (marked in the diagram with a dotted line) has a total size of 39 mm x 40 mm. [6]

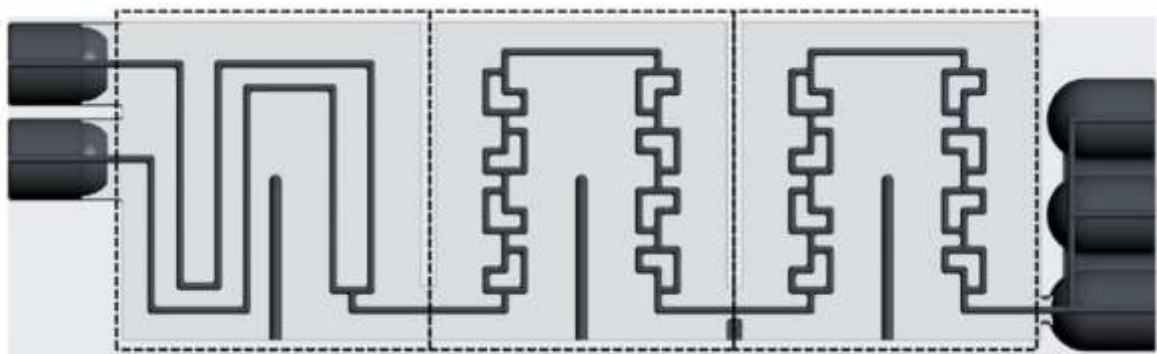


Figure 2-2: Structure of the internal geometry of the 3D printed reactor plate. The three sections from left to right: preheating section ("pre"), two reaction segments ("r1", "r2"). [3]

The following figure (Figure 2-3) shows basically the same design as above, but this reactor plate is extended by three reactor segments for a total of six segments. As you can see in the diagram, it also has a preheating segment ("pre") and five reaction segments ("r1", "r2", "r3", "r4", and "r5"). This plate was 3D printed from stainless steel using SLM (M6E).

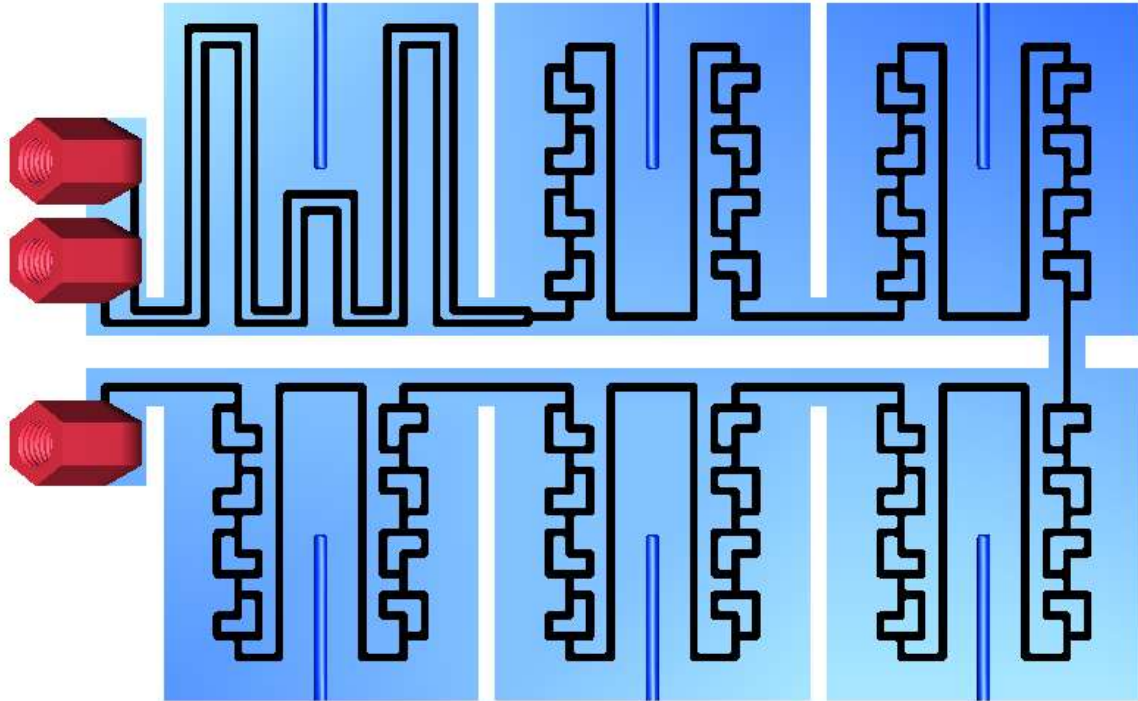


Figure 2-3: Structure of the internal geometry of the 3D printed reactor plate. The six sections from top left to bottom right: preheating section ("pre"), five reaction segments ("r1", "r2", "r3", "r4", "r5").

One additional reactor plate was used during this thesis which has the same characteristics (channel diameter) as M6E, but only consists of a total of three segments (two reaction sections) (M3Ed).

A precise categorization of the individual reactor plates used in this thesis with the exact data on the different sizes can be found in Chapter 5.1.

2.2.1 Selective laser melting (SLM)

The selective laser melting (SLM) process is used to produce components of stainless steel. With the SLM process, reactor plates with a very precise geometry can be produced. [5]

SLM is one of the powder bed-based processes. Here, a powder bed is present and a laser melts layer by layer and after solidification, a component is created. Here, the laser acts as its focalized energy beam, which melts the powder particles together. [6], [13], [14]

The following figure (Figure 2-4) shows the structure of such a SLM process. The powerful laser (approx. 100-400 W) melts a thin layer of particles in an inert gas atmosphere (argon, nitrogen). The layers are thus created on the building platform. Using a scraper, any uneven top layer is smoothed out and the plate is lowered by a predetermined distance (usually 0.02-0.1 mm) and new powder is applied to the bed. This process is repeated layer by layer. The model is usually created from a CAD design. The wall thickness depends on the size of the laser and is usually between 0.3 mm and 0.7 mm. [6]

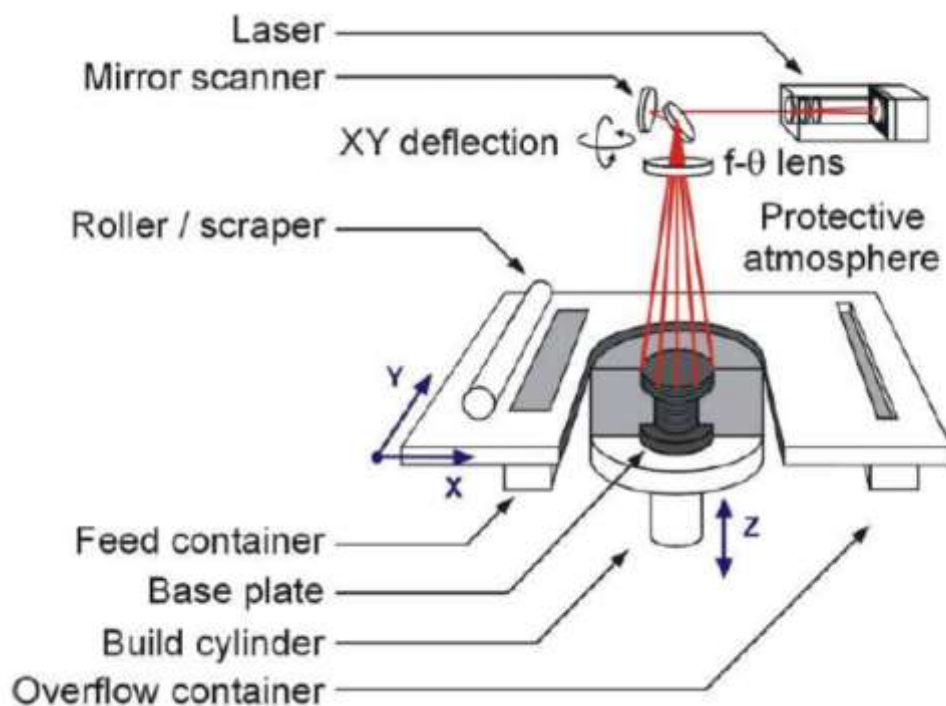


Figure 2-4: Schematic illustration of the basic set-up of a SLM printing device. [6]

A major disadvantage of SLM is the significant influence of the temperature distribution on the printing of very fine and especially fine internal structures. Here, the high and possible inconsistent temperatures can cause the printed piece to bend or internal structures to fuse or be distorted. Furthermore, it is possible that unmelted or only partially melted particles inside a component can block the channels or

change the structure unintentionally (very high surface roughness). [6], [15] As part of this thesis, the reactor plates were cleaned using high pressure to remove loose particles from the inside of the channels.

2.2.2 Stereolithography (SLA)

For this project, ceramic reactor plates were manufactured by Lithoz. The reactor plates were not produced using SLM, but with the help of lithography-based manufacturing. This process belongs to the stereolithographic technologies (SLA). [3], [16]

The principle behind SLA is the solidification of liquid resin through photopolymerization. Fundamentally, the SLA process is similar to the SLM process, which has already been described in more detail in the previous subchapter. The structure can be seen in Figure 2-5. [6]

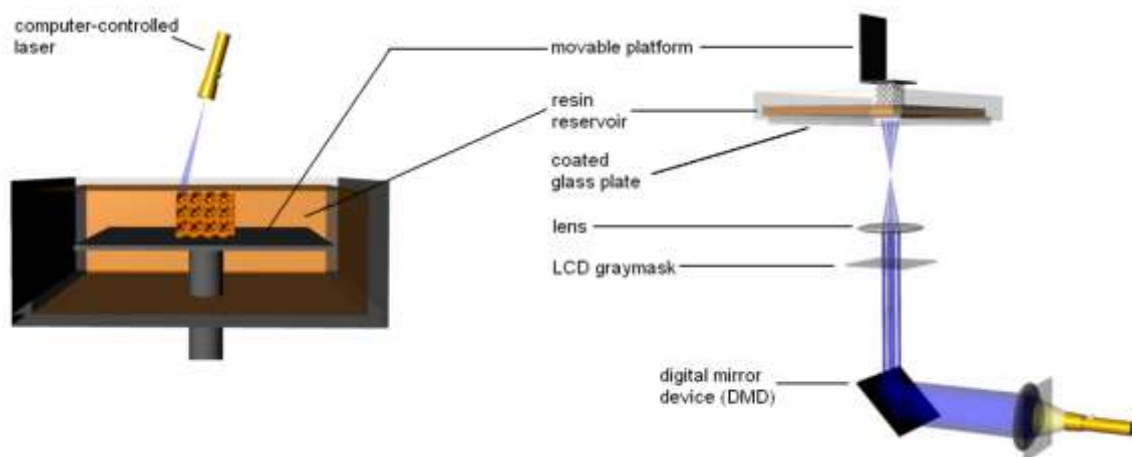


Figure 2-5: Left: Conventional SLA process, laser solidifies resin from top. Right: Different SLA process, laser solidifies resin from the bottom. [6], [17]

As can be seen in Figure 2-5 on the left, a platform is in a resin container and a predetermined geometry is “built” from above using a computer-controlled laser. The laser solidifies the resin layer by layer, while the platform sinks further and further down until the desired component is created. The thickness of the layers is determined by the advancement of the platform and is normally between 25 and 100 μm . One of the major disadvantages of this process, however, is that the top layer, which has just been created, comes in contact with air, which can lead to irregularities in the structure of the component (air pockets).

Another possible method can be seen in Figure 2-5 on the right. Here the principle is the same, but the laser shines from below through a transparent layer into the resin container. The component is lifted further and further out of the container towards the top. However, a disadvantage of this process is that the newly formed layer may stick to the underside of the resin container and thus tear loose when it is lifted further, which can both damage the container and ruin the structure of the component. One of the biggest advantages of this process is that less resin is required, as the container does not have to be as large as the entire component. Furthermore, the layer that has just been processed by the laser is not exposed to the ambient air, which results in fewer patches (air pockets) in the structure of the component. [6], [17]

Due to the layered and fine design, very complicated internal geometries can be produced with a relatively smooth surface. This makes this process particularly suitable for the production of microreactors. [6]

A CeraFab S65 [18] was used to print the ceramic reactor plate with three segments which is used in this thesis. [16] This printer uses the technology shown in Figure 2-5 on the right and is illustrated in Figure 2-6 below.

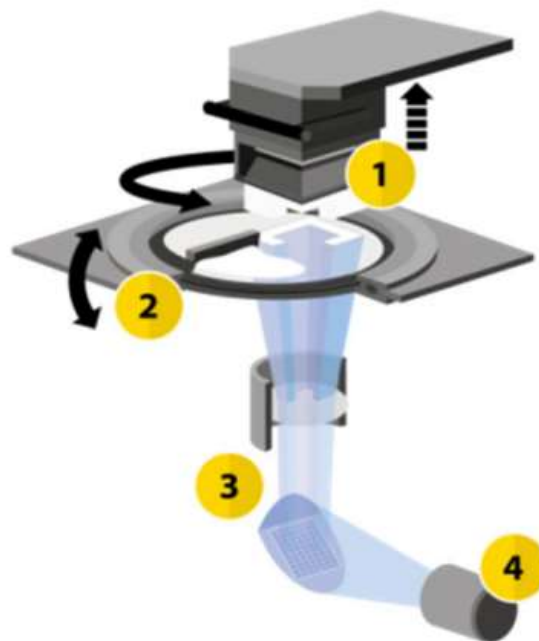


Figure 2-6: Schematic illustration of the CeraFab S56 printer [18]. (1) movable printer platform in Z-direction; (2) rotatable vat for material deposition; (3) optical system transmitting light from LED (4). [3]

Figure 2-6 shows an LED, which is redirected and sent through a lens onto the underside of a rotatable and transparent vat. This creates the component layer by layer, which is pulled further and further upwards. The thickness of the individual layers in this project was 25 μm . [3]

2.3 General calculations

The basic calculations are based on an existing work from Barbara Forster [2]. Nevertheless, the individual formulas are listed below.

In order to calculate the perceived heat flux \dot{Q}_i , the equation (2-1) can be used using the voltage from the Seebeck elements U_i and the calibration constants c_1 , c_2 and c_3 .

$$\dot{Q}_i = -(c_1 * U_i^2 + c_2 * U_i + c_3) \text{ for } i = pre, r1, r2 \quad (2-1)$$

The reaction enthalpy ΔH_R for the flow calorimeter is calculated using the molar flux \dot{n}_A of the substrate and the conversion X , using the equation (2-2).

$$\Delta H_R = \frac{\dot{Q}_{SE,pre} + \dot{Q}_{r1} + \dot{Q}_{r2} + \dot{Q}_{out}}{\dot{n}_A * X * 10^3} \quad (2-2)$$

The inserted heat fluxes \dot{Q} for the reaction enthalpy are derived according to the equations (2-3)-(2-5).

Using the equation (2-3), the exiting heat flux \dot{Q}_{out} can be calculated using the entering molar fluxes \dot{n} , the temperature difference dT_{out} and the specific heat capacity c_p .

$$\dot{Q}_{out} = \dot{n}_A * dT_{out} * c_{p,A} + \dot{n}_B * dT_{out} * c_{p,B} \quad (2-3)$$

The heat flux $\dot{Q}_{SE,pre}$ is simply the difference between the heat flux of the preheating plate \dot{Q}_{pre} and the entering heat fluxes via the feed streams \dot{Q}_A and \dot{Q}_B . This relation can be seen in the equation (2-4).

$$\dot{Q}_{SE,pre} = \dot{Q}_{pre} - \dot{Q}_A - \dot{Q}_B \quad (2-4)$$

Using the equation (2-5), the entering heat fluxes \dot{Q}_A and \dot{Q}_B can be calculated using the molar flux \dot{n} , the temperature difference dT_n and the specific heat capacity $c_{p,n}$.

$$\dot{Q}_n = \dot{n}_n * dT_n * c_{p,n} \text{ for } n = A, B \quad (2-5)$$

The individual temperature differences dT can be determined according to the equation (2-6) using the respective measured temperature T_m and the reactor temperature T_{react} .

$$dT_m = T_{react} - T_m \text{ for } m = A, B, out \quad (2-6)$$

The heat capacities c_p can be calculated using the equation (2-7) with the heat flux of the preheating plate \dot{Q}_{pre} , the entering molar fluxes \dot{n} and the temperature differences dT .

$$c_p = \frac{\dot{Q}_{pre}}{\dot{n}_A * dT_A + \dot{n}_B * dT_B} \quad (2-7)$$

2.4 Experimental overview

2.4.1 Residence time distribution (RTD)

In order to investigate the mixing behavior in a plate reactor, a residence time distribution (RTD) measurement can be carried out. This is usually necessary because theoretically simulated and calculated processes in a reactor can be influenced by various factors such as dead zones, channeling, inaccuracies in the manufacture of the reactor (possible clogged or too large channels), or impurities. In theory, an ideal plug flow is usually assumed for a plate reactor, as the channels in the reactor and the capillaries are tubular, but axial flows and velocities occur more frequently. [9], [10], [19]

In general, the residence time distribution is often used to characterize backmixing in macromixing or bulk mixing, as deviations from plug flow can be easily investigated here. [19]

As already described in Chapter 2.2, a microreactor has a very small capillary volume. This usually results in a parabolic and fundamentally laminar flow, which does not result in an ideal plug flow. As a result, the liquid does not flow evenly through the reactor and different elements arrive on the other side of the reactor at different times. This can be visualized and investigated using a RTD. [10]

To experimentally determine the residence time distribution, in this thesis a non-reactive tracer is pumped through the reactor using a step function. The quantity and concentration of the tracer is known exactly and the concentration coming out of the back of the reactor is measured as a function of time. This allows a distribution curve to be created in order to know the residence time of a quantity of liquid in the reactor. [10], [19]

The tracer is usually either a color or an electrolyte. When selecting the tracer, it is important that it should be inert, non-reactive and not interact with the reactor material. If this is the case, you can use a UV-Vis spectrometer at the output of the reactor to examine the concentration over time.

In general, a distinction can be made between step and pulse input.

With a pulse input, only liquid is first pumped through the reactor without a tracer. This continues until the measured signal is constant and stable. If this is the case, a liquid with tracer is sent through the reactor using a pulse. The concentration changes over time are analyzed at the reactor outlet and converted into the exit age distribution $E(t)$ by standardization using the tracer mass and the volumetric flow rate. The area under the resulting and standardized curve is equivalent to 1. A more detailed description of the pulse function can be found in the literature [10], but is not described any further here as the pulse function is not used in the thesis.

With the step input method, a constant liquid without tracer is first pumped through the reactor. As soon as this provides stable and constant results, an abrupt change is made to a solution with tracer and the time measurement is started. The

concentration of the tracer upstream of the reactor (c_0) is known. Now the concentration of the tracer at the back of the reactor will increase with continuous time until the starting concentration (c_0) is also reached there. To obtain a cumulative distribution $F(t)$ from this curve, the individual concentrations from the curve (c_i) are divided by the initial concentration (c_0). If the calculations were done right, following condition should be valid: if $t \rightarrow \infty$ then $F(t) \rightarrow 1$. [10]

Calculations of residence time distribution

The following calculations are based on [9] and [10].

If now the cumulative age distribution $F(t)$ is known from the values of the experiments, the following equation (2-8) can be established for the exit age distribution $E(t)$:

$$E(t) = \frac{dF(t)}{dt} \quad (2-8)$$

So, by integrating the $F(t)$ function it is possible to plot the $E(t)$ function. To be able to compare different experiments, the dimensionless time θ is used and given as seen in the equation (2-9).

$$\theta = \frac{t}{t_{res}} \quad (2-9)$$

Here, t_{res} is the mean residence time of the reactor. By using θ , the $E(\theta)$ curve can be normalized to:

$$E(\theta) = E(t) * t_{res} \quad (2-10)$$

Therefore, t_{res} can be defined as:

$$t_{res} = \int_0^{\infty} t * E(t) dt \cong \sum_{t=0}^{\infty} t * E(t) * \Delta t \quad (2-11)$$

The second part of the equation (2-11) can be used for a discrete measurement, as is the case with the conventional RTD measurement.

To investigate how far the flow behavior in a reactor deviates from that of an ideal plug flow reactor, the dispersion model is used.

The ideal plug flow is superimposed with a dispersion effect. This effect results from fluctuations in the flow and is described by the axial dispersion coefficient D_{ax} . D_{ax} describes the backmixing along a reactor.

The more backmixing there is, the further away the flow behavior is from the ideal plug flow and the higher D_{ax} is. However, in order to be able to make an actual statement about backmixing, the Bodenstein number Bo is used (ratio of convective mass transfer to axial dispersion), which can be represented using the equation (2-12) below.

$$Bo = \frac{u * L_{char}}{D_{ax}} = \frac{2}{\sigma_{\theta}^2} \quad (2-12)$$

The Bodenstein number is calculated using the flow velocity u , the characteristic length of the reactor L_{char} and the axial dispersion coefficient D_{ax} .

The higher the Bodenstein number (>100), the less backmixing exists. This in turn means that the flow behavior is very close to plug flow. The lower the Bodenstein number (<100), the more backmixing exists and the further away the flow behavior is from ideal plug flow and the more the flow resembles the one in a stirred tank reactor.

As can be seen in the equation (2-12), the Bodenstein number can also be calculated using variance σ_{θ}^2 (depending on the dimensionless time θ). This can also be calculated using the equation (2-13) below.

$$\sigma_{\theta}^2 = \frac{\sigma_t^2}{t_{res}^2} \quad (2-13)$$

In order to calculate the variance depending on the dimensionless time, the variance σ_t^2 can be calculated using the following equation (2-14).

$$\sigma_t^2 = \int_0^\infty (t - t_{res})^2 E(t) dt \cong \sum_{t=0}^\infty (t - t_{res})^2 E(t) \Delta t \quad (2-14)$$

Depending on the variance, the distribution of the RTD curve is wider or narrower. The greater the variance, the wider the distribution and vice versa. It can be seen from the equation that the greater the variance, the smaller the Bodenstein number and due to the already explained relation of the Bodenstein number to the flow behavior, it can be assumed that the smaller the Bodenstein number, the greater the backmixing and the greater the backmixing, the more asymmetrical the RTD curve.

The dependence of the Bodenstein number on the variance is only justified in the form shown in the equation (2-12) if the dispersion is low. The criteria for calculating the number of soil stones can be either:

- closed vessel: no dispersion at the reactor inlet or outlet
- open vessel: dispersion along all the length of the reactor

In the context of this work, an open vessel is assumed, whereby the Bodenstein number is calculated using the equation from Levenspiel and Smith [9], which is shown in the next equation (2-15) using the variance σ_θ^2 .

$$Bo_{o-o} = \frac{1}{\sigma_\theta^2} + \sqrt{\left(\frac{1}{\sigma_\theta^2}\right)^2 + \frac{8}{\sigma_\theta^2}} \quad (2-15)$$

Furthermore, the calculation of the Reynolds number is important for the analyses of the flow behavior. If the Reynolds number is below 2300 in a straight pipe, the flow is considered to be laminar, whereas if the Reynolds number is above 4000, it is considered to be turbulent. The Reynolds number Re is calculated using the fluid velocity u , the characteristic length L_{char} , the kinematic ν or dynamic η viscosity in combination with the density ρ as follows (equation (2-16)). [10]

$$Re = \frac{u * L_{char}}{\nu} = \frac{u * L_{char} * \rho}{\eta} \quad (2-16)$$

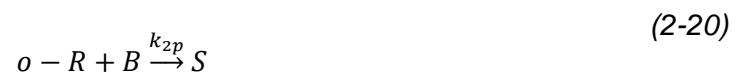
2.4.2 Bourne reaction

The Bourne reaction is a reaction named after Bourne [4], [20], as he developed it to better analyze the mixing behavior within a reactor. This involves the diazo coupling between 1-naphthol and diazotized sulfanilic acid. This method can be used to investigate not only coarse mixing behavior, but even micromixing. [4], [20]

There are also alternatives to the Bourne reaction to categorize the micromixing behavior within a reactor, but the Bourne reaction was chosen for the measurements in this work, as it is cheaper and there are already some results in the literature, which provides comparative values. [10], [21]

The reactants A and B are highly sensitive to temperature, light and time, which means that it is necessary to work cool and quickly in a darkened room. Additionally, the chemical preparation has to be done immediately before the experiments and cannot be prepared a long time in advance. If work is carried out too slowly, the product is decomposed, and the results are no longer representative. In addition, even the smallest inaccuracies in the preparation of the reactants or in the reaction sequence, or in the evaluation, have a very large impact on the result and distort it. [10]

The following equations ((2-17) - (2-20)) show the reactions taking place in the Bourne reaction. [10], [5]



In the equations ((2-17) - (2-20)), A stands for 1-naphthol and B for diazotized sulfanilic acid. In the primary coupling reactions, the para and ortho positions $p - R$ and $o - R$ are formed. These two resulting substances are monoazo dyes. In the

secondary coupling reaction, these two isomers ($p - R$, $o - R$) react further with B to form the bisazo dye S . For this reaction to work, A is present in 20% excess, while B is limiting. [10], [4], [5]

Earl studies described the reaction as a two-reaction scheme, which neglects the ortho position. However, this isn't accurate. The para and the ortho position (four-reaction scheme) is relevant/better representable. [4]

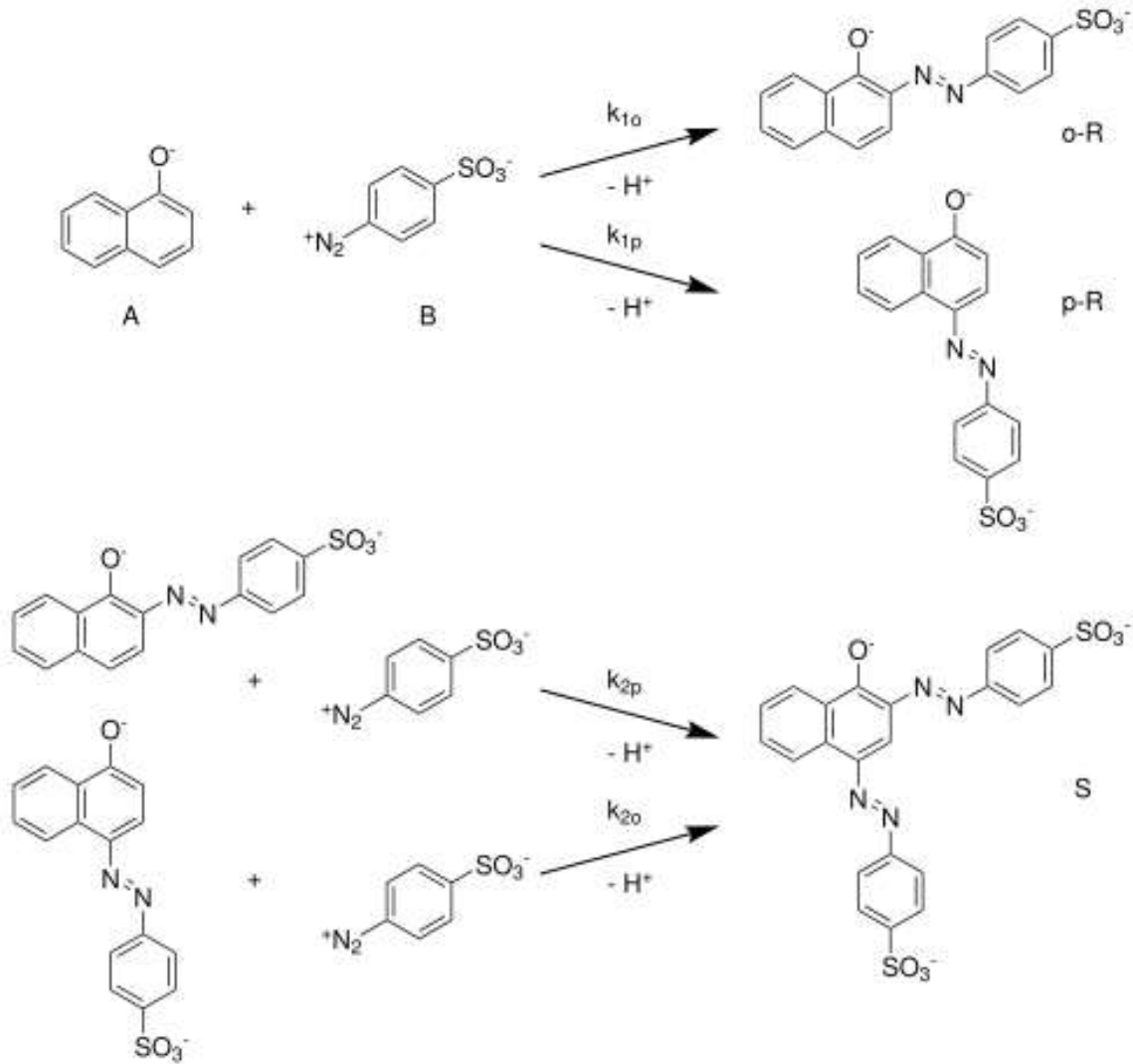
If there is very good mixing in a reaction, a lot of A reacts with B and the isomers no longer have a lot of B available to react further. However, if there is poor mixing, there is a lot of B in one place, which leads to more secondary coupling reactions (isomers react with B) and more S is formed. [10] [4]

The reaction rates for this reaction are $k_{1p}=12238 \pm 446 \text{ m}^3 \text{ mol}^{-1} \text{ s}^{-1}$, $k_{1o}=921 \pm 31 \text{ m}^3 \text{ mol}^{-1} \text{ s}^{-1}$, $k_{2o}=1.835 \pm 0.018 \text{ m}^3 \text{ mol}^{-1} \text{ s}^{-1}$ and $k_{2p}=22.25 \pm 0.25 \text{ m}^3 \text{ mol}^{-1} \text{ s}^{-1}$ according to Alessia Valotta [10]. However, in order to ensure a working reaction with these reaction rates, a pH value of 9.9, a room temperature of 25°C, an ionic strength of the sodium carbonate and the bicarbonate buffer of 444.4 mM must be given. [10]

In the following Scheme 2-1, the reaction scheme of the Bourne reaction can be seen.

As can be seen in the Scheme 2-1, the product consists of all the substances present (A , $p - R$, $o - R$, S) except B , as this has already reacted completely with the others to form S . A UV-Vis spectrometer (Chapter 5.4.1) is used for the analyses. The concentration can be determined by measuring the absorption of light by the sample. The extinction factor is taken from the literature [21] and included in the calculation and can be seen in Chapter 9.6.5. A wavelength of 390-700 nm is examined during the measurement. Assuming that the absorbance remains within a certain range (390 nm to 700 nm), the multiparameter regression can be calculated using the Lambert-Beer law. The yield of bisazo dye S Y_S can then be calculated using the concentrations c as it can be seen in the equation (2-21). [10]

$$Y_S = \frac{2 * c_s}{2 * c_s + c_{oR} + c_{pR}} \quad (2-21)$$



Scheme 2-1: Reaction scheme for the diazo coupling of 1-naphthol (A) and diazotized sulfanilic acid (B) giving the monoazo isomers p-R and o-R. The secondary coupling of p-R and o-R with B gives the bisazo dye S. [10]

Depending on the result of the yield of S Y_S , there are 3 different possible regimes:

- Kinetically controlled regime: $Y_S \ll 0.01$.
- Mixing controlled regime: $Y_S = 1$.
- Intermediate regime: $0.01 < Y_S < 1$.

The kinetically controlled regime results in very good mixing. This results in many primary coupling reactions. This results in a large number of ortho- and para-isomers, but there is not much B left to be able to react to S within a secondary coupling reaction. So, if the yield of S is very small, this means good mixing.

The mixing controlled regime results in very poor mixing, which leads to increased secondary coupling reactions and therefore to a large amount of product S being produced. If the yield of S is therefore very high, this means poor mixing.

The intermediate regime is the regime in between. Here, there can be good mixing in some cases and poorer mixing in others. [10], [20]

The most meaningful results are available at $0.004 \ll Y_S \ll 0.4$. Anything below 0.04 has a very low signal with the UV-Vis cell, since it is not sensitive enough and there are very large deviations due to the smallest impurities or inaccuracies. Anything above 0.4 shows that apparently B has reacted to some side products. [10], [20]

2.4.3 Solvent mixtures

When measuring the mixing enthalpy of solvent mixtures, the energy released is measured, which is generated/required when two different liquids are mixed. It is important to differentiate between a mixing enthalpy and a reaction enthalpy. The reaction enthalpy looks at the mechanisms involved in a reaction, whereas in a mixing enthalpy only two substances are mixed and do not react.

The enthalpy of mixing is highly dependent on the molecular and ionic mechanisms and interactions between the two liquids. The microscopic structure of the mixture is also relevant.

It is important to note that the mixing of two solvents can be endothermic or exothermic. If the mixing enthalpy is very high, the effect on the measurement of the reaction enthalpy can be high, as the measurement of an enthalpy is often carried out over the entire system. [22]

2.4.4 Neutralization reaction

The acid-base reaction (neutralization) has often been investigated in the past and therefore offers many reference values from the literature. In order to examine the validity of the results of the calorimeter, a neutralization can therefore be carried out and the results compared with literature values. [2], [5], [3], [23]

On closer examination, there is often no real neutralization reaction in which the product reaches a pH value of 7. Only in this case would the term “neutralization” really be accurate, but the basic reaction of an acid with a base is usually referred to as “neutralization” for the purposes of convenience. [2], [24]

Neutralization can be traced back to Arrhenius' acid-base theory. Arrhenius recognized that when an acid and a base are mixed, a neutral solution can be formed that is neither acidic nor basic. The solution behaves like a salt (NaCl) in water. Accordingly, the equation (2-22) can be defined as neutralization. [23]



In order to achieve such a behavior, acids build with H^+ -ions and bases with OH^- -ions aqueous solutions. If the reaction also builds water, it is called “neutralization”. [25], [23] Brønsted expanded Arrhenius' acid-base theory. [23]

Then, neutralization was based on the Brønsted-Lowry concept. If an acid and a base are combined, the acid releases protons (proton donor) and the base absorbs protons (proton acceptor). The strength of the acid or the base determines how strongly the protons are absorbed or released. [25], [26]

The basis for this concept is that acids are hydrogen compounds, while bases are hydroxides. The properties of the acid or base are based on the ions formed during dissociation in an aqueous solution. Acids produce H^+ -ions, while bases produce OH^- -ions.

In this thesis the neutralization of acetic acid with sodium hydroxide is used. There are many reasons for choosing especially this neutralization for a functionality test of the calorimeter, it being for instance highly exothermic and fast. [27] This reaction can be seen in the Scheme 2-2 bellow.



Scheme 2-2: Reaction of Acetic Acid with Sodium Hydroxide. [2]

For the reaction shown above (Scheme 2-2), the literature value for the reaction enthalpy is given at $-57.40 \text{ kJ mol}^{-1}$. [3], [23]

2.4.5 Nitration reaction

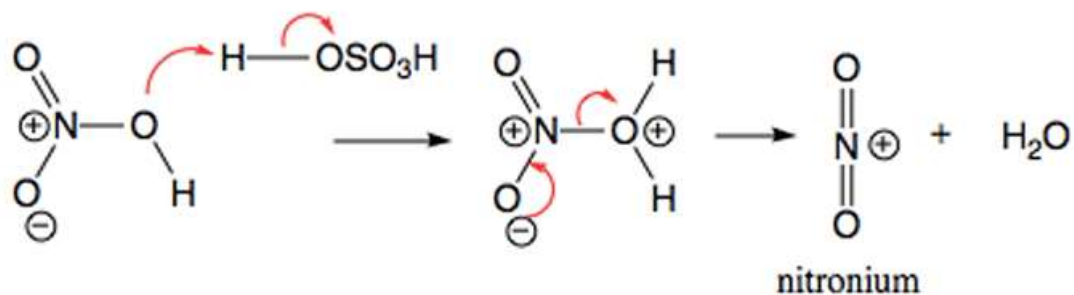
Reactions proceed at different speeds. Since microreactors with a very small volume are used in this work, the investigation of very fast reactions is particularly suitable. Here, nitration is examined in more detail, as this is an example of a very fast, highly aggressive and corrosive reaction that is dependent on mixing and is also strongly exothermic. [3], [28]

One of the great dangers of using nitrate ions is their highly exothermic but also partially unstable characteristics. This is particularly important for scale-up and should be taken into account, as this has already led to accidents in industry. This is another reason why the heat capacity should be investigated on a small scale (microreactor) in order to ensure sufficient heat exchange with the environment for cooling. Despite the small reaction volume, heat transfers are still recognizable here. [11], [28], [29]

In this thesis, nitration of toluene is investigated, which is why this chapter takes a closer look at the theory of precisely this reaction. The reaction is a two-phase liquid-liquid reaction.

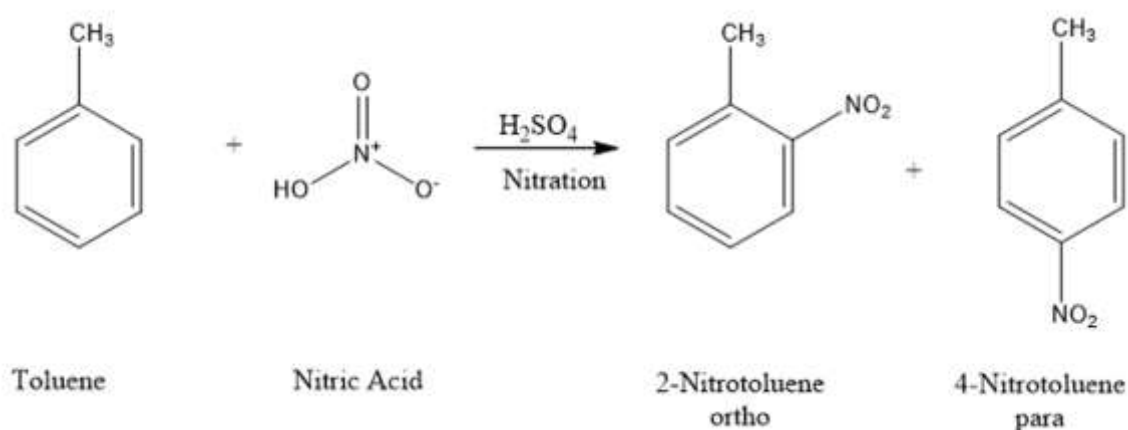
In general, toluene is nitrated using a mixture of concentrated nitric acid and sulphuric acid. The nitric acid receives a proton from the sulphuric acid and then forms a nitronium ion. This nitronium ion reacts with toluene and three isomers of nitrotoluene are formed. This process is called mononitration. The reaction can react almost completely, as sulphuric acid binds all water. A relatively large amount of sulphuric acid is required for this reaction and must be laboriously regenerated. During the reaction, toluene goes into the aqueous acid phase, where the reaction also takes place. [11] This process can be seen in the Scheme 2-3.

In general, nitration reactions are electrophilic. The highly reactive part is the nitronium ion, which is unstable. For this reason, it must be prepared from a nitric acid solution directly before an experiment.



Scheme 2-3: Generation of the nitronium ion with the help of sulphuric acid. [2]

The nitration of toluene is shown in the Scheme 2-4. [2]

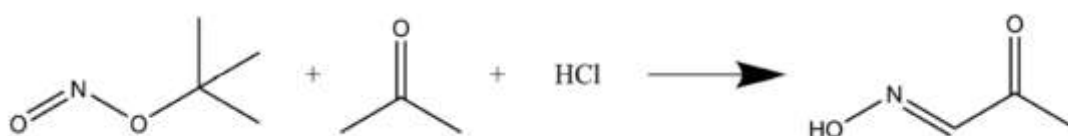


Scheme 2-4: Nitration of toluene: Toluene reacts with nitric acid to two main mononitro isomers (ortho and para). [2]

2.4.6 Nitrosylation reaction

Nitrosylation is a very corrosive reaction. For this reason, the reaction cannot be carried out in metal reactors without damaging them. In this thesis, nitrosylation is carried out in the ceramic reactor plate (C3E). In addition to most metals, the nitrosyl chloride can even corrode nickel-based alloys or gold.

The Scheme 2-5 below shows the nitrosylation reaction of tert-butyl nitrite with acetone and HCl. [3]



Scheme 2-5: Nitrosylation reaction of *tert*-butyl nitrite with acetone and HCL to 2-oxopropanal oxime.
[3]

As can be seen in the Scheme 2-5, tert-butyl nitrite reacts with acetone and hydrogen chloride in the nitrosylation reaction. [3]

During the reaction, nitrosyl chloride is formed in situ by the tert-butyl nitrite and the hydrochloric acid (HCL). This reacts rapidly with acetone to form α -nitrosylated acetone, which then evolves to 2-oxopropanal oxime. The final product is then quenched with an aqueous ammonium solution in order to take a sample.

This reaction and experiment set-up is shown in the Figure 2-7. [30]

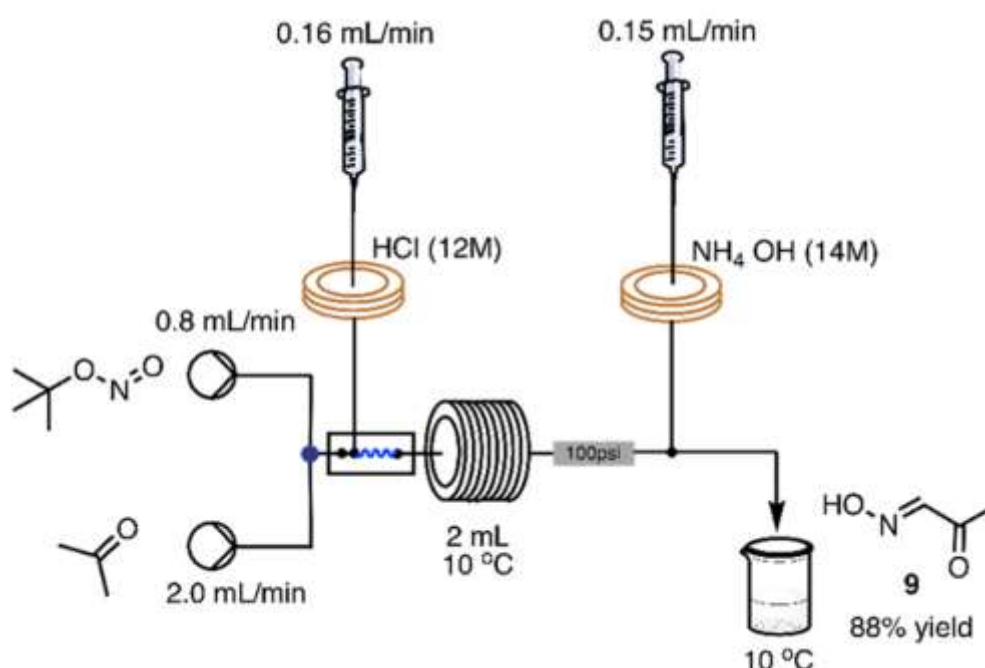


Figure 2-7: Schematical set-up of flow synthesis of Hydroximinoacetone (Nitrosylation). [30]

The flow rates shown in Figure 2-7 are adapted to the size of the microreactor in this thesis, but the basic procedure/set-up of the experiment in this thesis is the same as that shown in Figure 2-7.

3 Results and discussion

3.1 Selection of data

The selection of data was carried out as shown in Figure 3-1 and Figure 3-2 for all reactor plates.

As can be seen in Figure 3-1 and Figure 3-2 below, the values do not become constant immediately, but only stabilize after an initial deflection. This phenomenon was observed during the measurement of various reaction and mixing enthalpies as well as during calibration. When looking at the function of the calorimeter, it becomes clear why this is the case. Figure 3-2 shows that the voltage rises before becoming stable at the correct value (especially the second reaction segment “r2” where a lot of the reaction occurs in this example).

This becomes clear when looking at Figure 3-1 with the temperatures. The first moment the temperature rises, it rises so quickly that the calorimeter cannot compensate for this fast enough. It then tries to compensate and cools down too much (values of the voltage in Figure 3-2 rise). This must first stabilize before representative data can be obtained. In order to find a meaningful value, the average of as many values as possible is used. For this purpose, each curve is viewed individually and values are used from the point on, at which the values appear stable. This selection can be seen as an example in the graphs below using the green marked square. This procedure is used for the entire evaluation of the individual experiments in this thesis.

Furthermore, a certain amount of measurement noise can be seen when looking at the graph with the temperatures (Figure 3-1). This can be attributed to the precise and frequent temperature measurement with two decimal places, as the temperature changes greatly in relation to such a precise measurement.

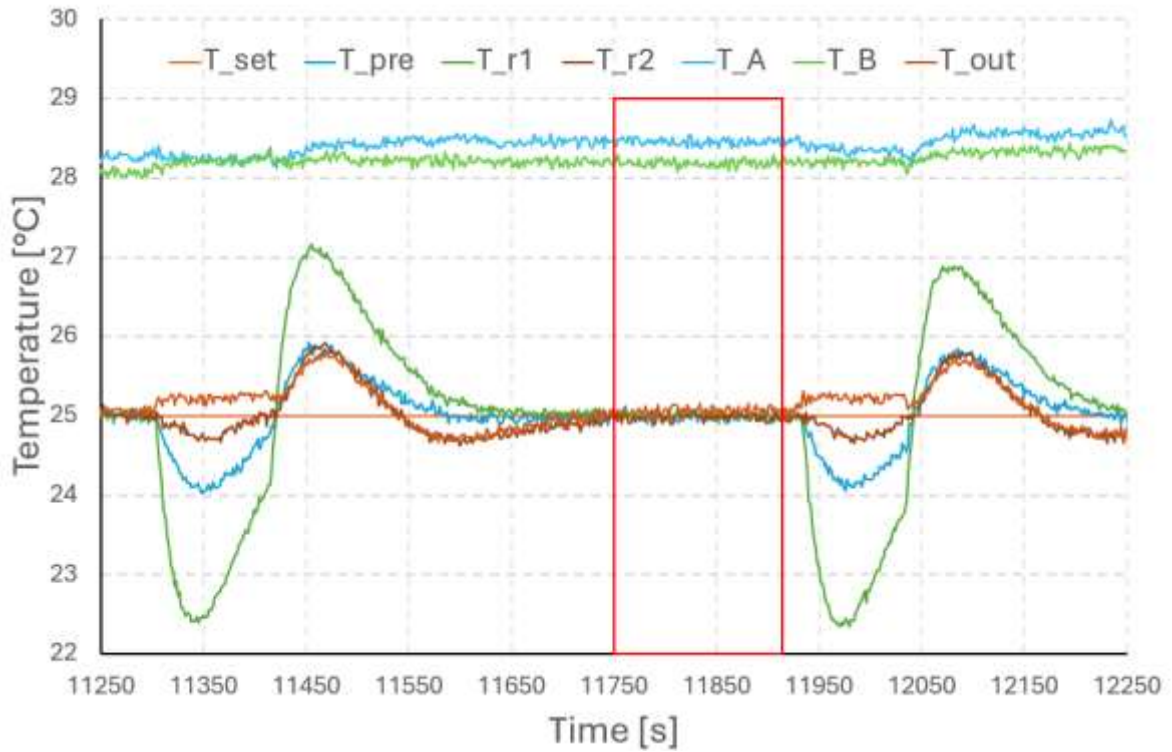


Figure 3-1: Temperature curve and selected values (red square) of the mixing of methanol-water. Different measured temperatures using a ceramic reactor plate with three segments (C3E) at 25°C.

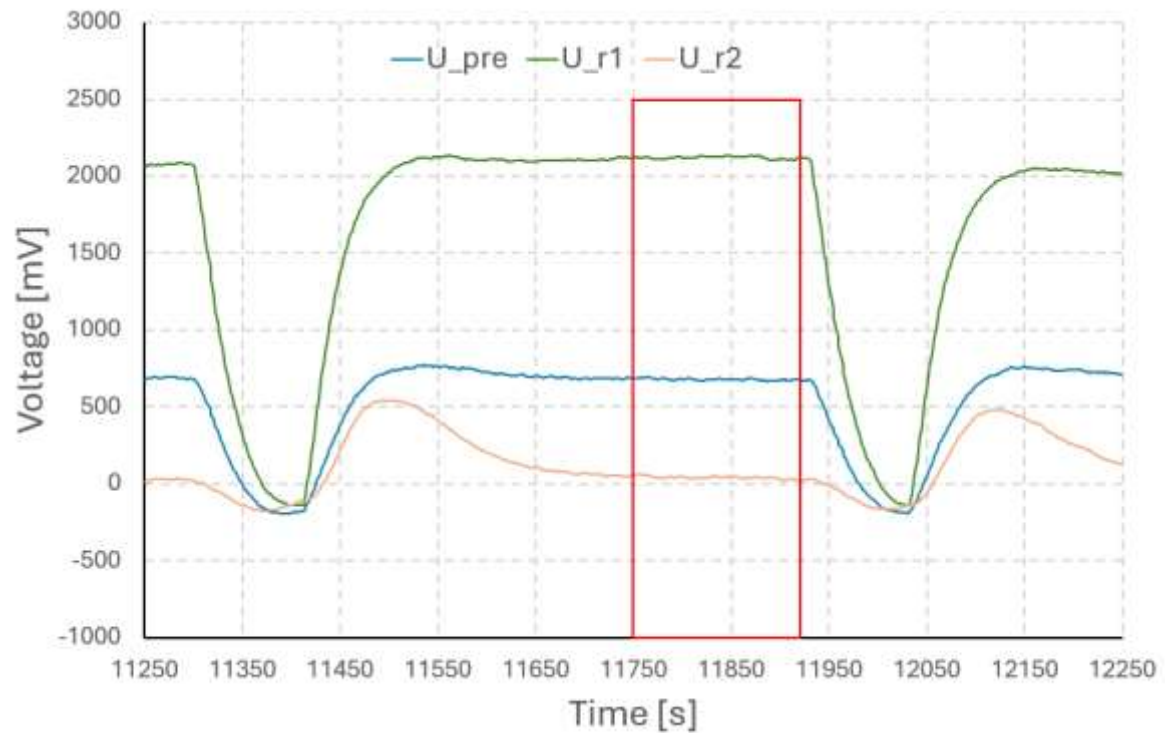


Figure 3-2: Measured signals of the Peltier elements and selected values (red square) of the mixing of methanol-water. Different measured signals using a ceramic reactor plate with three segments (C3E) at 25°C.

The ambient/room temperature also has a strong influence here, since the calorimeter is not optimally sealed to the environment. The effects of the ambient temperature on the results of the experiments can be attributed to the very precise calibration. Even the smallest deviations have a major impact on the calculated results. As the calibration is carried out at a specific room temperature, a deviation in the room temperature inevitably leads to a falsification of the results. The rising ambient temperature can be seen in the rising temperature of the liquids going into the reactor, which can also be seen in Figure 3-3.

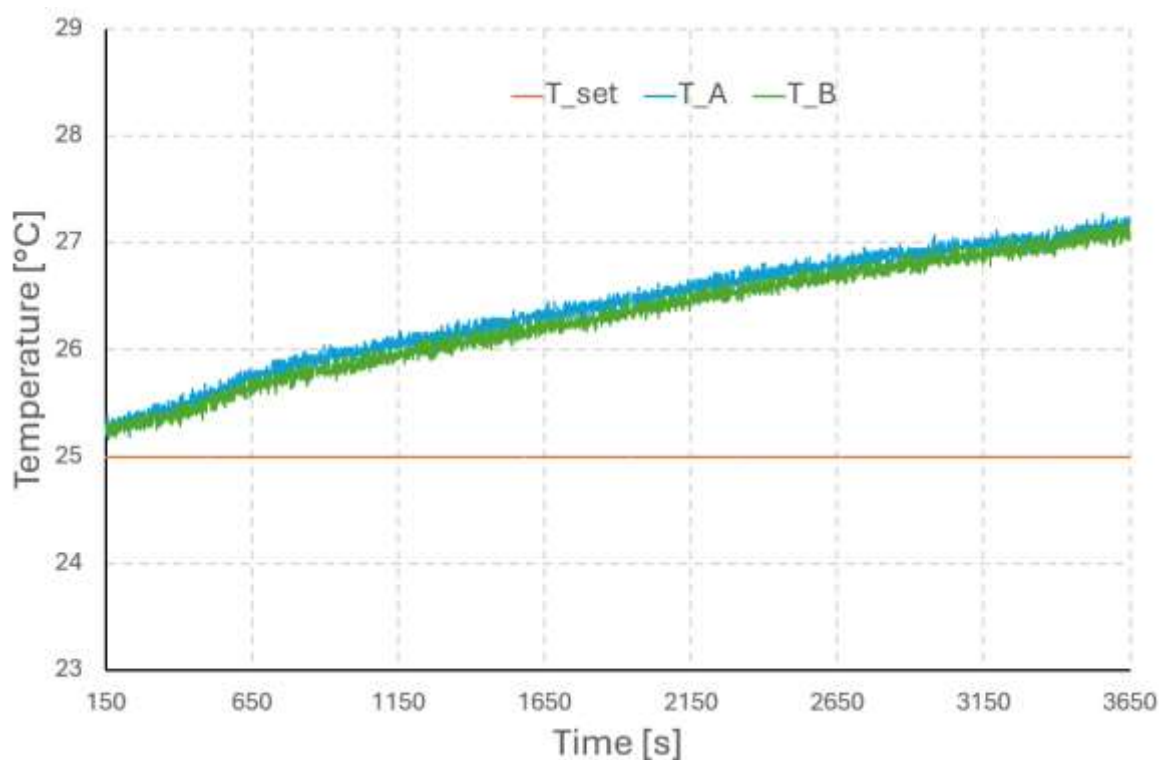


Figure 3-3: Temperature rising from 25.3°C to 27.1°C due to rising of the room temperature throughout the experiment.

In the course of this thesis, it was established that the detected signal (voltage) and calculated enthalpy values are constantly a little bit too high. To investigate the cause, experiments were started in which only pure water was passed through the calorimeter with the ceramic plate C3E at 18°C. The results of this can be seen in Table 3-1. To obtain these results, the mean value of each flow rate was calculated (number of done experiments are in Table 3-1). Here it can be seen that even with pure water, released enthalpy can be detected, although no reaction takes place. The reason for this could be heat caused by friction or the flow of the liquid through the very small capillaries in the calorimeter. However, due to the manufacturing

process of the reactor plates, it is also quite possible that some of the capillaries are somewhat smaller and/or slightly clogged. The plates were cleaned using a syringe that forces air through the plate to remove any excess particles from the manufacturing process. Isopropanol, acetone and ethanol are then passed through the plate using a syringe to eliminate other possible contaminants.

Table 3-1: Measuring only water passing through the ceramic reactor plate with three segments (C3E) with different flow rates. Number of experiments and the average detected signal.

Total flow rate	Number of experiments	Average detected signal
[mL min ⁻¹]	[-]	[W]
1.00	5	0.0026
2.00	5	0.0382
4.00	5	0.0964
5.00	3	0.0259
6.00	3	0.0562
7.00	3	0.0746

3.2 Residence time distribution (RTD)

Various reactor plates were used in the course of this work and are further described in Chapter 2.2 and Chapter 5.1. These have different channel diameters, and lengths and the material is stainless steel or ceramics (C3E, M3E, M3Ebd, M3Ed, M6E). This all has an influence on the duration of the liquid in the reactor and the mixing behaviour. In order to find out how long it takes for the liquid to flow through the entire reactor plate and possibly react, a residence time distribution must be investigated.

The detailed execution of the experiment and the set-up are described in more detail in Chapter 5.5. Two syringe pumps were used to pump solvent and tracer into the apparatus. The solvent is a mixture of ethanol 12wt% in water and for the tracer

anisole was added to the solvent to obtain 0.008v%. The absorbance of the light is measured at the output of the set-up and with the help of the data saved in an Excel file by the computer, the soil number can be calculated. Open-open parameters were used for the calculation. This is described in more detail in Chapter 2.4.1.

The standard operating procedure (SOP) of the experiment can be found in the appendix (Chapter 9.5.1).

The residence time distribution is examined using a step function, which is realized using a 6-port valve. Here, solvent without tracer or with tracer can be pumped alternately through the set-up.

First, the signal measurements must be normalized. Figure 3-4 shows an exemplary illustration of the normalized signal measurements for different flow velocities in the ceramic reactor plate (C3E).

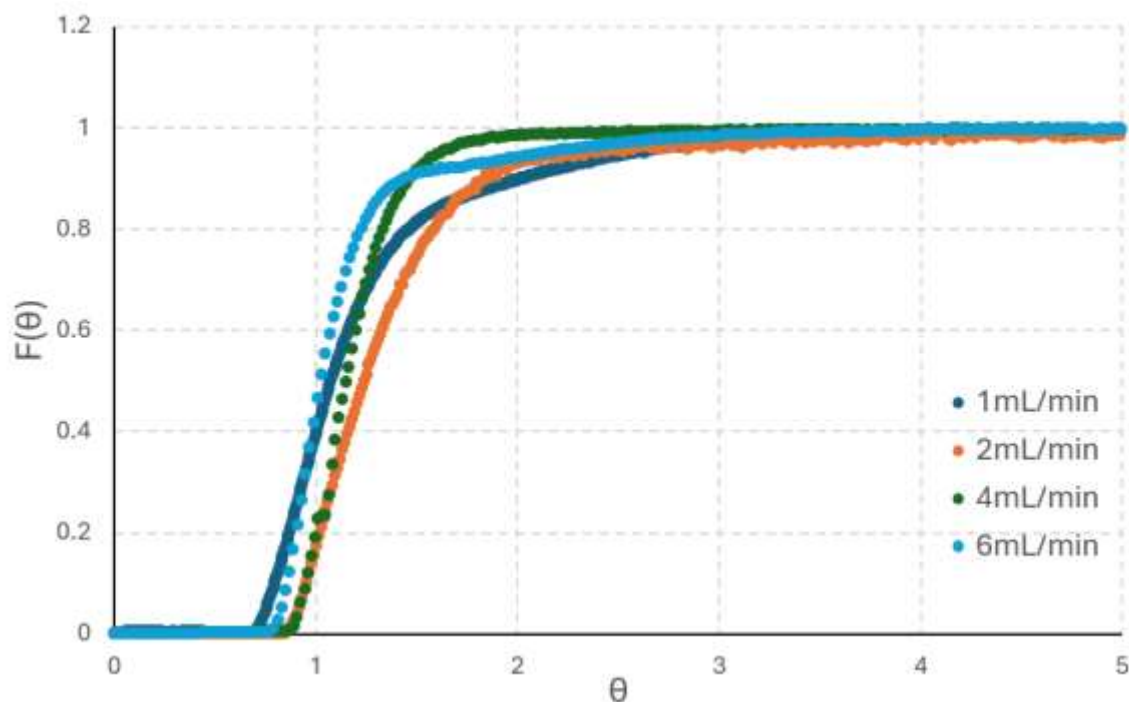


Figure 3-4: Normalized absorption plot of RTD measurements at various total flow rates using a ceramic reactor plate (C3E).

When looking at Figure 3-4, the F-curves reach values of approx. 0.20 - 0.40 after 1 theta. After approx. 2 theta, values of 0.90 - 0.95 are already reached. It can also be seen that the flow rate has an influence on the curve. The distance between the individually measured data points shows that the curve rises much faster at a higher

flow rate (experimental time), while at a lower flow rate many more data points were recorded within the rapid rise. This is due to the fact that theta represents the normalized time and the experimental time at low flow rates is much higher than that at high flow rates. Additionally, the curve becomes constant more quickly with a higher flow rate. With flow rates of 1 mL min^{-1} and 2 mL min^{-1} , for example, the F-curve only reaches 0.99 after 4 theta, while at 4 mL min^{-1} this is already achieved after 2 theta and at 6 mL min^{-1} at 3 theta.

Further, the respective Bodenstein numbers and the Reynolds numbers were calculated. The Reynolds number was calculated using the investigated flow rate which were tested from $0.295 \text{ mL min}^{-1}$ to 6 mL min^{-1} , resulting in Reynolds numbers in the range between $10.48 < \text{Re} < 213.06$. This clearly establishes that a laminar flow is present. The exact data can be found in the appendix (Chapter 9.5.2).

The Bodenstein numbers for the respective reactors were relatively constant across the different flow rates. Therefore, these data were averaged and the results with the standard deviation can be seen in the table below (Table 3-2).

Table 3-2: Results of the mean Bodenstein numbers for all reactor plates.

Reactor plate	Mean Bo + SD
	[-]
C3E	4.90 ± 0.80
M3E	3.43 ± 0.18
M3Ebd	2.91 ± 0.07
M3Ed	5.88 ± 0.97
M6E	5.29 ± 0.18

As already explained in Chapter 2.4.1, the Bodenstein number is a measure of how much backmixing exists. If the Bodenstein number is low, it can be assumed that there is a lot of backmixing. This is confirmed when looking at the results. M3Ebd stands out here. This reactor has a larger diameter, which results in a lower

superficial flow velocity and therefore a lower Reynolds number. This in turn means that the flow is calmer, resulting in more backmixing. Conversely, C3E and M3E with a smaller diameter result in a higher superficial velocity and therefore a more turbulent flow, which leads to less backmixing.

C3E, M3E and M3Ed each have the same inner diameter, which means that their superficial velocities are also the same. However, there are still slight deviations in the Bo number. This can possibly be explained by the inner surface structure of the reactor plates and the respective materials. The rougher surface of the metal plates compared to the much smoother surface of the ceramic plate results in much more turbulent flows, which leads to less backmixing. This is confirmed by the higher Bodenstein figures. M3Ed has a higher value for Bo than M3E, which can be attributed to the greater length of the capillaries for the same size of reactor plate. The volume flow has to change direction much more frequently, resulting in a much more turbulent flow behavior. Due to the greater chaos, there is less backmixing, which is reflected in the higher Bo number.

It is also noticeable that M6E has the same internal diameter as M3Ebd. The larger volume per segment, although the diameter is the same, results in a more turbulent flow behavior. This results in less backmixing, which explains the higher Bo number.

When calculating the RTD, it is important to exclude from the calculation the paths that must be traveled by the liquid that are outside the reaction segments of the reactor plate. This includes the capillaries between the pumps and the plate, the fittings, the preheating element in the reaction plate and the capillaries between the reaction plate and the UV-Vis cell. In the following graph the experimentally determined mean residence times are shown depending on the flow rate for each reactor plate.

The following graph (Figure 3-5) shows the results of the residence time for the different reactor plates depending on the flow rate.

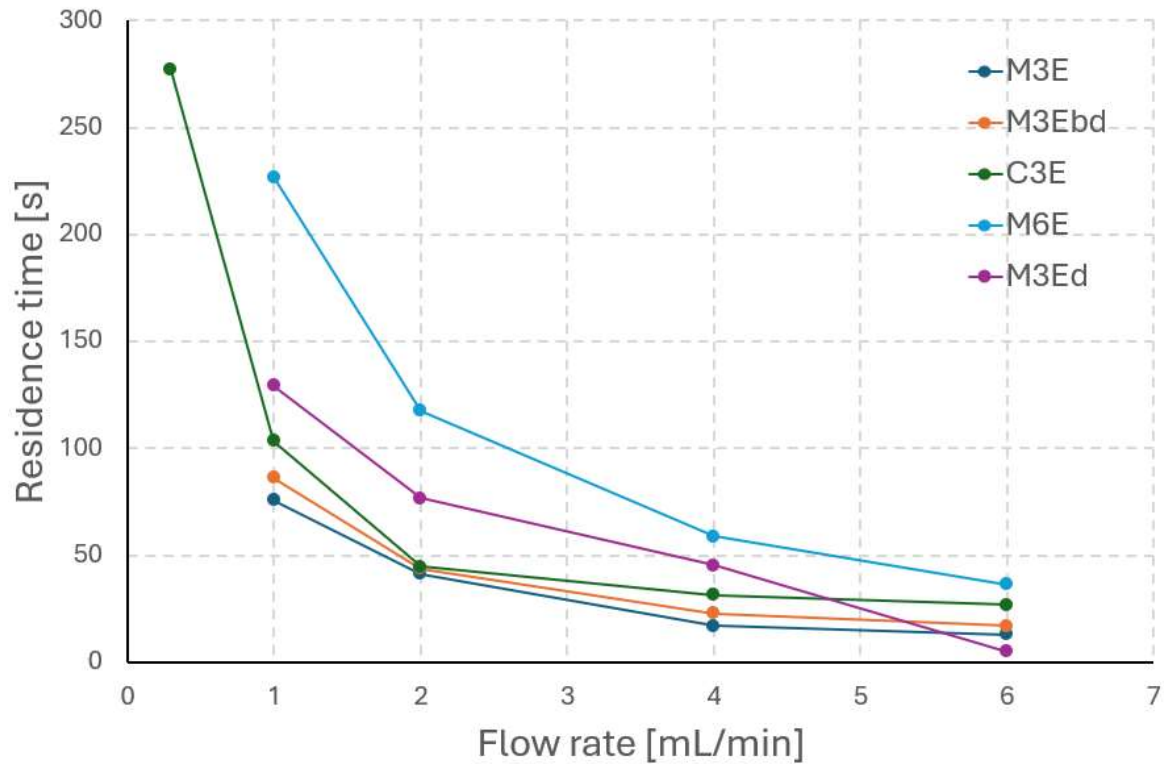


Figure 3-5: Results of the residence time distribution (RTD) for different reactor plates at different flow rates.

Figure 3-5 shows that the results decrease with increasing flow rate, as the liquid flows more quickly at higher velocities.

Nevertheless, the results of the residence times are much higher than the theoretical values, which can be seen in the appendix (Chapter 9.5.2). Possible reasons for this are previously undetected dead zones in the system, errors in the manufacture of the plates and thus a deviation from the intended geometry, error during measurements using the Flow Cell-Z-10 and Avantes [31], or the use of the SyrDos™ pump [32]. These pumps pump the liquid into the calorimeter with light pulses. This can lead to a deviation in the pump calibration, causing the actual flow rate to deviate from the desired flow rate. This would falsify the results. In future work, new experiments with syringe pumps [33] would be possible, but there was no time for this in the context of this work.

The exact data is listed in the appendix (Chapter 9.5.2).

3.3 Bourne reaction

To further investigate the mixing behaviour in the different reactor plates, the Bourne reaction was used. This reaction has been characterized precisely by Bourne et. al. [4] and therefore the experimental results can be compared with literature values. In the diazo coupling reaction 1-naphthol (reactant A) is used in excess and reacts with diazotised sulfanilic acid (reactant B). The whole reaction takes place at room temperature. The complete reaction scheme can be seen in Scheme 2-1. If perfect mixing would occur, all of reactant B would react with reactant A. But, if there is poor mixing, still existing reactant B reacts with the product and a secondary S-product (bisazo dye) is created. Therefore, the amount of the S-product (yield Y_s) quantifies the mixing behaviour and can be calculated using the equation (2-21). The higher Y_s , poorer mixing occurs and a low Y_s shows fast mixing and therefore, no limitation for mass transfer. [4]

The experimental set-up, the execution and a description of the measurements using UV-Vis-measurement can be seen in Chapter 5.6.

To incorporate the effect of the Reynolds number on the mixing behaviour, different flow rates were investigated. Before sample-taking (2 mL), to ensure steady state, the experimental set-up was flushed for three residence times before taking the sample. Further calculations are only valid, if Lambert-Beer-law is applicable and therefore the product has to be diluted 1+7 with buffer in order to decrease the concentration. After dilution the sample was measured with UV-Vis measurement.

A major problem with UV-Vis measurement is the durability of the light bulb used for this purpose. At the beginning of the experiments, it was not possible to obtain reproducible results. The reason for this is that the service life of the light bulb has been exceeded. Reproducibility can be guaranteed by using a new light bulb. Figure 3-6 shows the difference between the old and the new light bulb. The graph shows the scatter of the different measurements. Here it is clear from the lower scatter that the new light bulb is more reproducible.

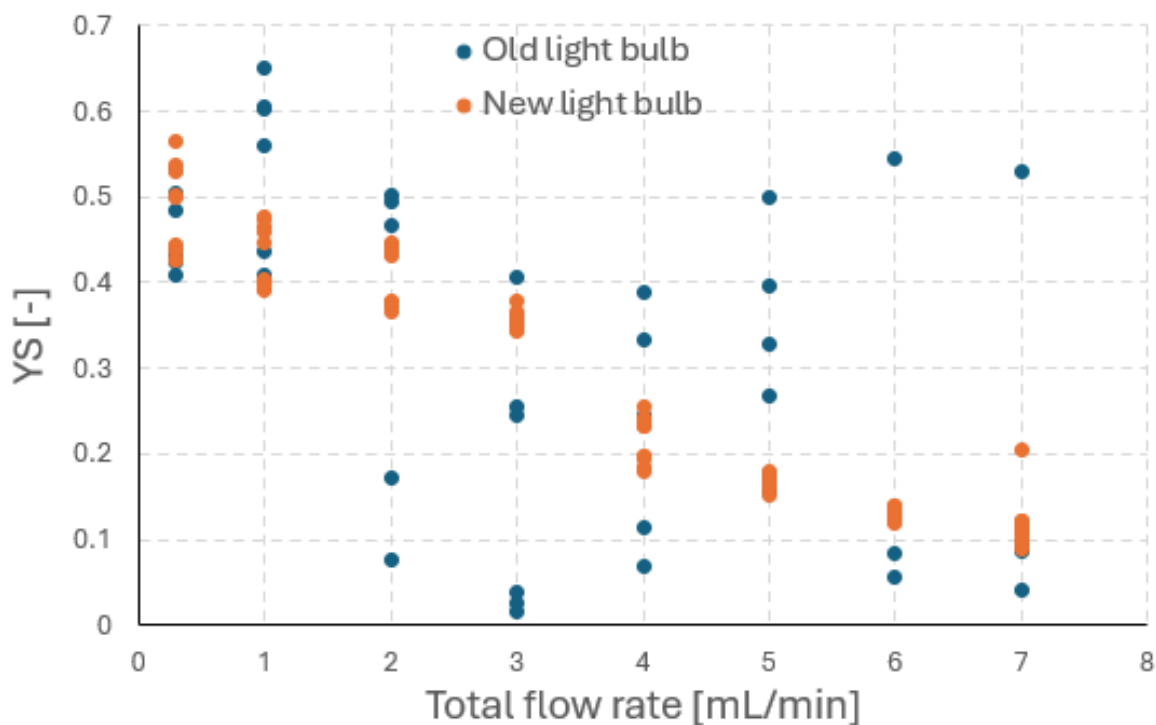


Figure 3-6: Difference between old and new light bulb for UV-Vis measurement using the Bourne reaction in order to test the ceramic reactor plate.

Using the Bourne reaction and the new light bulb, five different reactor plates were examined and a simple “T-piece” and an “AP04” were also considered as comparative values.

The AP04 has an inner diameter of 0.6 mm and mixing takes place using a split-and-recombine principle. The exact structure can be found in the literature [10]. The five reactor plates investigated are listed in Table 5-1 (C3E, M3E, M3Ebd, M3Ed, M6E) and the results can be seen in Figure 3-7.

As already described, Figure 3-7 shows the yield of the by-product S as a function of the total flow through the respective reactor plates. The lower the yield, the better the mixing in the reactor. It is clear to see that, regardless of the reactor plate, the yield decreases as the flow rate increases, i.e. mixing becomes more complete. The graph shows that AP04 has the best mixing, which can be explained by the fact that this reactor was developed precisely for good mixing.

Furthermore, it can be observed that when comparing the metal reactor plates, the one with three segments has the best mixing behavior (M3E). Here, the mixing behavior is significantly better (the yield significantly lower) than with the metal

plates with three segments and a larger diameter (M3Ebd), the large metal plate (M6E) or the metal plate with double the volume (M3Ed) and even the ceramic reactor plate (C3E).

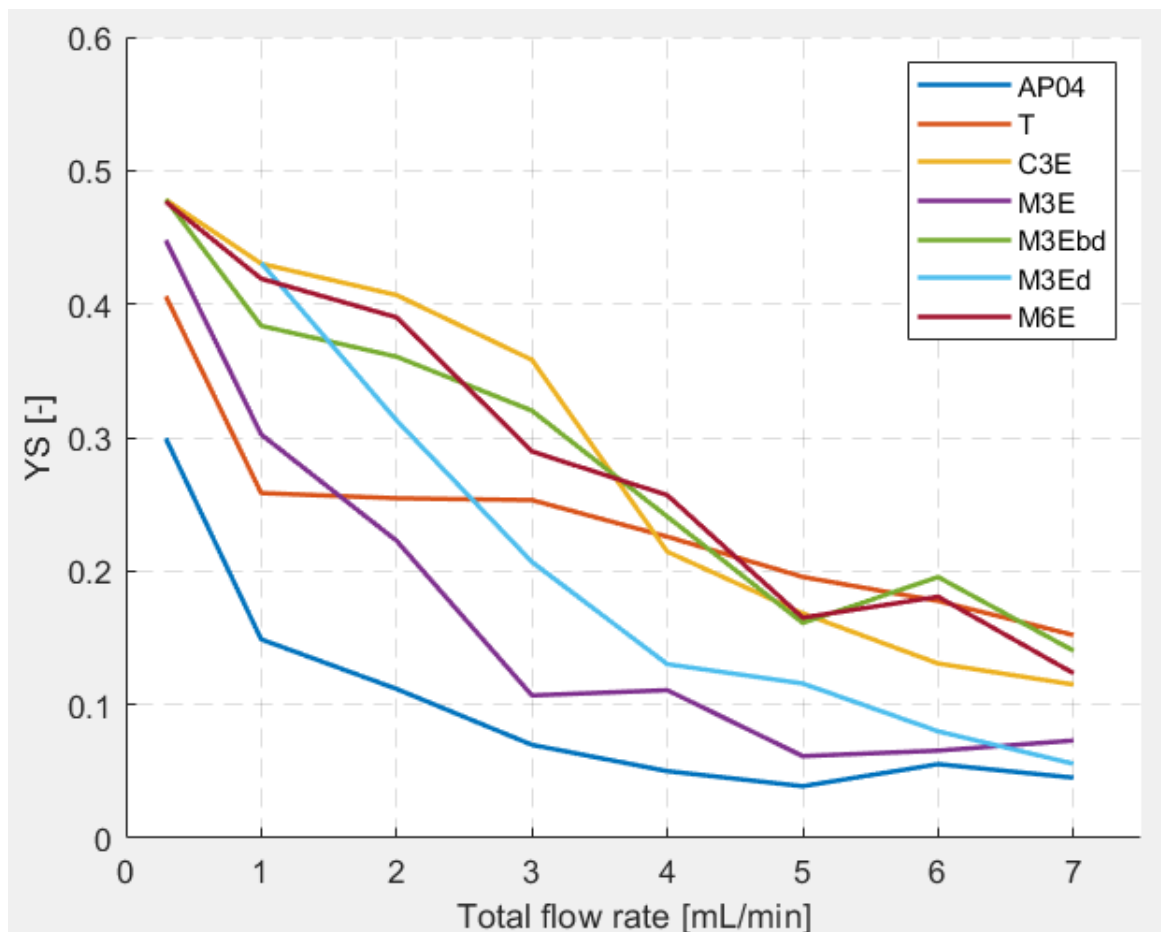


Figure 3-7: Results Bourne reaction using the new light bulb. Yield of product S depending on the total flow rate for seven different reactors (AP04, T, C3E, M3E, M3Ebd, M3Ed and M6E).

The reason for the better mixing behavior of M3E compared to C3E can be attributed to the difference between the surface roughness of the different materials. The exact production of the two plates has already been explained in Chapter 2.2. When manufacturing the ceramic reactor plate, a smooth surface is also possible inside the channels, while the metal reactor plates have rougher surfaces. In the production of metal plates, the process often results in loose metal powder inside the channels, which must be removed by air pressure before first use. However, it is possible that this has not been done completely and the more irregular surface on the inside can lead to greater turbulence and therefore better mixing.

When comparing M3E and M3Ebd, it is noticeable what a difference the larger diameter of the reactor plate channels makes. This results in less turbulence and therefore better mixing. Another possible reason for the better mixing with M3E is the production of the plate. When printing the smaller channels in the reactor plate, it is possible that some channel sections are blocked by the metal powder or the surface is inaccurate, which leads to increased turbulence.

The ceramic, metal reactor plate with three segments and a larger diameter and the one with six elements show comparable results with minor deviations. The fact that the two metal reactor plates have the same diameter and only the length of the channels is different may indicate that extending the reaction does not make a significant difference. Apparently, the reaction is already complete at the end of the third segment (second mixing element). The small deviations between the plates M3Ebd and M6E can be attributed to possible impurities, inaccuracies in the measurement or evaluation or minor blockages of the channels in the reactor plate. With a significantly higher number of experiments, the deviations could possibly be minimized.

When comparing M3E and M3Ed, it is noticeable that the longer capillaries exhibit poorer mixing behavior. The diameter is the same for both reactor plates. When comparing M3Edb and M6E, which also have the same diameter but different lengths, no significant differences in mixing behavior can be seen. The different mixing behavior of M3E and M3Ed can be attributed to possible clogged capillaries and thus a deviation from the optimal flow pattern/path.

The comparison between the T-Piece and the other reactors was used to see, how well something that is not explicitly designed as a reactor performs in comparison. This shows that at high flow rates, the yield is equal to or higher than that of the reactors, which means that the mixing is worse. At lower flow rates, on the other hand, the mixing is better compared to the reactor plates tested. However, this is only relevant at very low flow rates ($<1.75 \text{ mL min}^{-1}$) as at flow rates greater than 1.75 mL min^{-1} the mixing in the M3E is better and improves more and more as the flow rate increases.

To verify the experiments, the results of the Bourne reaction from this work are compared with those from previous experiments listed in the literature [5].

Figure 3-8 shows the results of these earlier experiments on the Bourne reaction. In comparison with the results in this thesis, it is clear that the results of the experiments with the reactor plate M3E and therefore the reactor plates are comparable. This means that the preparation and processing of the chemicals, the process of the experiment and the evaluation of the results can be assumed to be correct. When comparing the results with regard to the T-piece, the results obtained in this thesis are at higher flow rates similar to those in the literature [5], while the results at low flow rates deviate slightly from the literature values. Therefore, at higher flow rates the measurement method is more accurate. Various deviations are due to possible impurities, deviations in the measurement or small printing errors in the reactor plates.

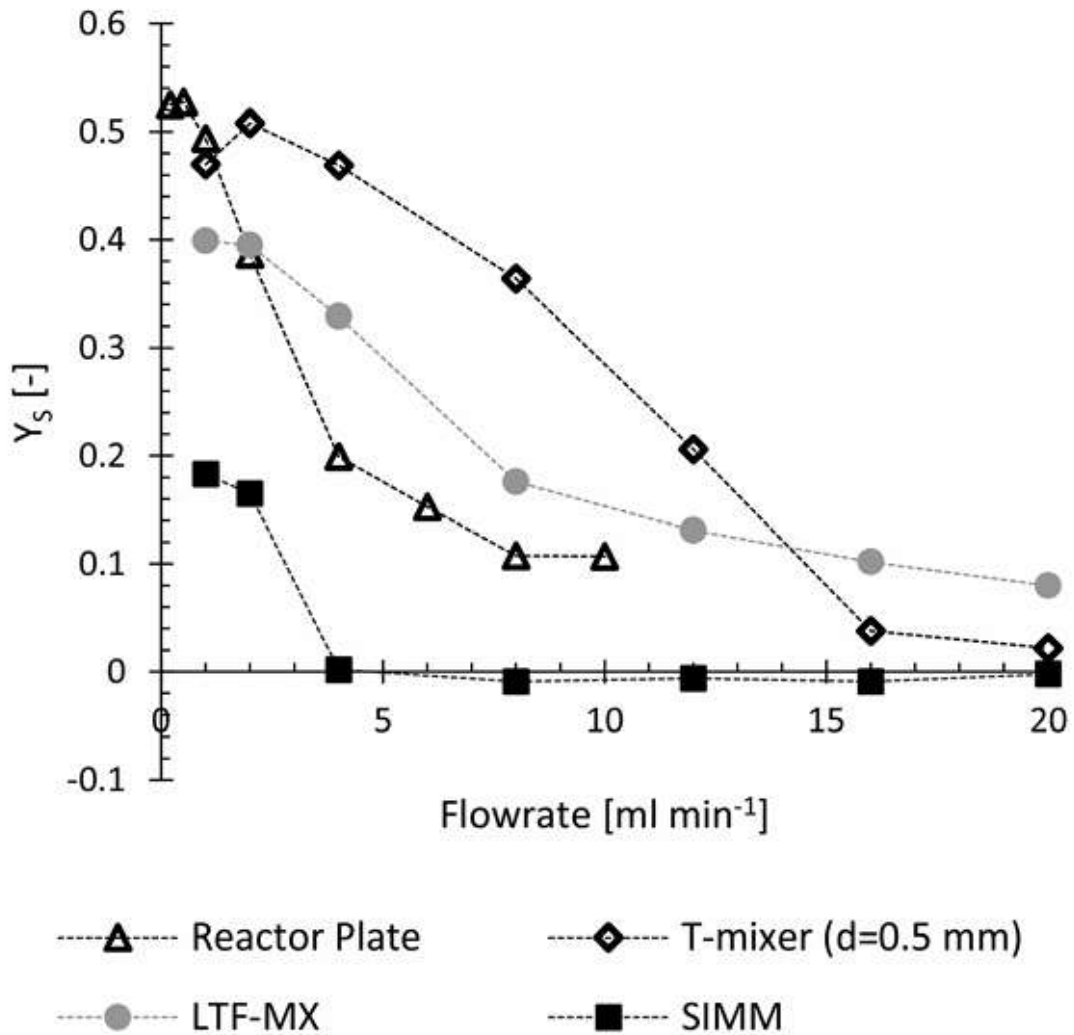


Figure 3-8: Comparison of the performance of a reactor plate (comparable to M3E), T-mixer, a X-mixer (Little Things Factory GmbH, type X), Slit interdigital micromixer SIMM-V2_ss (Institut für Mikrotechnik Mainz GmbH) during Bourne reaction previously done in other literature. [5]

3.4 Solvent mixtures

Mixing enthalpies of solvent mixtures are well studied and are registered at lower enthalpy values. Therefore, first of all the mixing enthalpy experiment with water and methanol was investigated. After determining the accuracy of the calorimeter, two not so well studied mixing enthalpies were investigated, TEG with water and TEG with 1-propanol. The exact experimental procedure is described in Chapter 5.7.

3.4.1 Methanol-water

As already described, a large number of literature values can be used in the experiment to measure the enthalpy when mixing methanol and water. [34], [35], [36]

The literature values are measured at different ratios and in order to be able to compare them, different ratios between methanol and water are also compared in this thesis. However, the first question was, what effect the flow rate during the mixing has on the results. For this reason, different flow rates were first tested using the same ratio. Methanol and water were pumped into the reactor in a volumetric ratio of 1:1 using syringe pumps [33]. In addition, two different temperatures were investigated in order to detect any possible differences/influences.

Figure 3-9 shows these values in comparison to the literature value (orange line). The literature value with a molar ratio of 0.3 (volumetric ratio methanol:water of 1:1) at 25°C is a mixture enthalpy of $-0.84 \text{ kJ mol}^{-1}$. [34], [35], [36]

The literature [34] and [36] did not indicate that the flow rate could have a possible effect on the enthalpy of mixing, while various flow rates between 0.1 ml min^{-1} and 0.5 ml min^{-1} were measured in the literature [35]. Here, the measured enthalpies only show such small differences depending on the flow rate that these were declared as measurement inaccuracies. Accordingly, the measured enthalpy of mixing is also defined here as independent of the flow rate.

The exact dates are listed in the appendix (Chapter 9.7.1).

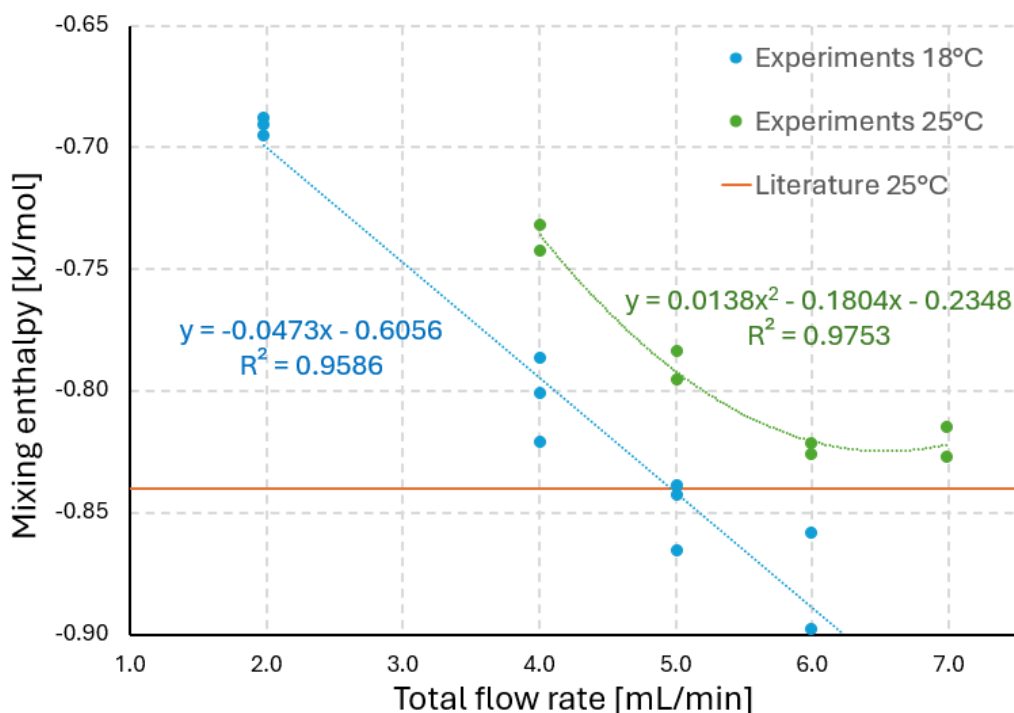


Figure 3-9: Mixing methanol-water at different temperatures and different total flow rates with volumetric ratio methanol:water 1:1 in the ceramic calorimeter with three segments (C3E) and comparing results to the literature value.

When looking at Figure 3-9 and comparing the values obtained with the literature value, it should be noted that the literature value was measured at a temperature of 25°C. When looking at the experimental data at 18°C, it is noticeable that they come closer and closer to the literature value as the flow rate increases. However, if the flow rate is higher than 5 mL min⁻¹, more mixing enthalpy is released and it no longer appears to approach the experimental value. Even without taking the literature value of 25°C into account, the trend curve (as shown in Figure 3-9) appears to decrease constantly and does not stabilize at an ideal value.

If the curve of the experiments at 25°C is viewed in comparison, a clear trend can be seen. Here, the values approach the ideal literature value more and more as the flow rate increases. The highest accuracy and most representative are the results at 6 mL min⁻¹. However, the results here are also slightly higher than the literature value, which has already been discussed and analyzed in Chapter 3.1.

Based on the experiments shown in Figure 3-9, a total flow rate of 6 mL min⁻¹ was set for the following experiments, as this comes closest to the literature value and still provides representative results. In the following experiments different

compositions were tested. The system was set to a temperature of 25°C and an attempt was made to keep the ambient temperature (room temperature) at a constant 25°C, in order to best match the calibration.

This was particularly important as the enthalpy generated is very low and therefore the differences between the individual compositions of the liquids and the associated results are minimal, which can also be seen in Figure 3-10 and in the results in Table 3-3. Some experiments had to be repeated, as the room temperature varied greatly in some experiments and the calibration of the calorimeter therefore no longer provided accurate results. The results used in Table 3-3 below were taken from experiments at constant room temperature in order to ensure reproducibility. Table 3-3 also shows the amount (n) of the representative values for each particular composition.

Table 3-3: Mixing reaction methanol-water at different ratios at 25°C in the ceramic calorimeter with 3 segments (C3E) with a total flow rate of 6 mL min⁻¹ and the amount of done experiments (n).

X_{water}	n	Mixing enthalpy
[-]	[-]	[J mol⁻¹]
0.900	1	-579.7
0.840	2	-745.7
0.771	1	-825.5
0.692	2	-854.5
0.600	3	-845.7
0.491	3	-793.3
0.360	3	-688.4
0.200	3	-474.6

In order to better visualize the results obtained and to be able to compare them with the literature values [34], [35], [36]., they are plotted in the following Figure 3-10.

The data values of the literature can be seen in the appendix (Chapter 9.7.2).

Looking at Figure 3-10, it is noticeable that the values form a parabola and that the difference between the individual mixing enthalpies depending on the ratio between methanol and water is very small, especially at the apex. For example, the difference between a mixture of $x_{\text{water}} = 0.600$ and $x_{\text{water}} = 0.692$ is only 8.8 J mol^{-1} .

It can be seen in Figure 3-10, that even the results of the calorimeter at very low enthalpy values are well comparable with the literature ones, which indicates that the calorimeter functions acceptably.

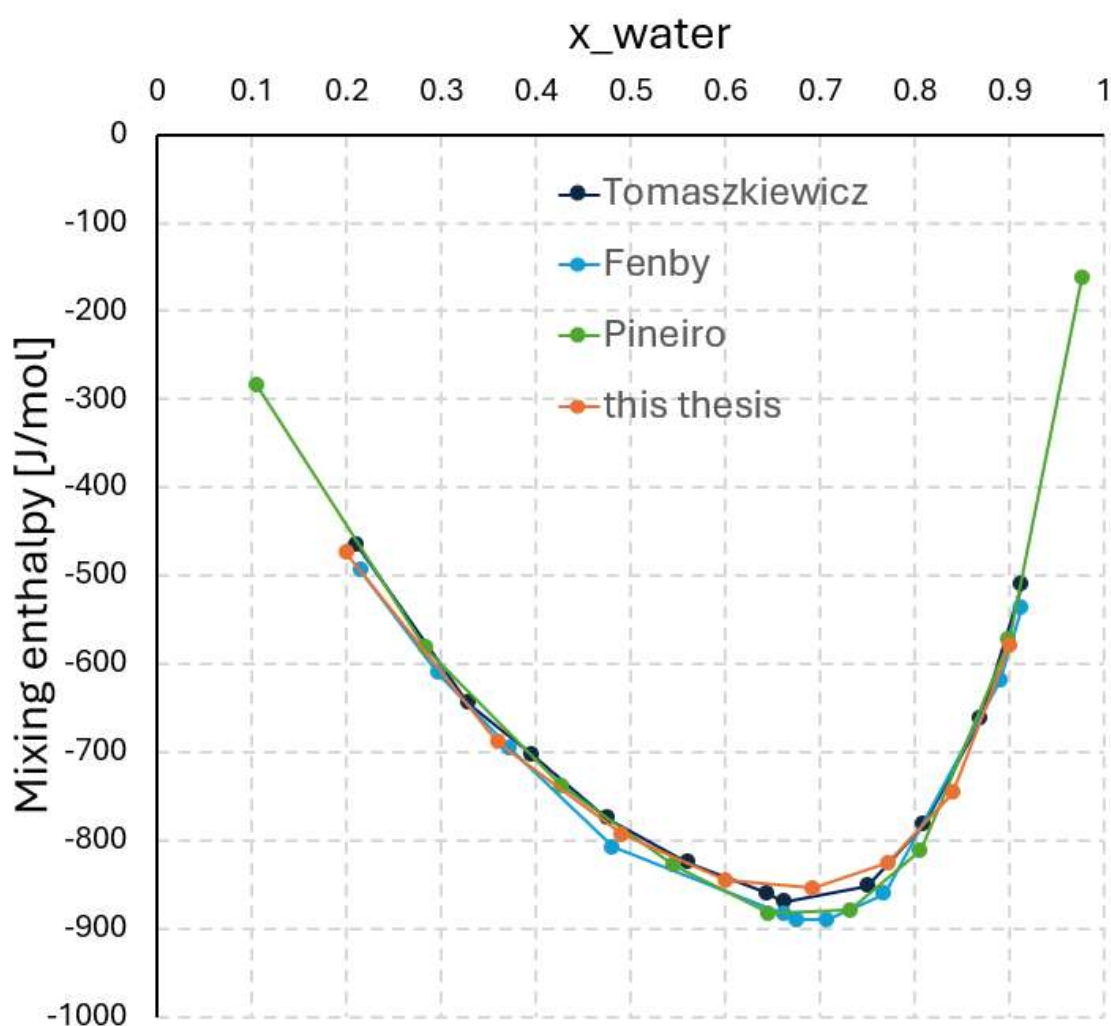


Figure 3-10: Comparing the results of the mixing enthalpies for the mixture methanol-water with literature values at 25°C .

3.4.2 Triethylene glycol (TEG)-water and Triethylene glycol (TEG)-1-propanol

After validating the results of the calorimeter using the mixing of methanol and water, new experiments with not much established chemicals were investigated. The interaction between TEG and water and between TEG and 1-propanol was analyzed. The experimental procedure can be found in Chapter 5.7.2.

One of the biggest problems in handling TEG is the very high viscosity (47.8 mPa at 20°C [37]), as this resulted in an extreme increase in pressure in the microreactor. This led to the syringe pump [33] not working and it was necessary to switch to a SyrDos[™] pump [32]. However, this pump also had problems pushing the liquid through the reactor, especially at low temperatures. The experiments were therefore carried out at 25°C and then at the much higher temperatures of 40°C and 55°C. For this purpose, the liquids (especially the TEG) were preheated in advance to counteract the high viscosity as well as possible. In addition, the set flow rate and the actual flow rate were checked several times, but there were various problems with fittings remaining tight due to the excess pressure. The flow rates were in between 1 and 2 mL min⁻¹.

Triethylene glycol (TEG)-water

As already described in Chapter 3.1, the values obtained during the experiment were again fundamentally too high. A few tests were carried out with pure water, and these were then subtracted from the mixing enthalpies obtained from the experiment. The averaged and corrected values are shown in Figure 3-11. The exact data and the number of experiments can be seen in the appendix (Chapter 9.7.3).

It can be seen in Figure 3-11 that the curves from the higher temperatures show a clear trend with increasing composition. In addition, it can be seen that at low composition, more mixing enthalpy is emitted the higher the temperature. At high composition, the results approach each other. Especially at high temperatures, it is noticeable that with a higher proportion of water, less mixing enthalpy is released. The viscosity of TEG has a very large influence, especially at low temperatures, as only a few representative experiments were possible, which can be seen in Chapter 9.7.3.

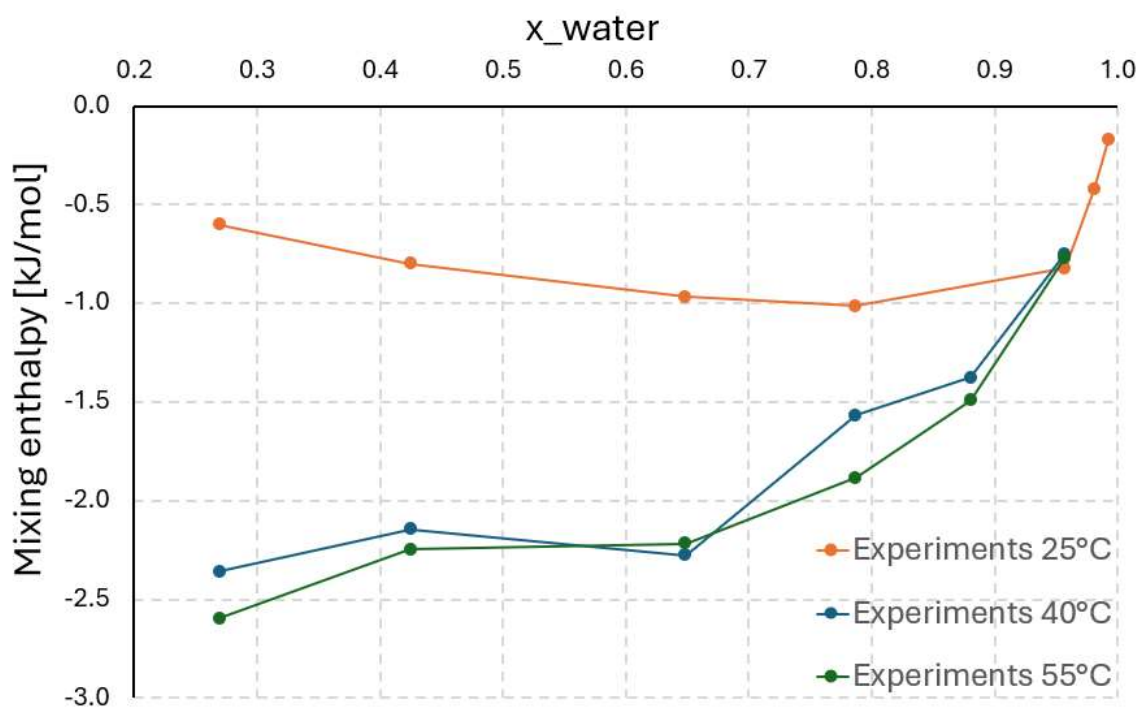


Figure 3-11: Mixing enthalpies of TEG-water at different temperatures (25°C, 40°C and 55°C) using the ceramic calorimeter with three segments (C3E).

Triethylene glycol (TEG)-1-propanol

As already established and described in Chapter 3.1, the values obtained during the experiment were again fundamentally too high. A few tests were carried out with pure 1-propanol, and these were then subtracted from the mixing enthalpies obtained from the experiment. The averaged and corrected values are shown in Figure 3-12. Each value was measured once. The exact data can be seen in the appendix (Chapter 9.7.4).

When looking at the results in Figure 3-12, it can be seen that all three curves follow a clear trend. However, it is noticeable that the curve at 25°C is much more constant than at higher temperatures. As with the mixing of TEG and water, all three curves converge as the composition increases and become similar. However, if the proportion of 1-propanol is higher, the curves diverge from another and the reaction shows a much higher mixing enthalpy release at higher temperatures.

A closer look at the values of the experiment at 25°C reveals that there actually is a curve and not a constant value. However, the differences between the individual values are so small that it is reasonable to assume that the deviation from each other could possibly be reduced by using several more data points.

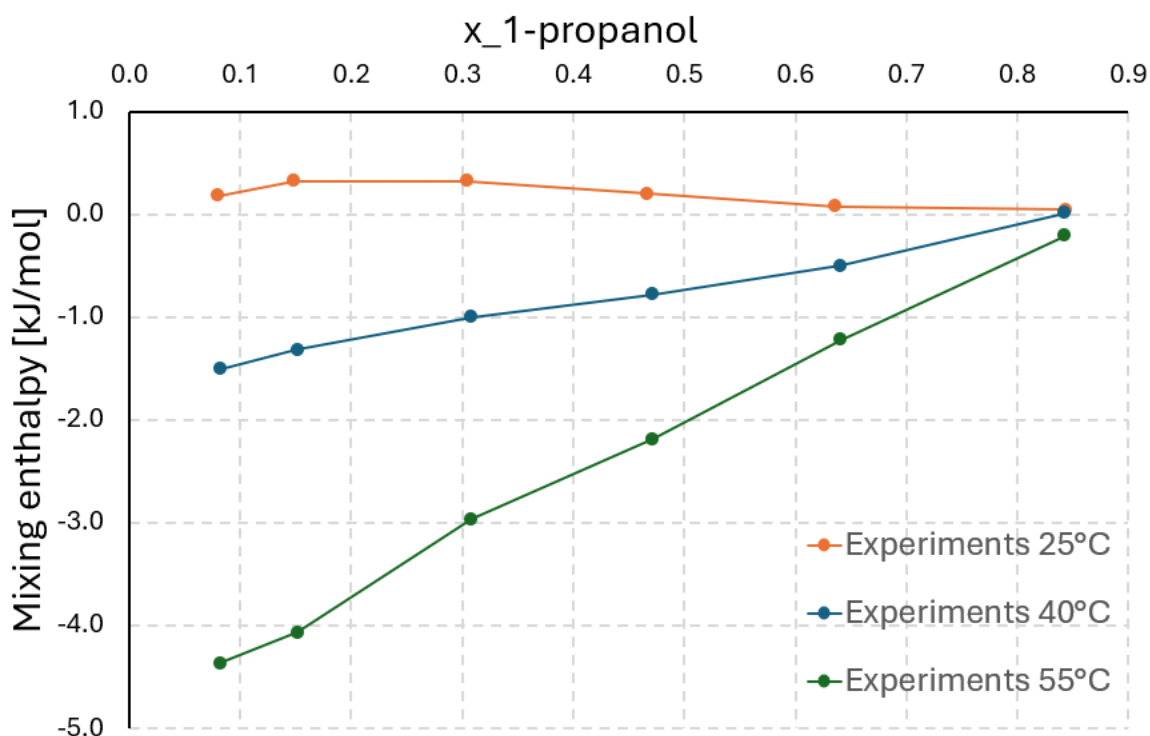


Figure 3-12: Mixing enthalpies of TEG-1-propanol at different temperatures (25°C, 40°C and 55°C) using the ceramic calorimeter with three segments (C3E).

3.5 Neutralization reaction

The neutralization of acetic acid with NaOH was tested for additional validation of the calorimeter. The results were then compared with literature values [23]. The experiment was carried out in the ceramic reactor plate with three segments (C3E) and in a stainless steel reactor plate with six segments (M6E). The experimental procedure can be found in Chapter 5.8.

3.5.1 Neutralization in ceramic reactor plate (C3E)

The measured flow rates and ratios are shown in Table 3-4 and compared to the literature value for the reaction enthalpy of $-57.4 \text{ kJ mol}^{-1}$ [23]. Table 3-4 shows the measured values at a room temperature of 22°C, while Table 3-5 shows the measured data at a room temperature of 28°C. As it can be seen, the experiment at 22°C was done for seven different total flow rates, while the one at 28°C was only done for two different flow rates.

In Table 3-4 and Table 3-5, only the mean reaction enthalpies and the calculated standard deviation can be seen. There was a big influence of the temperature in the laboratory on the results. As it can be seen in the tables below, the total flow rate 1.5 mL min^{-1} and 2.5 mL min^{-1} have been measured multiple times on different days. The temperature in between these days varies from 22°C to 28°C . These variations had a significant impact on the results. After more calibrations with different environmental temperatures, the deviation between the results from the same total flow rates, decreased, but nevertheless, it can be seen that the surrounding temperature still has a huge impact on the results, because of the highly sensitive reaction and temperature sensors.

Table 3-4: Neutralization of acetic acid with NaOH using the C3E calorimeter and different flow rates. Average detected signal, reaction enthalpy deviation from literature [23] and the amount of experiments (n). Room temperature was 22°C .

Flow rate [mL min ⁻¹]	n [-]	Average detected signal [W]	Mean +SD ΔH_R [kJ mol ⁻¹]	Mean deviation from literature [23] [%]
1.00	2	-0.25	-58.74 ± 6.14	2.34
1.50	3	-0.67	-59.29 ± 1.49	3.29
2.00	3	-0.72	-62.44 ± 2.68	8.77
2.50	3	-1.11	-59.31 ± 3.46	3.33
4.00	4	-1.68	-56.02 ± 5.82	2.41
5.00	2	-2.17	-57.91 ± 7.47	0.88
6.00	2	-2.63	-58.62 ± 6.54	2.13

Table 3-5: Neutralization of acetic acid with NaOH using the C3E calorimeter and different flow rates. Average detected signal, reaction enthalpy deviation from literature [23] and the amount of experiments (n). Room temperature was 28°C.

Flow rate [mL min ⁻¹]	n	Average detected signal [W]	Mean +SD ΔH_R [kJ mol ⁻¹]	Mean deviation from literature [23] [%]
1.50	3	-0.71	-62.85 ± 0.97	9.49
2.50	3	-1.10	-58.74 ± 0.75	2.34

When looking at the results in Figure 3-13, it is noticeable that generally (except one at the total flow rate of 4 mL min⁻¹) more reaction enthalpy is emitted than it should be according to the literature [23]. This can be attributed to the problem with the generally too high values discussed in Chapter 3.1 and has already been investigated with the measurement of pure water (no reaction). Taking into account the measurements with water, the neutralization values are even more comparable with the literature value. In Table 3-6 the percentage of the value of pure water in comparison to the total measured value is presented.

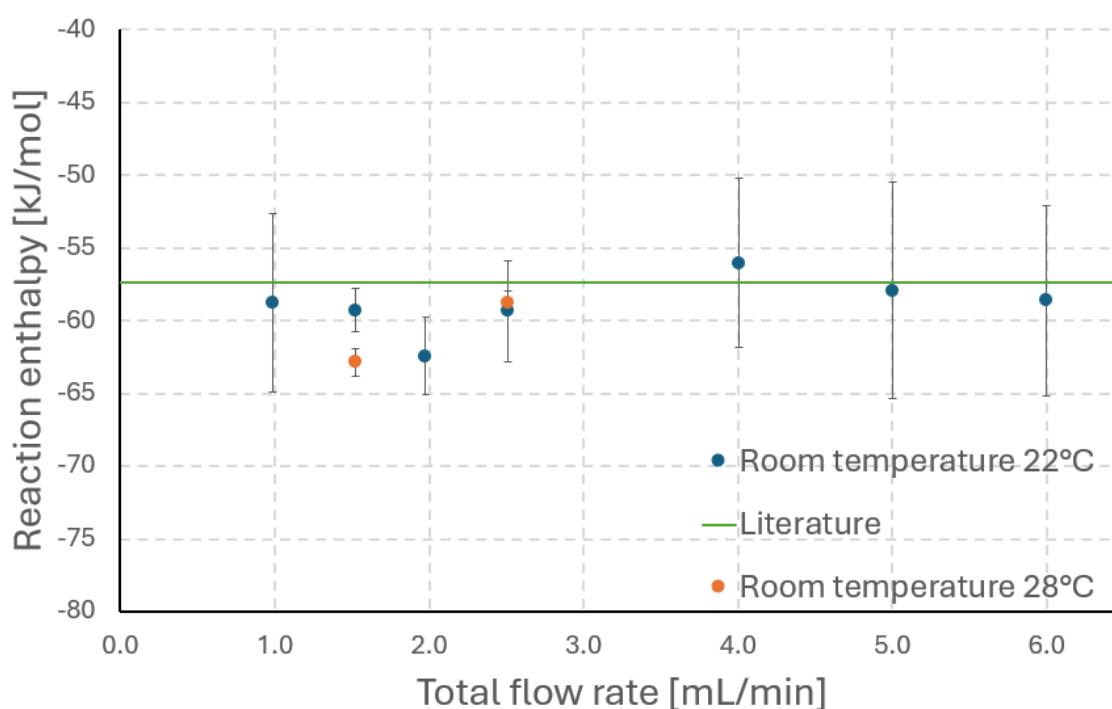


Figure 3-13: Neutralization reaction with C3E at different flow rates. Comparing different room temperatures to literature value [23] (green line).

As it can be seen in Figure 3-13, overall, the results are well comparable to the literature values and are repeatable but highly dependable on the surrounding conditions.

Table 3-6: Amount of difference pure water in comparison to neutralization signal for different flow rates in ceramic calorimeter with 3 segments (C3E).

Flow rate	Percentage of neutralization signal
[mL min ⁻¹]	[%]
1.00	1.02
2.00	5.33
4.00	5.72
5.00	1.19
6.00	2.14

3.5.2 Neutralization in stainless steel reactor plate (M6E)

In order to validate the large calorimeter (M6E), neutralization tests were also carried out with it. Different flow rates were tested at two different temperatures (25°C and 30°C). The literature value is given as -57.4 kJ mol⁻¹ [23]. The results are shown in Figure 3-14.

Figure 3-14 shows that the measured values of the reaction enthalpy at very low flow rates deviate greatly from the literature value. These are not representative. But if the flow rate is increased, the two curves approach the ideal value. However, the curve at 25°C continues to rise even after the literature value, which the curve at 30°C does not do. This curve becomes more and more similar to the ideal value and only has a deviation of 5% at a flow rate of 10 mL min⁻¹.

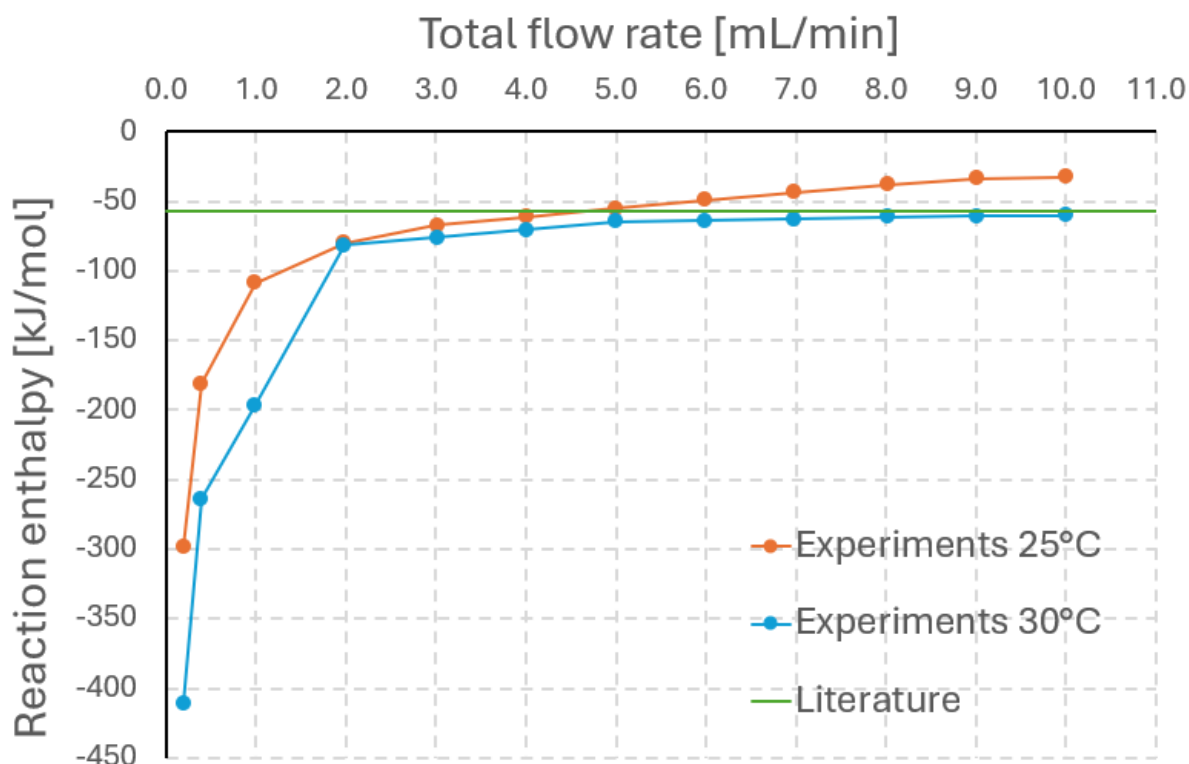


Figure 3-14: Neutralization reaction of acetic acid with NaOH using the stainless steel reaction plate with 6 Segments (M6E) at two different temperatures (25°C, 30°C) and the literature value for comparison.

One possibility as to why the values could have deviations is that the large reactor plate at the outlet has no possibility for a temperature measurement. For this reason, the temperature at the outlet was measured at a distance of 5 cm in the course of the emerging capillary. The path between the calorimeter outlet and the temperature sensor therefore contains an area in which the actual emerging temperature is changed. For future tests, a new stainless steel reactor plate with 6 segments was commissioned for printing, in which a temperature sensor can be placed directly at the outlet, as is the case with the small reactor plates.

3.6 Nitration reaction

The nitration of toluene with nitric acid and sulfuric acid was carried out due to its highly aggressive nature and a further opportunity to validate the calorimeter, as literature values already exist for this reaction. The reaction enthalpy is known from literature values and should be $-125.52 \pm 2.56 \text{ kJ mol}^{-1}$. [2], [3], [11], [38]

The exact reaction equation, the set-up and the execution of the experiment can be found in Chapter 2.4.5 and Chapter 5.9. Basically, a mixture of $\text{HNO}_3\text{:H}_2\text{SO}_4$ and toluene was pumped into the calorimeter with the ceramic reactor plate (C3E) in a volumetric ratio of 1:4 using a syringe pump [33] and then quenched with a NaOH solution. The whole experiment was done at 30°C. At the outlet many samples were taken and analyzed using HPLC.

Due to the highly aggressive and corrosive properties of the reaction, various problems with dissolved fittings and seals occurred during the experiments, resulting in leaks. In addition, the syringe in the syringe pump slowly began to dissolve from the inside out during the experiment. As a result, it was never possible to test many different flow rates during one experiment, and therefore, many unrepresentative results were obtained.

The HPLC analyses showed clear peaks for the ortho (2-nitrotoluene) and para (4-nitrotoluene) compound (comparison with calibration curves). These peaks were measured at retention times of 4.3 and 4.8 min. Another clear peak could be recognized at 6.5 min, which shows the unsubstituted toluene.

In some cases, the samples also contained many by-products or other substances, which can be attributed to impurities or reactions with the material of the calorimeter, as already described. However, the concentrations here were very low and were therefore neglected, as only the ortho and para variants and the measured toluene are relevant. If the concentration of the by-products was too high, the experiment was repeated.

Three different total flow rates were examined in the experiment, which can be seen in Table 3-7. The experiment was repeated until sufficient representative data was obtained for each total flow rate (number of representable experiments n is shown in Table 3-7). The data was then averaged and can be seen in Table 3-7.

The flow rates investigated are very low (0.50, 0.75, 1.00 mL min⁻¹) compared to other reactions investigated, as otherwise the reaction would not have provided clear results. This is noticeable when looking at the toluene conversion. As the total flow rate increases, it decreases, which means that no complete reaction can take place during the experiment at very high flow rates.

The reaction enthalpy released also decreases as the total flow rate increases, which confirms this once again. Furthermore, the standard deviation of the individual flow rates is relatively high, which can be attributed to the aggressive behavior of the reaction, possible impurities, inaccuracies in the preparation of the samples or possible inaccuracies in the HPLC measurement.

The individual reaction enthalpies of each total flow rate were averaged again to obtain an overall value of $-123.45 \pm 24.34 \text{ kJ mol}^{-1}$. This represents a deviation from the literature value of 1.7%.

Table 3-7: Nitration reaction of toluene with nitric acid and sulfuric acid at different flow rates and amount of experiments (n). Measured toluene conversion using HPLC analysis and reaction enthalpy with calculated deviation from literature [2], [3], [11], [38].

Flow rate [mL min ⁻¹]	n [-]	Mean toluene conversion [%]	Mean + SD ΔH_R [kJ mol ⁻¹]	Mean deviation from literature [%]
0.50	4	30.84	-132.49 ± 20.41	5.55
0.75	2	19.27	-130.18 ± 8.29	3.71
1.00	3	15.20	-106.93 ± 33.06	14.9

3.7 Nitrosylation reaction

Nitrosylation is another highly corrosive reaction, which is why it was carried out in the ceramic calorimeter (C3E). The exact description and execution of the experiment can be found in Chapter 2.4.6 and Chapter 5.10.

The reactants are tert-butyl nitrite, hydrochloric acid and acetone. After the reactor plate, an ammonia solution was used for quenching.

In the experiment, a sample was taken every 3 min after the first 5 min. The samples were then diluted so that they could be analyzed using HPLC (Chapter 5.4.2).

The evaluation of the HPLC analysis shows two large peaks. One is the product pyruvic aldehyde 1-oxime and the other is the limiting product tert-butyl nitrite (comparison with calibration curves). These became visible after a retention time of 0.54 and 0.73 min. A few by-products were also detected, but the concentrations were so low that they could be neglected.

As already described, nitrosylation is a very aggressive reaction, which meant that many experiments either had to be aborted due to leaks in the calorimeter or did not produce representative results. Only the realistic values were used for the evaluation. The aim here was to show a possible trend.

Table 3-8 clearly shows that the yield increases rapidly as the temperature rises. This trend can also be clearly seen with only one representative result in some cases. It can be assumed that with a larger number of values, the accuracy of these could be increased, but the trend in yield should be the same.

Additionally, it can be assumed that an even higher yield could be achieved at even higher temperatures. However, attention must be paid to the maximum temperature of the chemicals, as these could cause difficulties at excessively high temperatures.

If the mean value is formed from the various reaction contents over the different temperatures, the average is $-325.71 \pm 15.97 \text{ kJ mol}^{-1}$.

At very low temperatures and correspondingly low yields, small deviations due to measurement inaccuracies, impurities or the quench have a very large effect on the overall results of the reaction. Relatively speaking, the effects on the results are smaller at higher yields than at lower yields. Accordingly, the question arises as to how representative the results of the reaction enthalpy are at yields below 20%.

Based on this, the mean value of the reaction enthalpies for the two experiments with a yield above 20% was calculated for comparison, which was established to be $-317.04 \pm 11.11 \text{ kJ mol}^{-1}$.

Table 3-8: Nitrosylation reaction results at different temperatures, the reaction yield and the reaction enthalpy.

Temperature [°C]	Number of experiments [-]	Mean reaction yield [%]	Mean ΔH_R [kJ mol ⁻¹]
10	3	7.49	-308.77
18	1	10.36	-341.28
25	1	13.09	-344.40
40	4	23.84	-328.15
50	1	43.25	-305.93

To better illustrate the results of the individual temperatures, these are shown in comparison to the calculated mean value of the reaction enthalpies of the reactions with a yield above 20% in Figure 3-15.

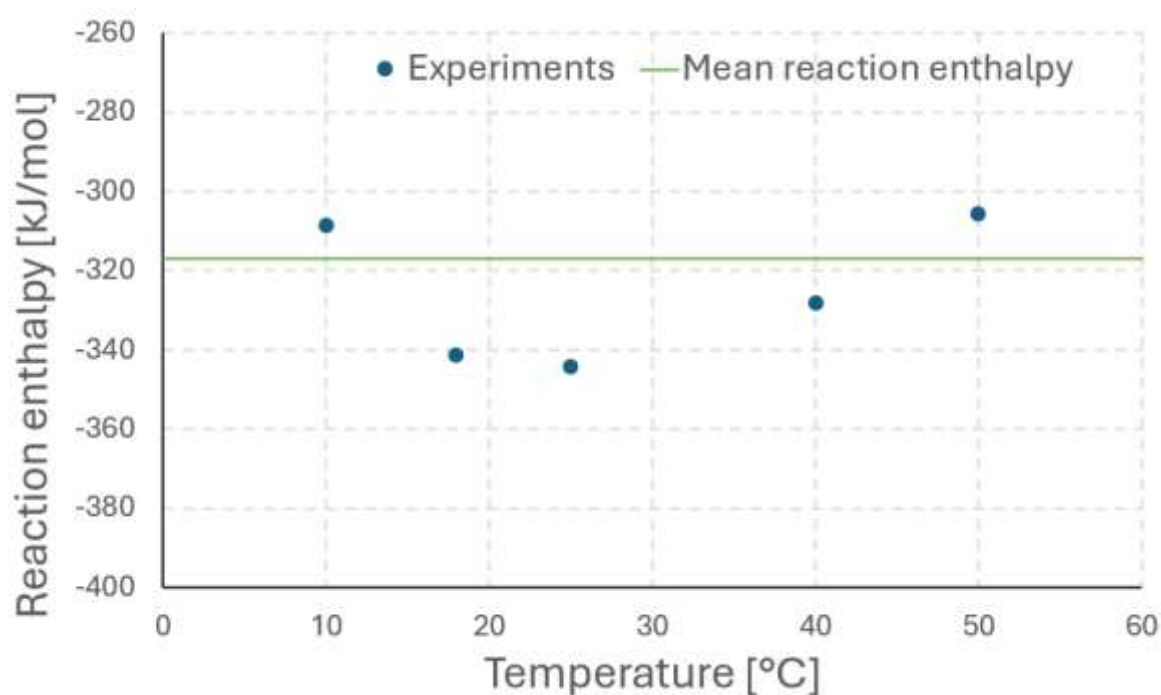


Figure 3-15: Nitrosylation of *tert*-butyl nitrite with hydrochloric acid and acetone: results visualized in a graph compared to the mean reaction enthalpy of the reactions having a yield above 20%.

Figure 3-15 shows that there is no particular trend with increasing temperature, but it is questionable how accurate these individual points are due to the number of valid experiments.

Figure 3-16 below shows a section of an experiment in a ceramic reactor plate at 10°C. The measured volts over time are shown in the respective segments of the reactor plate.

Shown is an experiment that starts at the time stamp of 13700 s. The experiment was stopped at 14500 s and only pure acetone was pumped. This was continued until the straight lines leveled off and became constant. At the time stamp of 14900 s, the pumps were switched off and it was waited until the baseline stabilized. The measurements were ended at the time stamp of 15300 s.

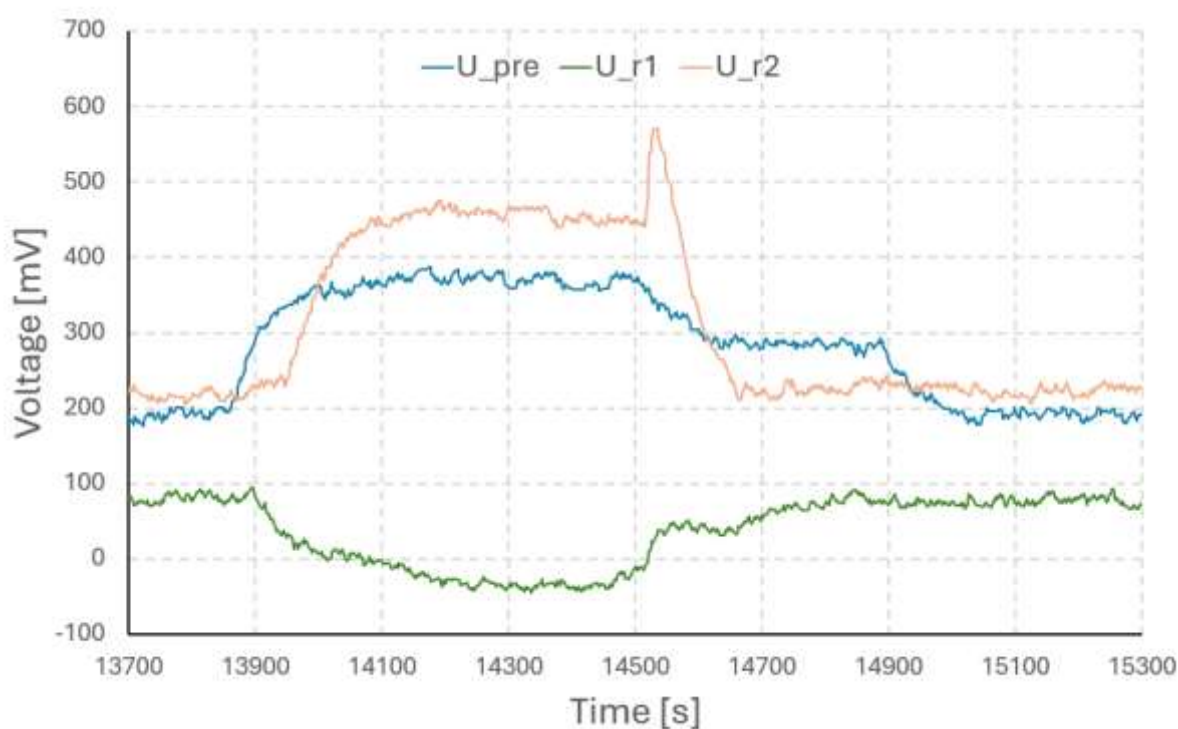


Figure 3-16: Nitrosylation of *tert*-butyl nitrite with hydrochloric acid and acetone: Example of signal curve from Peltier elements at 10°C in a ceramic calorimeter with 3 segments (C3E).

Looking at the individual curves in Figure 3-16, U_pre (blue line) is the perceived signal in the preheating segment (pre). In this segment, there is not yet any mixing and therefore no possible reaction. This segment only serves to bring the flows to the desired temperature (in this case 10°C). The graph shows a small increase in the measured amount of volts. This is due to the fact that the volume flow enters the

reactor plate at room temperature and must then be cooled down to 10°C. After no reactants, but only more acetone is pumped through the reactor plate, the curve drops slightly, but still does not go directly back to the base line. This shows that the inflowing acetone still needs to be cooled, but not as much energy is required for this as with the reactants.

Furthermore, it can be seen that the reaction in the first reaction segment (r_1 , shown via U_{r1} (green line)) is endothermic. This can be concluded from the fact that the detected signal decreases, which in return means that the reactor plate must be heated. This can also be seen in the comparison of the same signal between the steady-state condition during the reaction (14200-14500 s) and the base-line (15100-15250 s). After the reaction has ended and only pure acetone is pumped, the curve quickly stabilizes back to the base line, regardless of whether acetone is still being pumped or not, as no more reaction takes place, and the acetone already has the desired temperature due to the preheating element.

When looking at the measured signal in the second reaction segment (r_2 , shown by U_{r2} (pink line)), it is noticeable that the curve rises late, which is due to the fact that the reaction has not yet reached this segment. It reaches a steady state very quickly and shows that the exothermic reaction is taking place in this segment, hence the necessity of cooling. After no more reaction takes place, the curve quickly settles on the base line and stabilizes there, regardless of whether acetone is still being pumped or not, as no more reaction takes place and therefore no cooling/heating is required.

Figure 3-17 shows the exact same experiment but carried out at 40°C.

In this experiment, the measurement was started at the time stamp 8700 s. The change from substrates to pure acetone took place at 10700 s, until finally at 11600 s the pumps were switched off and the measurements ended.

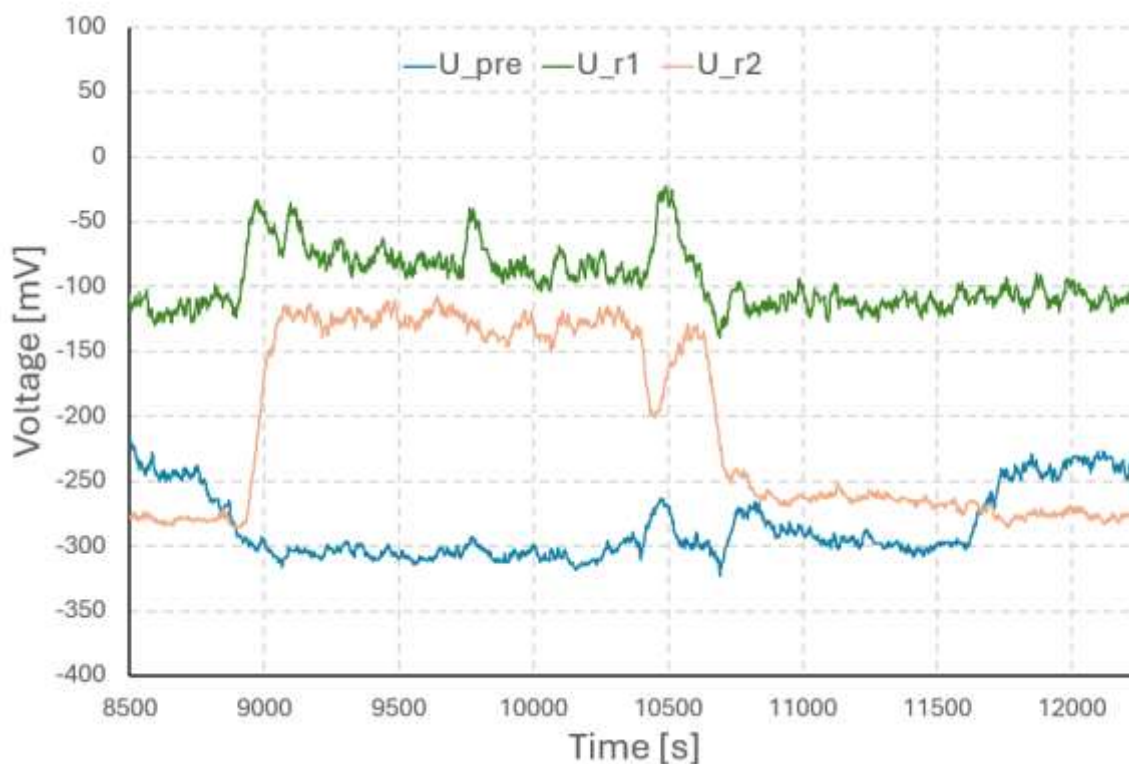


Figure 3-17: Nitrosylation of *tert*-butyl nitrite with hydrochloric acid and acetone: Example of signal curve from Peltier elements at 40°C in a ceramic calorimeter with 3 segments (C3E).

The results depicted in Figure 3-17 clearly show that no endothermic reaction can be seen. When looking at the two reaction segments (r_1 , r_2), it is noticeable that both rise upwards and therefore reflect an exothermic reaction, as the reactor plate has to be cooled down. It can also be seen that the curve of the first reaction segment (U_{r1} (green line)) is higher than that of the second one (U_{r2} (pink line)), which was not the case at the lower temperature. This suggests that a large part of the reaction has already happened in r_1 .

In summary, it can be said that the mixing process of the two reactants exhibits endothermic mixing behavior at low temperatures, while this is no longer detectable at higher temperatures. In addition, it can be seen that the reaction takes place earlier with increasing temperature, i.e. it proceeds faster. However, the endothermic mixing behavior at low temperatures has no significant difference for the overall process enthalpy.

4 Conclusion and outlook

The aim of this work was to validate an existing continuous flow calorimeter, developed within the group, with different microreactor plates and, in the best case, to optimize it. To this end, a wide variety of experiments were carried out in order to cover as many different reaction characteristics as possible.

In the experimental part of this work, the 6 different reactor plates were first examined for their properties with regard to mixing behavior. For this purpose, a residence time distribution (RTD) analyses and a characterization using the Bourne reaction approach were carried out.

The RTD is used to investigate the residence time within the reactor. This is relevant for various other experiments and also for various cleaning processes. Furthermore, a possible backmixing and the flow regime can be determined by calculating the Bodenstein number and the Reynolds number. The experiments showed that each of the microreactor plates exhibits laminar behavior and operates under extreme backmixing. This became clear as the Bodenstein number was below 10 for all reactor plates and the Reynolds number was $10.48 < Re < 213.06$. The residence time was generally unrealistically high for all reactor plates (for example, the ceramic reactor plate with 2 reaction segments had a residence time of 277.01 s in comparison to 65.08 s theoretical residence time). This is because the SyrDos™ pump [32] used may have been the wrong pump due to its pulsating pumping method, or the pumps may not have been calibrated accurately enough in advance to counteract incorrect pulsing. Furthermore, the internal geometry may not correspond to the intended one due to a manufacturing error or wear, or there are various “dead zones” in the system that would have to be excluded from the calculation. Another possibility for the difference in the measured and the calculated residence time could be the analysis method using a UV-Vis cell [31] with AVASOFT, as this shows many inaccuracies in handling and evaluation.

Future experiments could investigate whether other volumes need to be subtracted in the experimental setup, whether the SyrDos™ pump [32] needs to be calibrated differently, or whether the syringe pumps would be more suitable for this experiment, or whether the analysis method could be improved.

By carrying out the Bourne reaction [4], the mixing behavior within the reactor plates was investigated even better. The reaction allows a statement to be made about how well two liquids can be mixed using the reactor plate. In the experiments, all five reactor plates were again examined and additionally compared with an AP04 (uses split-and-recombine principle for mixing and has an inner diameter of 0.6 mm [10]) and an ordinary T-piece in the mixing performance. The result was that mixing is generally better with a higher flow rate. When comparing the individual reactors, it could be seen that M3E achieved better mixing than the other reactor plates made of metal or ceramic. A yield of S of less than 0.15 was detected with a flow rate of 3 ml/min. In comparison, the other reactor plates have a significantly higher yield of the product S, indicating a worse mixing behaviour. This means that the best mixing occurs with M3E. The experiments also showed that the length of the reactor makes no significant difference in the case of the Bourne reactions, as the reaction is largely completed at the end of r2 within the reactor plate. The reactor plates with a larger diameter and the ceramic reactor plate also exhibits poorer mixing. The smoother ceramic surface appears to produce less mixing than the rougher surface of the stainless steel.

In order to investigate the function of the calorimeter for very low enthalpy values, the enthalpy of mixing two solvents was examined. On the one hand, methanol and water were mixed, as this system has already been investigated several times in the past and there are therefore many literature values for comparison. On the other hand, the mixtures of Triethylene glycol (TEG) and water as well as Triethylene glycol (TEG) and 1-propanol were examined. After testing the appropriate flow rate to obtain representative results, the flow rate for the reaction was set at 6 mL min⁻¹ and the temperature to 25°C since the literature values were also measured at 25°C. Comparing these results only small deviation and a good comparability between the results of the experiments and the literature values can be seen. As the mixing enthalpy values are very close to each other, precise work, exact measurements and analyses are particularly important in this experiment. The difference between

$x_{\text{water}} = 0.600$ and $x_{\text{water}} = 0.692$ is only 8.8 J mol^{-1} . When looking at the results of mixing TEG and water, it is noticeable that more mixing enthalpy is released at higher temperatures. The viscosity of TEG could have a huge influence on the results. TEG was warmed up to the temperature of the experiment before the tests and at lower temperatures the deviation of the actual flow rate from the desired flow rate may be greater. This is clearly visible at low compositions, while the enthalpies of the mixtures become more similar as the proportion of water increases. When examining TEG and 1-propanol, it is noticeable that the reaction at 25°C gives significantly more constant values for the enthalpy of mixing depending on the composition. At higher temperatures, however, the mixture of TEG and 1-propanol behaves similarly to TEG and water.

Neutralization experiments were also carried out as part of this work. Here, 1 M of sodium hydroxide (NaOH) is used as the base and 1 M acetic acid as the acid. The experiment was carried out once in the C3E and once in the M6E for seven different flow rates ($1.0, 1.5, 2.0, 2.5, 4.0, 5.0, 6.0 \text{ mL min}^{-1}$). During the experiments with the C3E, the ambient temperature fluctuated greatly, which meant that many additional calibrations had to be carried out to make the data meaningful. Nevertheless, it can be assumed that the data therefore have a very high standard deviation (up to 7.47 kJ mol^{-1}). However, if the results are compared with the literature value of $-57.4 \text{ kJ mol}^{-1}$ [23] there is a maximum deviation of up to 3.33%. The only exception are the experiments at a flow rate of 2.0 mL min^{-1} where the deviation from the literature value stands out at 8.77%. However, it must be questioned whether this value would not be even closer to the literature value if the experiment were repeated more often. In future experiments, however, care should be taken to keep the ambient temperature as constant as possible, as this has a very large influence on the results. Furthermore, neutralization in M6E was tested at 25°C and at 30°C . It can be seen that the results below 2 mL min^{-1} are not representative values. However, from a higher flow rate onwards, the results come closer and closer to the literature value. At a temperature of 25°C , which corresponds approximately to room temperature, the values are not constant, whereas at 30°C the values become constant and at 10 mL min^{-1} only deviate 5% from the literature value.

Nitration reactions of toluene with HNO_3 and H_2SO_4 were tested in this work in order to test highly aggressive reactions and then compare them with the literature value $125.52 \pm 2.56 \text{ kJ mol}^{-1}$. [2], [11], [3], [38]. $\text{HNO}_3\text{:H}_2\text{SO}_4$ and toluene were tested in a volumetric ratio of 1:4 in C3E at 30°C and then quenched with NaOH. The samples were analyzed by HPLC, and peaks were seen with retention times of 4.3 min (ortho structure), 4.8 min (para structure) and 6.5 min (unsubstituted toluene). Due to the very aggressive reaction, many experiments had to be carried out to obtain representative results. The flow rates 0.50 , 0.75 , 1.00 mL min^{-1} were tested and then the average was calculated as $-123.45 \pm 24.34 \text{ kJ mol}^{-1}$. This represents a deviation from the literature value of 1.7%.

In order to test another highly aggressive reaction, nitrosylation reactions were tested in C3E at different temperatures (10 , 18 , 25 , 40 , 50°C). Tert-butyl nitrite, acetone and hydrochloric acid were used to perform the reaction and an ammonia solution was used for quenching. The samples were taken every 3 min after initial 5 min and analyzed using HPLC. Peaks were seen with retention times of 0.54 min (pyruvic aldehyde 1-oxime; product) and 0.73 min (tert-butyl nitrite). The different results were averaged to $-325.71 \pm 15.97 \text{ kJ mol}^{-1}$. The yield also rises sharply with increasing temperature. When considering only the yields above 20% (40 and 50°C), the average value for the reaction enthalpy is $-317.04 \pm 11.11 \text{ kJ mol}^{-1}$. When comparing the experimental results with the average value of the experiments with a yield above 20%, only slight deviations can be observed, which could be further minimized with a higher number of experiments. It is also noticeable that endothermic mixing occurs in the first reaction segment (r_1), particularly at low temperatures. When comparing with higher temperatures, this is no longer the case. Here the influence on the measurement of enthalpy is smaller. In future experiments, the endothermic behavior when mixing the reactants could be investigated in more detail.

5 Experimental

5.1 Reactor plates

As described in the previous chapters, different designs of the calorimeter were used. Which reactor plate was used in which experiment can be read in the corresponding chapter.

The various reactor plates were manufactured either from ceramic or stainless steel using 3D printing (SLM or SLA). The different parameters of the reactor plates can be seen in the table below (Table 5-1). The calculated overall volumes can be seen in Table 9-5 in the appendix (Chapter 9.3).

Table 5-1: Different used reactor plates and their characteristics.

Name	Material	number of segments [-]	Channel diameter [μm]	V per preheating element [μL]	V per mixing element [μL]
C3E	Ceramic	3	800	98	111
M3E	Stainless steel	3	800	98	111
M3Ebd	Stainless steel	3	1000	153	173
M3Ed	Stainless steel	3	800	98	170
M6E	Stainless steel	6	1000	153	170

5.2 Experimental set-up

5.2.1 Overall set-up

The set-up for the flow calorimeter varies slightly for each experiment, although the overall set-up does not, which can be seen in Figure 5-1 below.

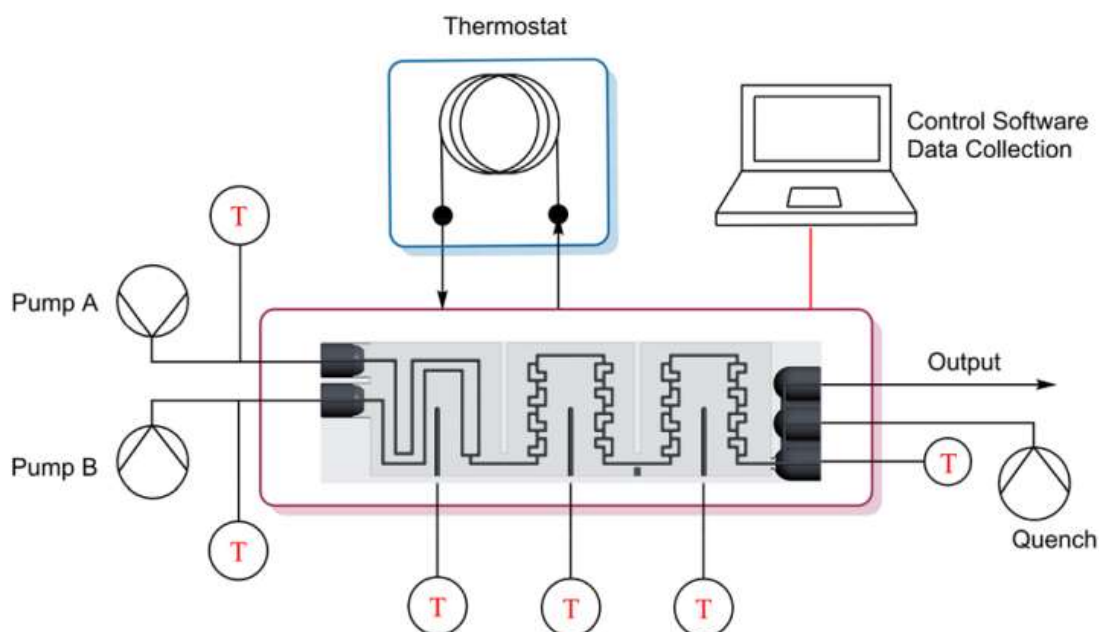


Figure 5-1: Overall experimental set-up of the calorimeter with two pumps, a thermostat [7], a computer for data collection, a quench possibility and 6 temperature sensors. [3]

As it can be seen in Figure 5-1, for demonstrational purpose a reactor plate with three segments is used. The different reactor plates with three segments are used in the small calorimeter, while the large calorimeter uses a reactor plate with six segments (M6E). Overall, the set-up of the large calorimeter is the same as for the small one.

The two reagents/chemicals are pumped through the reactor plate with the help of two pumps (pump A and pump B). As described in Chapter 2.2, the two liquids are preheated within the first reactor element (preheating element) and interact with each other in the following. After exiting the reactor plate, there is a possibility for a quench (if necessary). The sample is either taken at room temperature or in an ice bath, depending on the reaction's requirements. Afterwards the sample can be further analyzed.

5.3 Calibration of the calorimeter

The exact structure of the calorimeter is described in detail in Chapter 2.1. All designs have Seebeck elements, which are installed between Peltier elements and the reactor plate. The output is the voltage depending on the work of the Peltier elements to heat/cool the reactor plate to a set temperature. There is a proportionality between the temperature difference between the reactor plate and the Peltier element. Using this output, the heat flux can be calculated.

For this purpose, however, the dependence between the cooling capacity and the specified voltage must be established in advance by means of a calibration. To make this possible, heating foils are attached to the bottom of the reactor plate, which gradually increase the energy influx during a running calibration. Each heating foil covers its own segment in the reactor plate, which means that each segment could be calibrated individually. With the aid of the calibration, a correlation can be established in order to find out which energy flux correlates to which output voltage value of the Seebeck element in an experiment depending on the temperature.

The SOP for calibration can be found in the appendix (Chapter 9.4.1).

Due to the high accuracy of the sensors, imperfections in the regulation circuits and the used set-up, a repetition of the calibration with exactly the same settings results in a small deviation of the results.

The performed calibrations are listed in the appendix (Chapter 9.4.2). The figures below show an example of the calibration of a ceramic calorimeter with three elements (C3E) (Figure 5-2) and of a stainless steel reactor plate with six elements (M6E) (Figure 5-3) at 25°C each.

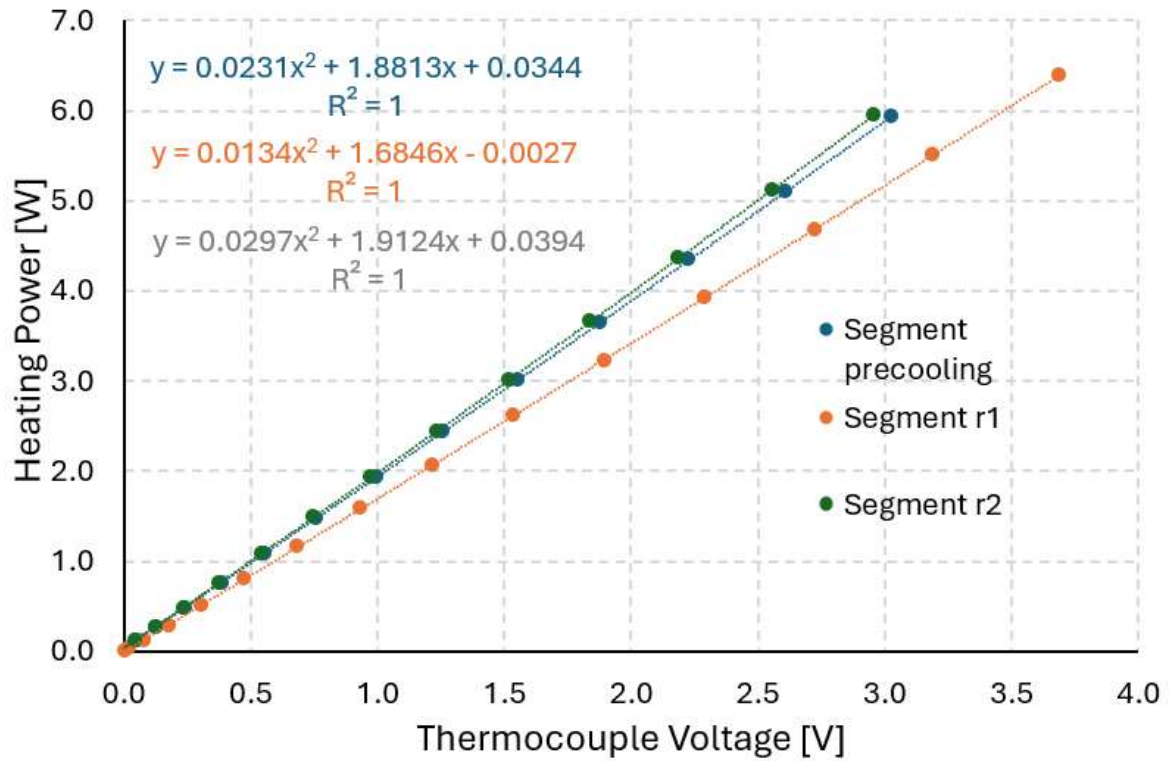


Figure 5-2: Calibration curve of ceramic calorimeter with three segments (C3E) at 25°C with a room temperature of 25°C and thermostat [7] set to 28°C.

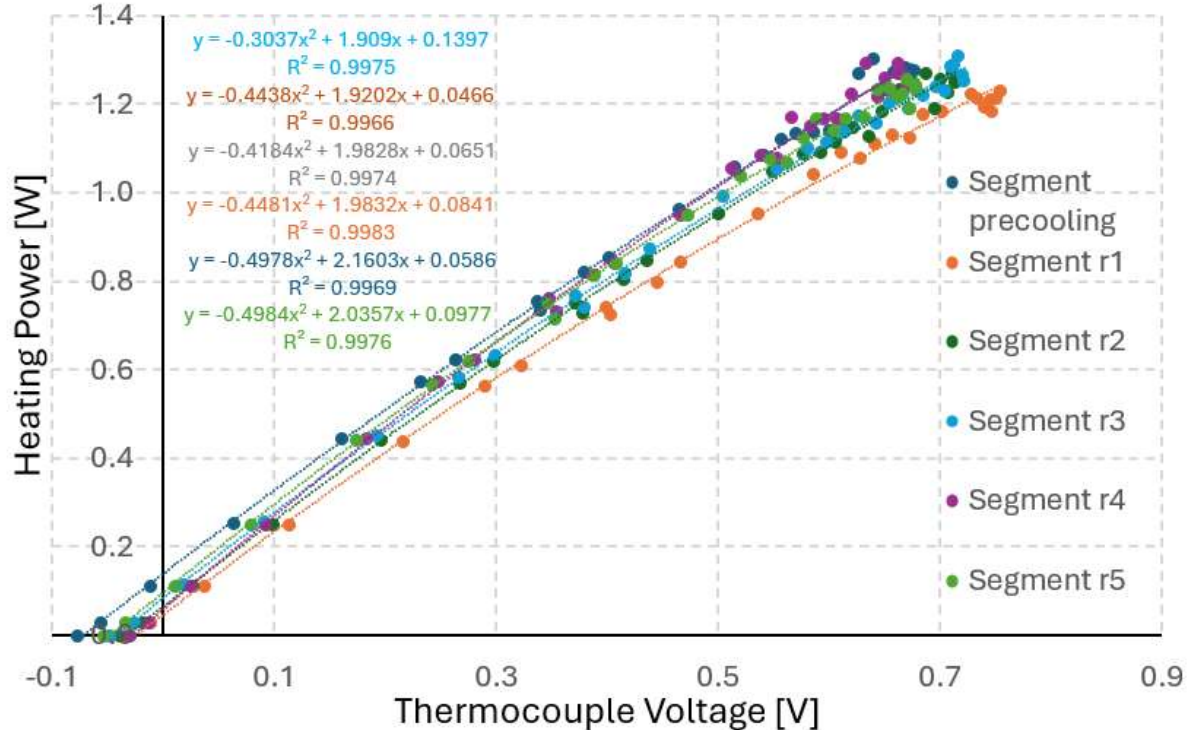


Figure 5-3: Calibration curve of stainless steel calorimeter with six segments (M6E) at 25°C with a room temperature of 25°C and thermostat [7] set to 28°C.

In the course of the experiments, it turned out that the ambient temperature had a very large influence on the results and already on the calibration. As a result, the calorimeter had to be recalibrated for higher room temperatures. To show the difference in calibration due to the ambient temperature, a calibration of a ceramic calorimeter with three segments (C3E) for 25°C at an ambient temperature of 28°C is also shown in Figure 5-4. It is notable that the curves are looking similar, but looking at the equations, there is a difference noticeable.

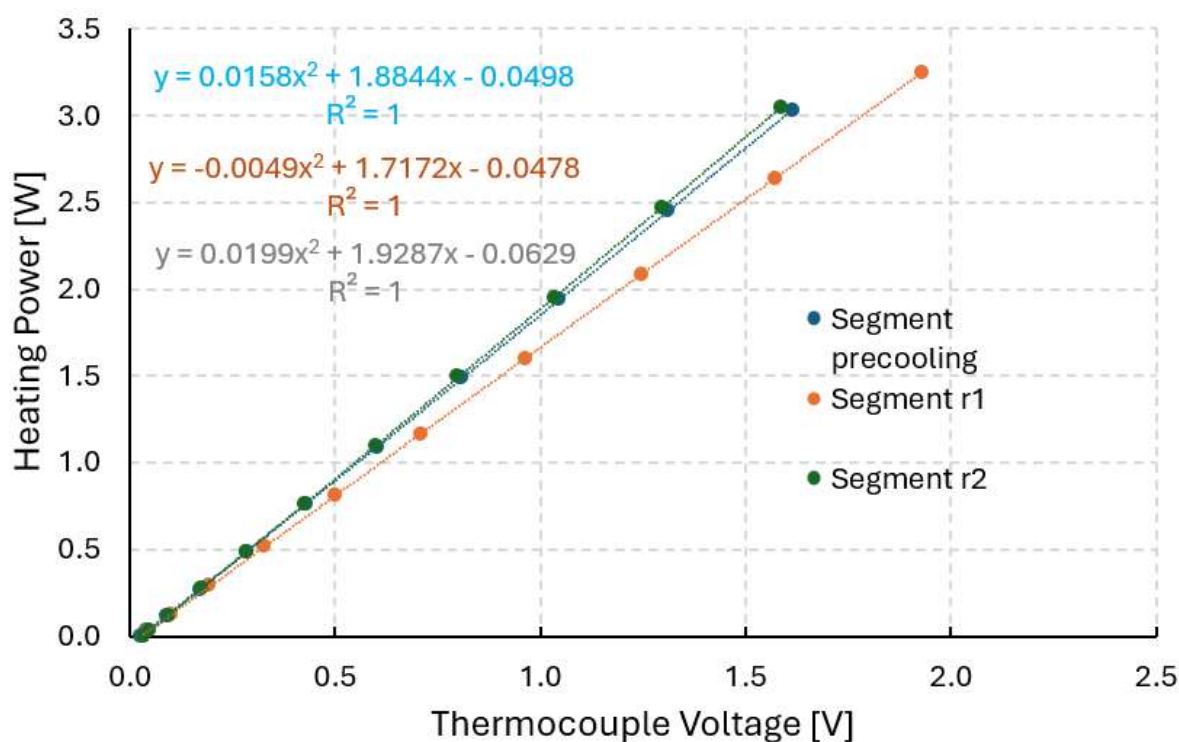


Figure 5-4: Calibration curve of ceramic calorimeter with three segments (C3E) at 25°C with a room temperature of 28°C and thermostat [7] set to 28°C.

5.4 Methods for analyses

In the course of this thesis, some experiments are analyzed using different methods. On the one hand UV-Vis spectroscopy and on the other hand HPLC analysis are used. The theory behind these two methods is described in more detail in this chapter.

5.4.1 UV-Vis spectroscopy

For UV-Vis spectroscopy, a spectrophotometer is used, which measures the absorption of light that has been passed through a liquid. [39]

Some functional groups within the liquid absorb the light differently than others, which means that the quantity of these groups can be measured by measuring the absorption.

As the analysis method is based on light waves, the wavelength λ and the frequency ν are important. If you multiply these together, you get the speed of light.

The energy of electromagnetic radiation (light) can be calculated using the equation (5-1). The energy E is calculated using Planck's constant $h = 6.63 * 10^{-34}$, the frequency of the light ν , or the speed c_{light} and the wavelength of light λ .

$$E = h * \nu = \frac{h * c_{light}}{\lambda} \quad (5-1)$$

Molecules can be stimulated by an external stimulus to jump from a basic state to a higher molecular orbit. In the case of UV-Vis Spectroscopy, this stimulus is a beam of light and the resulting absorption of the radiation. Since, depending on the functional group, different amounts of energy are needed to reach this excited state of the molecules, the functional group can be better analyzed by analyzing this state. [10], [40]

The peaks detected in the absorbance can be used to identify the composition and concentration of a sample. [39], [40]

However, one of the greatest weaknesses of UV-Vis spectroscopy in the application of micro processes is that the sensitivity has a high influence on the evaluation of results due to the lower volume. Here, the optical path length can be strongly influenced by the liquid. This is further described with the Lambert-Beer law. [39], [41]

However, the Labert-Beer law must be valid, which is given by the following conditions [10], [42]:

- There is a homogeneous distribution of the molecules.
- There is no light scattering or photochemical reaction in the sample.
- There is no light from the light beam outside of the sample.
- There is only independent absorption of the substances.
- There is only absorption below 1.

In order to be able to carry out a measurement in the UV-Vis range, valence electrons must be present that already reach an excited state at low excitation energy. These are present in many organic and inorganic components, which means that they can also be examined with UV (190 - 390 nm) or VIS (390 - 770 nm). [10], [40], [41]

The Lambert-Beer law is used to calculate the concentration using the values of the absorption A , which is shown in the following equation (5-2).

$$A = \log \frac{I_0}{I} = \varepsilon * c * l \quad (5-2)$$

Using the equation (5-2), the dimensionless absorbance A can be calculated using the molar extinction factor ε , the concentration of the absorbed medium c , the original intensity of the light beam I_0 , the intensity of the light beam after passing the medium I and the path length l . [10]

To calculate a local absorption A_{tot} , the sum can be used, as can be seen in the equation (5-3) below.

$$A_{tot} = \log \frac{I_0}{I} = \sum_{i=1}^n \varepsilon_i * c_i * l \quad (5-3)$$

This equation can be used to calculate any concentration of a solution if the extinction factor ε for the respective wavelength of the substance is known. The extinction factor can either be measured by analyzing the pure substance with known concentrations or by using literature values. [10]

In this thesis, for example, the Bourne reaction and the RTD was analyzed with a UV-Vis spectrometer and the extinction factor for Bourne reaction was taken from literature values [4]. These can be found in Chapter 9.6.5.

A UV-Vis flow cell (Flow Cell-Z-10, Avantes [31]) was used for the measurements in this thesis. The used UV light source was the AvaLight-DS-DUV [43] and the used detector was the AvaSpec-ULS2048 [44].

5.4.2 HPLC analysis

A high performance liquid chromatography (HPLC) analysis can be carried out to analyze samples from the experiments. The conversion of the substrate can also be determined here.

Within the scope of this project the HPLC system 1100 from Agilent Technologies [45] is used with a UV-Vis diode array detector, an online degasser, an autosampler, a quaternary pump and a column compartment. The used column for the organic components is a reversed phase column (Thermo Scientific Accucore^{THC} 18,50 mm x 4.6 mm; 2.6 μm particle size) [46]. The used column for the pyridines is the Thermo Scientific Hypersil BDS Cyano Column (250 mm x 4 mm; 5 μm particle size) [47]. The samples were analyzed at 25°C with a flow rate of the mobile phase of 1 mL min⁻¹ for 15 min. The analyses were carried out at 222 nm.

In this thesis, a mixture of methanol and aqueous phosphoric acid was used as the mobile phase. This mixture is prepared with a volumetric ratio of 6:4 (MeOH:aqueous phase). The aqueous phosphoric acid is prepared in advance in a volumetric ratio of 300:1 (water to phosphoric acid). This mixture is later used for various sample dilutions.

To enable HPLC analysis, the samples had to be diluted. In case of this thesis, this often requires dilution by a factor of 200. The sample is diluted using the mobile phase of the HPLC analysis. For this purpose, 100 μL of the sample is diluted with 900 μL of the dilution solution and in a second step, 50 μL of the already diluted sample is diluted again with 950 μL .

In order to be able to access the possible products to the respective peaks during the evaluation, a calibration curve was created for each of these in advance. These calibration curves were used from the preliminary work [2], [3], as they were performed in the same laboratory.

5.5 Residence time distribution (RTD)

The residence time distribution is an effective experiment to determine the needed time for the liquid to go through the reactor plate. The set-up of the experiment differs a little bit from the overall set-up (Figure 5-1), as it can be seen in Figure 5-5.

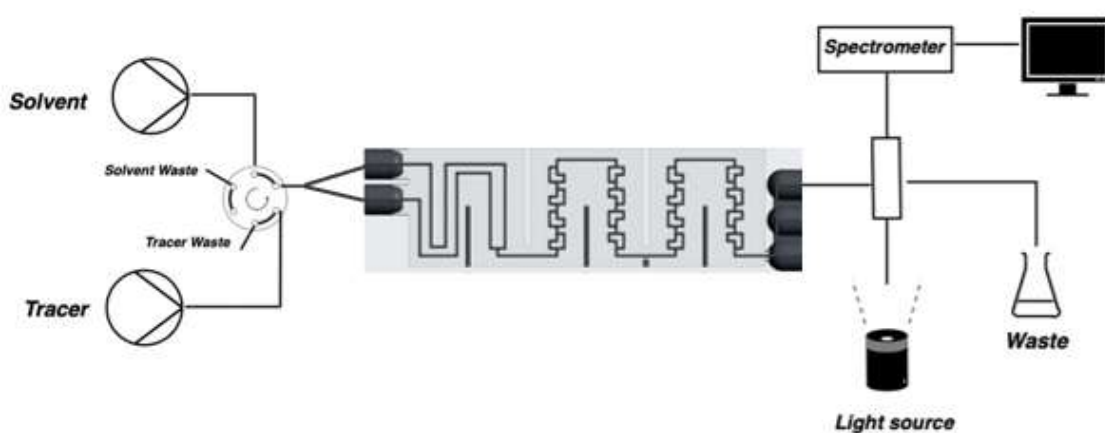


Figure 5-5: Schematic experimental set-up residence time distribution (RTD) using a 6-port valve and a UV-Vis cell [31].

Two Lambda syringe pumps [33] with stainless steel syringes [48] were used, one filled with solvent and the other one filled with tracer. In between the pumps and the reactor plate, there is a 6-port injection valve [49]. After the reactor plate, there is a UV-Vis cell (spectrometer) [31] instead of the quench.

Figure 5-6 shows the schematic set-up of a 6-port valve. It can be seen how the connections must be routed in order to be able to create a step function.

Step input

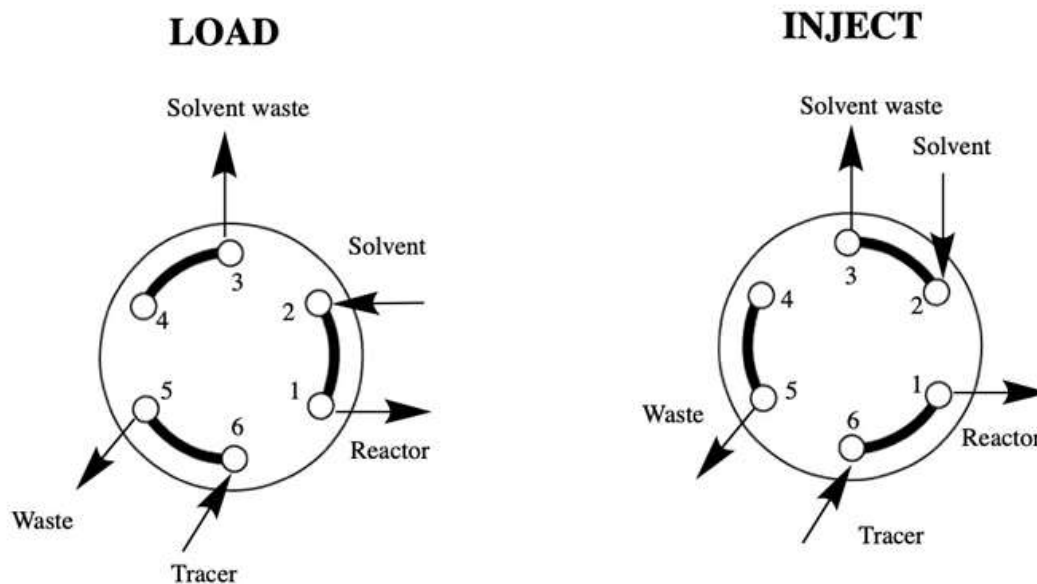


Figure 5-6: Graphical representation of the capillary connections of a 6-port valve used at RTD experiments. [10]

The solvent is a mixture of 12wt% ethanol in water. For the tracer, 0.008v% Anisole was mixed with the solvent. The solvent is pumped through the whole set-up, until the signal of the UV-Vis cell is considered constant. The signal is measured with AVASOFT.

In order to achieve the most accurate measurement possible, a baseline correction must be carried out. For this purpose, the absorbance is measured at a wavelength at which anisole does not interfere with the measurement, therefore is not absorbed (500 nm-506 nm). The measurement was done at 268 nm-276 nm.

First, the 6-port valve is switched to only pump tracer free solvent until the base line is stabilized and corrected. Afterwards, the 6-port valve is switched in order to pump the tracer. The exact time of the switch is important for later calculations. The experiment is carried out, until the signal detected in the UV-Vis cell appears to be stable.

More detailed instructions (SOP) for the settings of AVASOFT and the measurements can be found in the appendix (Chapter 9.5.1).

5.6 Bourne reaction

In order to investigate the mixing behaviour in each reaction plate, the Bourne reaction is carried out. Therefor the buffer, reagent A (1.2 mM 1-naphthol solution in a carbonate/bicarbonate buffer (pH 9.9, ionic strength 888.8 mM)) and reagent B (1 mM solution of diazotised sulfanilic acid) have to be prepared in advance. The buffer can be prepared in stock, whereas the reagents have to be prepared newly every day.

The theory behind this reaction is further described in Chapter 2.4.2.

The general set-up of the experiment can be seen in Figure 5-7.

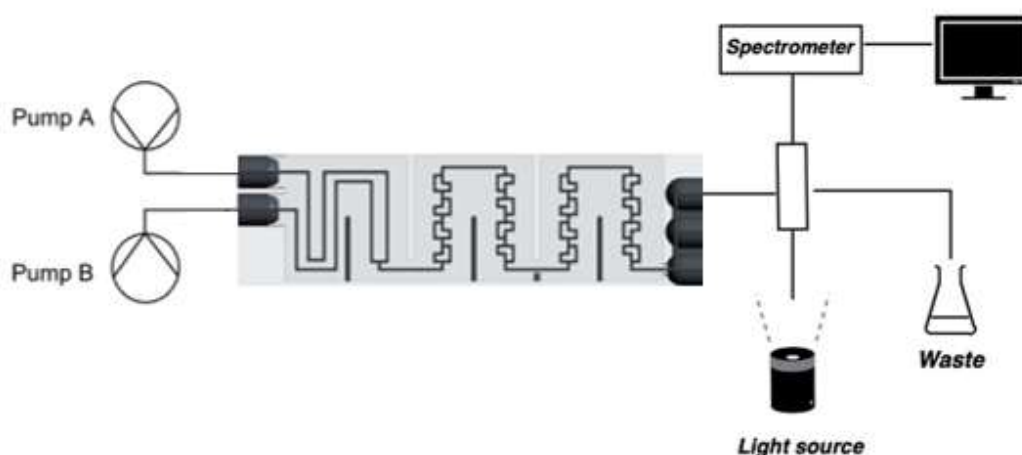


Figure 5-7: Schematic experimental set-up of Bourne reaction using a UV-Vis cell [31].

The five reactor plates investigated are listed in Table 5-1 (C3E, M3E, M3Ebd, M3Ed, M6E. In addition, a T-piece and an AP04 [10] with an internal diameter of 0.6 mm were tested.

This measurement is carried out at room temperature and doesn't have to be cooled, because there is no temperature change coming from the reaction. As a result, the various reactor plates are not always inserted into and removed from the calorimeter. For the experiment, the syringes [48] with the syringe pumps [33] are connected directly to the reactor plates using capillaries. It is important that the capillaries are non-transparent. For the experiments in this work, aluminium foil is wrapped around the capillaries and stainless steel syringes are used.

In order to guarantee steady state, the experiment was run for three residence times each time before collecting a 2 mL sample. The sample was covered in tin foil to ensure as little exposure to light as possible and was directly analyzed to ensure the least possible decomposition of the product. The analysis occurred within 10 minutes after sample taking.

All the chemicals and a complete checklist of the preparation can be seen in the appendix (Chapter 9.6.1 and Chapter 9.6.2) and are based on previously done work from Alessia Valotta [10].

5.6.1 Evaluation of Bourne reaction

The analyses of the samples took place via UV-Vis measurements. The concentration of the product received after the reaction is too high to be analyzed with the Avantes flow cell, therefore, to ensure measurability, the product has to be diluted with buffer first. For the dilution 0.7 mL of the product solution was diluted with 5 mL buffer (pH 9.9, ionic strength 444.4 mM). The step by step instructions for the measurement can be seen in the appendix (Chapter 9.6.3). General settings in the AVASOFT software were: "Integration Time" was set to 1.05 ms, "Averaging" was set to 100, exported wavelengths were between 390 nm and 700 nm with intervals of 10 nm and saved in ASCII files. To flush the cell and take light and dark references, the buffer used for the dilution of the product was used.

The total absorption of the samples was measured and therefore the concentration of each dye can be calculated using the following equation (5-4) given for the total absorption A , if the Lambert-Beer law is valid (Absorption in the range between 0.1 and 1) [4]:

$$A = \varepsilon_{pR} * c_{pR} * l + \varepsilon_{oR} * c_{oR} * l + \varepsilon_S * c_S * l \quad (5-4)$$

Here, ε is the molar extinction coefficient of a dye at a specific wavelength, c is the dye concentration and l is the optical path length. The extinction coefficients of all components for each measured wavelength are known [4] and can be seen in Chapter 9.6.5. Therefore, with the help of a standard-multi-parameter-regression with least square fitting method, each concentration can be calculated using a MATLAB code which can be seen in the appendix (Chapter 9.6.4).

5.7 Solvent mixtures

The calorimeter can be used to measure a change in temperature during the mixing of two solvents. Therefore, three different solvent systems were investigated as part of this thesis. On the one hand methanol-water, on the other hand TEG-water and TEG-1propanol.

The set-up can be seen in Figure 5-1 just without the quench. For the measurements the ceramic reactor plate with three segments (C3E) was used.

5.7.1 Methanol-water

The mixing behavior between methanol and water was investigated, as this has already been extensively studied in various other literature [34], [35], [36] and therefore various literature values exist for comparison. This allows the accuracy of the calorimeter to be determined and the validity to be confirmed. Because of the very low enthalpy values when investigating the solvent system methanol and water, precise and accurate measurements are very important.

Before the experiments can be carried out with different compositions, the impact of the flow rate on the results were investigated. For this purpose, methanol and water were pumped into the calorimeter using syringe pumps in a volumetric ratio methanol: water of 1:1 (molar ratio = 0.3). Different flow rates were measured, and two different temperatures (18°C and 25°C) were also investigated. At 18°C the flow rates 2, 4, 5 and 6 mL min⁻¹ were measured and at 25°C the flow rates 4, 5, 6 and 7 mL min⁻¹ were analyzed.

In the existing literature, the mixing enthalpy was measured at 25°C for different compositions. In order to be able to compare the values as accurately as possible, the following experiments in this work are also carried out at 25°C.

In the following experiments, various compositions of methanol and water were tested with a total flow rate of 6 mL min⁻¹ in order to identify a trend and subsequently compare these with literature values. 6 mL min⁻¹ was chosen as the flow rate, as this has produced the most representative and accurate results in previous experiments, which can be found in Chapter 3.4.

5.7.2 Triethylene glycol (TEG)-water and Triethylene glycol (TEG)-1-propanol

Once the accuracy of the chromatograph has been established, the mixing enthalpy of TEG-water and TEG-1-propanol has not yet been researched very often. The two mixing experiments (TEG-water and TEG-1-propanol) are exactly the same in set-up and procedure, with the only exception that one of the liquids is different (water or 1-propanol).

Triethylene glycol (TEG) was analyzed at different temperatures. Different compositions were tested at three different temperatures (25°C, 40°C and 55°C). In the experiment, the water or 1-propanol was pumped using a syringe pump [33], while the TEG was pumped using a SyrDos™ pump [32] in order to counteract the high pressure due to the high viscosity of TEG. In addition to the stronger pump, the high viscosity was also counteracted by preheating. In the experiments, TEG was preheated to the respective temperature in advance.

Due to the high viscosity, there were some difficulties with the flow rate, so they were not always the same, but they were always between 1 and 2 mL min⁻¹.

5.8 Neutralization reaction

The basic standard set-up (Figure 5-1) without a quench is used for the neutralization reaction and the ceramic reactor plate is tested. The resulting enthalpy is measured during a neutralization reaction. This is measured because this reaction has already been measured many times and many reference values are available in the literature. This allows the calorimeter to be validated. The theory behind the reaction is described in more detail in Chapter 2.4.4. In the reaction, 1 M of sodium hydroxide (NaOH) is used as the base and 1 M acetic acid as the acid. For the experiment, the base and the acid are pumped through the reactor plate at different speeds and ratios with two syringe pumps [33]. Overall, seven different total flow rates were investigated multiple times each at 18°C and the mean value and the standard deviation were calculated in order to be able to compare them to literature values.

5.9 Nitration reaction

Nitration was carried out as a further validation of the calorimeter and highly aggressive chemicals. The experiment was based on a previous thesis which was done on the same calorimeter. The results and conclusions were taken into account and necessary adjustments were made to the concentrations, flow rates and general conditions. [2]

In this thesis, only experiments with the mono-nitration of toluene are examined in more detail. Furthermore, concentrated nitric acid and the homogeneous catalyst sulfuric acid are used.

The experimental set-up is the original set-up which can be seen in Figure 5-1, even with the quench. The reaction equation can be found in Chapter 2.4.5. The reaction enthalpy is known from literature values. This should be $-125.52 \pm 2.56 \text{ kJ mol}^{-1}$. [2], [11], [3], [38]

The nitration was carried out in the ceramic calorimeter (C3E) at 30°C (thermostat temperature [7] is 33°C), as an experiment at 25°C does not provide representative results. At 25°C the influence of the room temperature is too high and therefore the following experiments were carried out at 30°C. A 1:1 v:v solution of $\text{HNO}_3\text{:H}_2\text{SO}_4$ is prepared in advance. The prepared solution and toluene are pumped through the calorimeter with syringe pumps with a volumetric flow rate of 1:4.

After the calorimeter, the liquid is quenched with a NaOH solution. This quench is added to the outgoing stream in a volumetric ratio of 4:1. The purpose of the quench is to prevent further conversion of toluene.

The experiments were carried out often and quickly due to the highly aggressive reaction. The reaction attacked the entire apparatus during the experiment. For example, even the fittings and syringes dissolved during the experiment.

Three different total flow rates were examined several times until several representative results were obtained. The different investigated total flow rates were 0.50, 0.75 and 1.00 mL min^{-1} .

Several samples were taken and prepared (diluted according to Chapter 5.4.2) for HPLC analyses. Due to varying results, the respective samples were analyzed several times in the HPLC.

5.10 Nitrosylation reaction

Nitrosylation was chosen as an experiment to test another very aggressive reaction.

The nitrosylation reaction in this work is based on the previously investigated experiments from Godineau et al. [30]. The corrosive properties (corrodes most metals and alloys) only permit an experiment in a ceramic calorimeter (C3E). The experimental set-up is the standard set-up with quench and an additional back pressure regulator (set to 3 bar) [50] as shown in Figure 5-8.

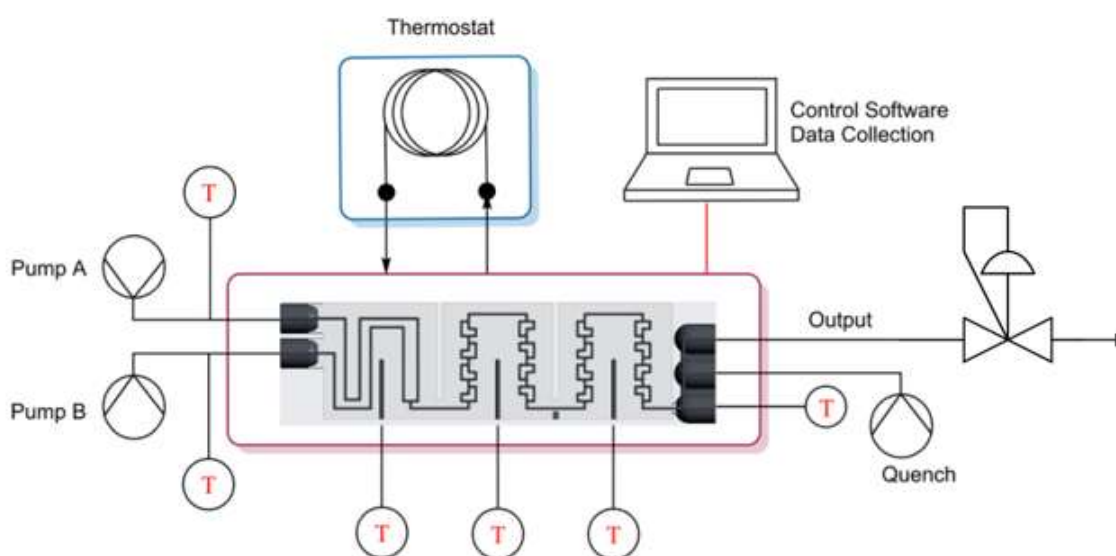


Figure 5-8: Schematic experimental set-up of nitrosylation reaction using a thermostat [7] and a back pressure regulator [50].

The flow rates from the literature [30] had to be adapted for the experiment in a microreactor. This is because in the literature cited a reactor with a reactor volume of 2.0 mL was used, while the ceramic reactor plate has a reactor volume of only 222 μL . Therefore, the overall flow rate is reduced from 2.96 mL min^{-1} by the factor 10.

In addition, the amount of hydrochloric acid (HCl) required is halved and each half is added to the other two reactants in advance, as the calorimeter is only designed to mix two liquids together and not three. After the liquid exits the reactor plate, it was quenched with an ammonia solution. The exact preparation of the substrates can be seen in Table 5-2.

The substrates were pumped through the reactor using syringe pumps [33] (substrate A and quench) and a SyrDos™ pump [32] (substrate B).

Table 5-2: Substrate and quench preparation for nitrosylation reaction.

	Chemicals	Amount [mL]
Substrate A	Tert-butyl nitrite	3.20
	Acetone	4.00
Substrate B	12 M Hydrochloric Acid	0.64
	Acetone	4.00
Quench	Ammonia	1.00
	Water	3.00

The experiment was carried out continuously at different temperatures (10, 18, 25, 40 and 50°C) for approximately 30 minutes at a time. The temperature of the thermostat [7] was set to 18, 21, 28, 45, 57°C. The duration of the experiment was set at this length in order to be able to observe possible changes during the course of the experiment.

After quenching, starting after 5 min, a sample is taken every 3 min, which is then analyzed in the HPLC (Chapter 5.4.2).

6 References

- [1] T. A. Frede, M. C. Maier, N. Kockmann, and H. Gruber-Woelfler, "Advances in Continuous Flow Calorimetry," *Org. Process Res. Dev.*, vol. 26, no. 2, pp. 267–277, 2022, doi: 10.1021/acs.oprd.1c00437.
- [2] B. Forster, "Continuous Reaction Calorimetry - Investigation of key steps of pharmaceutical syntheses," no. June, 2022.
- [3] S. Soritz *et al.*, "Thermokinetic analyses of metal-sensitive reactions in a ceramic flow calorimeter," *React. Chem. Eng.*, 2024, doi: 10.1039/d4re00014e.
- [4] J. R. Bourne, O. M. Kut, J. Lenzner, and H. Maire, "Kinetics of the Diazo Coupling between 1-Naphthol and Diazotized Sulfanilic Acid," *Ind. Eng. Chem. Res.*, vol. 29, no. 9, pp. 1761–1765, 1990, doi: 10.1021/ie00105a004.
- [5] M. C. Maier, M. Leitner, C. O. Kappe, and H. Gruber-Woelfler, "A modular 3D printed isothermal heat flow calorimeter for reaction calorimetry in continuous flow," *React. Chem. Eng.*, vol. 5, no. 8, pp. 1410–1420, 2020, doi: 10.1039/d0re00122h.
- [6] M. Leitner, "Development of a continuous flow reaction calorimeter for milli- and micro-fluidic applications," no. May, 2020.
- [7] T. Fisher and S. Isotemp, "Fisher Scientific Isothemp thermostat," pp. 1–6.
- [8] V. Hessel and H. Löwe, "Organische Synthese mit mikrostrukturierten Reaktoren," *Chemie-Ingenieur-Technik*, vol. 76, no. 5, pp. 535–554, 2004, doi: 10.1002/cite.200406165.
- [9] Octave Levenspiel, *Chemical reaction engineering*, vol. 35, no. 9. 1980.
- [10] V. Alessia, "Design of 3D printed microreactors for Continuous Flow Synthesis," no. August, pp. 79–107, 2019.
- [11] R. Halder, A. Lawal, and R. Damavarapu, "Nitration of toluene in a microreactor," *Catal. Today*, vol. 125, no. 1–2, pp. 74–80, 2007, doi: 10.1016/j.cattod.2007.04.002.
- [12] M. B. Plutschack, B. Pieber, K. Gilmore, and P. H. Seeberger, "The Hitchhiker's Guide to Flow Chemistry â€", *Chem. Rev.*, vol. 117, no. 18, pp. 11796–11893, 2017, doi: 10.1021/acs.chemrev.7b00183.
- [13] C. Y. Yap *et al.*, "Review of selective laser melting: Materials and applications," *Appl. Phys. Rev.*, vol. 2, no. 4, 2015, doi: 10.1063/1.4935926.
- [14] T. G. Spears and S. A. Gold, "In-process sensing in selective laser melting (SLM) additive manufacturing," *Integr. Mater. Manuf. Innov.*, vol. 5, no. 1, pp. 16–40, 2016, doi: 10.1186/s40192-016-0045-4.

-
- [15] J. P. Kruth, G. Levy, F. Klocke, and T. H. C. Childs, "Consolidation phenomena in laser and powder-bed based layered manufacturing," *CIRP Ann. - Manuf. Technol.*, vol. 56, no. 2, pp. 730–759, 2007, doi: 10.1016/j.cirp.2007.10.004.
- [16] A. Valotta *et al.*, "3D printed ceramics as solid supports for enzyme immobilization: an automated DoE approach for applications in continuous flow," *J. Flow Chem.*, vol. 11, no. 3, pp. 675–689, 2021, doi: 10.1007/s41981-021-00163-4.
- [17] F. Melchels, J. Feijen, and D. Grijpma, "A review on stereolithography and its applications in biomedical engineering," vol. 22, no. 5, pp. 965–971, 2009.
- [18] Lithos, "CeraFab S65," 2024. <https://lithoz.com/de/3d-drucker/cerafab-s65/> (accessed Feb. 04, 2024).
- [19] S. R. L. Gobert, S. Kuhn, L. Braeken, and L. C. J. Thomassen, "Characterization of Milli- and Microflow Reactors: Mixing Efficiency and Residence Time Distribution," *Org. Process Res. Dev.*, vol. 21, no. 4, pp. 531–542, 2017, doi: 10.1021/acs.oprd.6b00359.
- [20] J. R. Bourne, O. M. Kut, and J. Lenzner, "An Improved Reaction System To Investigate Micromixing in High-Intensity Mixers," *Ind. Eng. Chem. Res.*, vol. 31, no. 3, pp. 949–958, 1992, doi: 10.1021/ie00003a042.
- [21] M. C. Fournier, L. Falk, and J. Villiermaux, "A new parallel competing reaction system for assessing micromixing efficiency - Experimental approach," *Chem. Eng. Sci.*, vol. 51, no. 22, pp. 5053–5064, 1996, doi: 10.1016/0009-2509(96)00270-9.
- [22] A. Podgoršek, J. Jacquemin, A. A. H. Pádua, and M. F. Costa Gomes, "Mixing Enthalpy for Binary Mixtures Containing Ionic Liquids," *Chem. Rev.*, vol. 116, no. 10, pp. 6075–6106, 2016, doi: 10.1021/acs.chemrev.5b00379.
- [23] E. Riedel and H.-J. Meyer, *Allgemeine und Anorganische Chemie*. 2013.
- [24] C. E. Mortimer and U. Müller, "19 Säure-Base-Gleichgewichte," *Chemie Das Basiswissen der Chemie*, pp. 293–315, 2019, doi: 10.1055/b-0039-171985.
- [25] H. Wachter and A. Hausen, "18. Säuren Und Basen," *Chemie für Mediziner*, pp. 107–128, 2019, doi: 10.1515/9783111712352-014.
- [26] H. P. Latscha, K. Uli, and K. Helmut, *Organische Chemie*, vol. 25, no. 3. 1892.
- [27] M. Moser, A. G. Georg, F. L. Steinemann, D. P. Rütli, and D. M. Meier, "Continuous milli-scale reaction calorimeter for direct scale-up of flow chemistry," *J. Flow Chem.*, vol. 11, no. 3, pp. 691–699, 2021, doi: 10.1007/s41981-021-00204-y.
- [28] J. Antes *et al.*, "Analysis and improvement of strong exothermic nitrations in microreactors," *Chem. Eng. Res. Des.*, vol. 81, no. 7, pp. 760–765, 2003, doi: 10.1205/026387603322302931.
- [29] D. J. Am Ende, P. J. Clifford, and D. L. Northrup, "The role of reaction calorimetry in the development and scale-up of aromatic nitrations," *Thermochim. Acta*, vol. 289, no. 2, pp. 143–154, 1996, doi: 10.1016/S0040-6031(96)03065-1.

- [30] E. Godineau *et al.*, "A Convergent Continuous Multistep Process for the Preparation of C4-Oxime-Substituted Thiazoles," *Org. Process Res. Dev.*, vol. 22, no. 8, pp. 955–962, 2018, doi: 10.1021/acs.oprd.8b00095.
- [31] Avantes, "Avantes Flow Cell-Z-10," 2024. <https://www.avantes.com/products/accessories/micro-flow-cells/> (accessed Feb. 04, 2024).
- [32] S. Ckp, H. Dosieren, and V. K.- Kleinstmengen, "SyrDos™ CKP."
- [33] L. laboratory Instruments, "Operation Manual Syringe Pump / Infusion Pump," [Online]. Available: https://www.holmarc.com/syringe_pump.php.
- [34] I. Tomaszewicz, S. L. Randzio, and P. Gierycz, "Excess Enthalpy in the methanol-water system," vol. 22, pp. 3–20, 1986.
- [35] Á. Piñero, Á. Olvera, G. García-Miaja, and M. Costas, "Excess molar enthalpies of tetrahydrofuran or diisopropyl ether + 1-alkanols at 298.15 K, using a newly designed flow mixing cell for an isothermal microcalorimeter," *J. Chem. Eng. Data*, vol. 46, no. 5, pp. 1274–1279, 2001, doi: 10.1021/je0100645.
- [36] D. V. Fenby and A. Chand, "Thermodynamic study of deuterium exchange in water + methanol systems," *J. Chem. Soc. Faraday Trans. 1 Phys. Chem. Condens. Phases*, vol. 74, pp. 1768–1775, 1978, doi: 10.1039/F19787401768.
- [37] Roth, "Safety sheet TEG," vol. 2006, no. 1907, pp. 1–12, 2016.
- [38] C. Y. Chen and C. W. Wu, "Thermal hazard assessment and macrokinetics analysis of toluene mononitration in a batch reactor," *J. Loss Prev. Process Ind.*, vol. 9, no. 5, pp. 309–316, 1996, doi: 10.1016/0950-4230(96)00022-8.
- [39] F. B. Myers and L. P. Lee, "Innovations in optical microfluidic technologies for point-of-care diagnostics," *Lab Chip*, vol. 8, no. 12, pp. 2015–2031, 2008, doi: 10.1039/b812343h.
- [40] J. Yue, J. C. Schouten, and T. Alexander Nijhuis, "Integration of microreactors with spectroscopic detection for online reaction monitoring and catalyst characterization," *Ind. Eng. Chem. Res.*, vol. 51, no. 45, pp. 14583–14609, 2012, doi: 10.1021/ie301258j.
- [41] K. Swinney and D. J. Bornhop, "Detection in capillary electrophoresis," *Electrophoresis*, vol. 21, no. 7, pp. 1239–1250, 2000, doi: 10.1002/(SICI)1522-2683(20000401)21:7<1239::AID-ELPS1239>3.0.CO;2-6.
- [42] W. Mantele and E. Deniz, "UV–VIS absorption spectroscopy: Lambert-Beer reloaded," *Spectrochim. Acta - Part A Mol. Biomol. Spectrosc.*, vol. 173, pp. 965–968, 2017, doi: 10.1016/j.saa.2016.09.037.
- [43] Avantes, "AvaLight-DH-S Deuterium-Halogen Light Source," pp. 90–91.
- [44] Avantes, "AvaSpec-ULS2048x64-EVO SensLine High UV and NIR Sensitivity Spectrometer," pp. 49–50.

-
- [45] A. Technologies, "Agilent 1100 Series HPLC Value System Users's Guide," p. 76, 1999.
- [46] Thermo Fisher Scientific Inc., "Thermo Scientific Accucore HPLC Columns," p. 56, 2012, [Online]. Available: <https://assets.thermofisher.com/TFS-Assets/CMD/brochures/TG-20666-Accucore-HPLC-Columns-TG20666-EN.pdf>.
- [47] T. Scientific, "Thermo Scientific Hypersil BDS column."
- [48] KdScientific, "Stainless steel syringes."
- [49] I. H. & Science, "6-Port Valve V-450." https://www.idex-hs.com/store/product-detail/injection_valve_2_position_6_port_040_black/v-450 (accessed Feb. 04, 2024).
- [50] Z. F. Technology and S. made Simple, "Back pressure regulator," 2024. <https://www.zaiput.com/product/back-pressure-regulators/> (accessed Feb. 04, 2024).

7 List of figures

Figure 2-1: Structure of the calorimeter using a reactor plate with 3 segments. From the bottom up: base plate, heating foils, reactor plate, Seebeck elements, Peltier elements, casing elements to secure everything together, metal cooling blocks. [2], [5], [6]	3
Figure 2-2: Structure of the internal geometry of the 3D printed reactor plate. The three sections from left to right: preheating section ("pre"), two reaction segments ("r1", "r2"). [3]	5
Figure 2-3: Structure of the internal geometry of the 3D printed reactor plate. The six sections from top left to bottom right: preheating section ("pre"), five reaction segments ("r1", "r2", "r3", "r4", "r5").	6
Figure 2-4: Schematic illustration of the basic set-up of a SLM printing device. [6] 7	
Figure 2-5: Left: Conventional SLA process, laser solidifies resin from top. Right: Different SLA process, laser solidifies resin from the bottom. [6], [17]	8
Figure 2-6: Schematic illustration of the CeraFab S56 printer [18]. (1) movable printer platform in Z-direction; (2) rotatable vat for material deposition; (3) optical system transmitting light from LED (4). [3].....	9
Figure 2-7: Schematical set-up of flow synthesis of Hydroximinoacetone (Nitrosylation). [30]	23
Figure 3-1: Temperature curve and selected values (red square) of the mixing of methanol-water. Different measured temperatures using a ceramic reactor plate with three segments (C3E) at 25°C.	25
Figure 3-2: Measured signals of the Peltier elements and selected values (red square) of the mixing of methanol-water. Different measured signals using a ceramic reactor plate with three segments (C3E) at 25°C.	25

Figure 3-3: Temperature rising from 25.3°C to 27.1°C due to rising of the room temperature throughout the experiment.	26
Figure 3-4: Normalized absorption plot of RTD measurements at various total flow rates using a ceramic reactor plate (C3E).	28
Figure 3-5: Results of the residence time distribution (RTD) for different reactor plates at different flow rates.....	31
Figure 3-6: Difference between old and new light bulb for UV-Vis measurement using the Bourne reaction in order to test the ceramic reactor plate.	33
Figure 3-7: Results Bourne reaction using the new light bulb. Yield of product S depending on the total flow rate for seven different reactors (AP04, T, C3E, M3E, M3ebd, M3ed and M6E).....	34
Figure 3-8: Comparison of the performance of a reactor plate (comparable to M3E), T-mixer, a X-mixer (Little Things Factory GmbH, type X), Slit interdigital micromixer SIMM-V2_ss (Institut für Mikrotechnik Mainz GmbH) during Bourne reaction previously done in other literature. [5]	36
Figure 3-9: Mixing methanol-water at different temperatures and different total flow rates with volumetric ratio methanol:water 1:1 in the ceramic calorimeter with three segments (C3E) and comparing results to the literature value.	38
Figure 3-10: Comparing the results of the mixing enthalpies for the mixture methanol-water with literature values at 25°C.	40
Figure 3-11: Mixing enthalpies of TEG-water at different temperatures (25°C, 40°C and 55°C) using the ceramic calorimeter with three segments (C3E).	42
Figure 3-12: Mixing enthalpies of TEG-1-propanol at different temperatures (25°C, 40°C and 55°C) using the ceramic calorimeter with three segments (C3E).	43
Figure 3-13: Neutralization reaction with C3E at different flow rates. Comparing different room temperatures to literature value [23] (green line).....	45

Figure 3-14: Neutralization reaction of acetic acid with NaOH using the stainless steel reaction plate with 6 Segments (M6E) at two different temperatures (25°C, 30°C) and the literature value for comparison.	47
Figure 3-15: Nitrosylation of tert-butyl nitrite with hydrochloric acid and acetone: results visualized in a graph compared to the mean reaction enthalpy of the reactions having a yield above 20%.	51
Figure 3-16: Nitrosylation of tert-butyl nitrite with hydrochloric acid and acetone: Example of signal curve from Peltier elements at 10°C in a ceramic calorimeter with 3 segments (C3E).	52
Figure 3-17: Nitrosylation of tert-butyl nitrite with hydrochloric acid and acetone: Example of signal curve from Peltier elements at 40°C in a ceramic calorimeter with 3 segments (C3E).	54
Figure 5-1: Overall experimental set-up of the calorimeter with two pumps, a thermostat [7], a computer for data collection, a quench possibility and 6 temperature sensors. [3]	60
Figure 5-2: Calibration curve of ceramic calorimeter with three segments (C3E) at 25°C with a room temperature of 25°C and thermostat [7] set to 28°C.	62
Figure 5-3: Calibration curve of stainless steel calorimeter with six segments (M6E) at 25°C with a room temperature of 25°C and thermostat [7] set to 28°C.	62
Figure 5-4: Calibration curve of ceramic calorimeter with three segments (C3E) at 25°C with a room temperature of 28°C and thermostat [7] set to 28°C.	63
Figure 5-5: Schematic experimental set-up residence time distribution (RTD) using a 6-port valve and a UV-Vis cell [31].	67
Figure 5-6: Graphical representation of the capillary connections of a 6-port valve used at RTD experiments. [10]	68
Figure 5-7: Schematic experimental set-up of Bourne reaction using a UV-Vis cell [31].	69

Figure 5-8: Schematic experimental set-up of nitrosylation reaction using a thermostat [7] and a back pressure regulator [50].....	74
Figure 9-1: Laboratory checklist for Bourne reaction.....	105

8 List of tables

Table 3-1: Measuring only water passing through the ceramic reactor plate with three segments (C3E) with different flow rates. Number of experiments and the average detected signal.	27
Table 3-2: Results of the mean Bodenstein numbers for all reactor plates.	29
Table 3-3: Mixing reaction methanol-water at different ratios at 25°C in the ceramic calorimeter with 3 segments (C3E) with a total flow rate of 6 mL min ⁻¹ and the amount of done experiments (n).	39
Table 3-4: Neutralization of acetic acid with NaOH using the C3E calorimeter and different flow rates. Average detected signal, reaction enthalpy deviation from literature [23] and the amount of experiments (n). Room temperature was 22°C.	44
Table 3-5: Neutralization of acetic acid with NaOH using the C3E calorimeter and different flow rates. Average detected signal, reaction enthalpy deviation from literature [23] and the amount of experiments (n). Room temperature was 28°C.	45
Table 3-6: Amount of difference pure water in comparison to neutralization signal for different flow rates in ceramic calorimeter with 3 segments (C3E).	46
Table 3-7: Nitration reaction of toluene with nitric acid and sulfuric acid at different flow rates and amount of experiments (n). Measured toluene conversion using HPLC analysis and reaction enthalpy with calculated deviation from literature [2], [3], [11], [38].	49
Table 3-8: Nitrosylation reaction results at different temperatures, the reaction yield and the reaction enthalpy.	51
Table 5-1: Different used reactor plates and their characteristics.	59
Table 5-2: Substrate and quench preparation for nitrosylation reaction.	75

Table 9-1: List of Abbreviations.....	88
Table 9-2: List of Symbols.....	89
Table 9-3: List of greek symbols.....	91
Table 9-4: List of chemicals.....	92
Table 9-5: Different used reactor plates and their calculated overall volumes.....	94
Table 9-6: Calibration values for the Seebeck Elements for ceramic calorimeter with 3 segments (C3E). Temperature of calibration: 10°C; of thermostat: 13°C; of the room around: 23°C. Mean $R^2=0.9998$	96
Table 9-7: Calibration values for the Seebeck Elements for ceramic calorimeter with 3 segments (C3E). Temperature of calibration: 18°C; of thermostat: 21°C; of the room around: 23°C. Mean $R^2=0.9999$	96
Table 9-8: Calibration values for the Seebeck Elements for ceramic calorimeter with 3 segments (C3E). Temperature of calibration: 25°C; of thermostat: 28°C; of the room around: 23°C. Mean $R^2=1$	96
Table 9-9: Calibration values for the Seebeck Elements for ceramic calorimeter with 3 segments (C3E). Temperature of calibration: 25°C; of thermostat: 28°C; of the room around: 28°C. Mean $R^2=1$	97
Table 9-10: Calibration values for the Seebeck Elements for ceramic calorimeter with 3 segments (C3E). Temperature of calibration: 30°C; of thermostat: 33°C; of the room around: 25°C. Mean $R^2=0.9991$	97
Table 9-11: Calibration values for the Seebeck Elements for ceramic calorimeter with 3 segments (C3E). Temperature of calibration: 40°C; of thermostat: 45°C; of the room around: 23°C. Mean $R^2=0.9997$	97
Table 9-12: Calibration values for the Seebeck Elements for ceramic calorimeter with 3 segments (C3E). Temperature of calibration: 40°C; of thermostat: 45°C; of the room around: 23°C. Mean $R^2=1$	98

Table 9-13: Calibration values for the Seebeck Elements for ceramic calorimeter with 3 segments (C3E). Temperature of calibration: 40°C; of thermostat: 48°C; of the room around: 23°C. Mean $R^2=0.9996$	98
Table 9-14: Calibration values for the Seebeck Elements for ceramic calorimeter with 3 segments (C3E). Temperature of calibration: 50°C; of thermostat: 57°C; of the room around: 28°C. Mean $R^2=0.9999$	98
Table 9-15: Calibration values for the Seebeck Elements for ceramic calorimeter with 3 segments (C3E). Temperature of calibration: 55°C; of thermostat: 63°C; of the room around: 23°C. Mean $R^2=0.9998$	99
Table 9-16: Calibration values for the Seebeck Elements for stainless steel calorimeter with 6 segments (M6E). Temperature of calibration: 25°C; of thermostat: 28°C; of the room around: 22°C. Mean $R^2=0.9974$	99
Table 9-17: Calibration values for the Seebeck Elements for stainless steel calorimeter with 6 segments (M6E). Temperature of calibration: 30°C; of thermostat: 33°C; of the room around: 22°C. Mean $R^2=0.9964$	99
Table 9-18: Experimental results residence time distribution (RTD), Bodenstein number and Reynolds number depending on flow rate, measured on C3E.	101
Table 9-19: Experimental results residence time distribution (RTD), Bodenstein number and Reynolds number depending on flow rate, measured on M3E.	102
Table 9-20: Experimental results residence time distribution (RTD), Bodenstein number and Reynolds number depending on flow rate, measured on M3Ebd. ...	102
Table 9-21: Experimental results residence time distribution (RTD), Bodenstein number and Reynolds number depending on flow rate, measured on M3Ed.	103
Table 9-22: Experimental results residence time distribution (RTD), Bodenstein number and Reynolds number depending on flow rate, measured on M6E.	103
Table 9-23: Extinction coefficients for Bourne Reaction for para-isomer (p-P), ortho-isomer (o-R) and S-product. [4], [10]	109

Table 9-24: Mixing reaction methanol-water experimental results at 18°C for volumetric ratio 1:1; different flow rates.....	110
Table 9-25: Mixing reaction methanol-water experimental results at 25°C for volumetric ratio 1:1; different flow rates.....	111
Table 9-26: Mixing reaction methanol-water literature values Tomaszekiewicz. [34]	112
Table 9-27: Mixing reaction methanol-water literature values Fenby. [36]	113
Table 9-28: Mixing reaction methanol-water literature values Pineiro. [35]	114
Table 9-29: Mixing reaction experimental results TEG-water at 25°C.....	115
Table 9-30: Mixing reaction experimental results TEG-water at 40°C.....	115
Table 9-31: Mixing reaction experimental results TEG-water at 55°C.....	116
Table 9-32: Mixing reaction experimental results TEG-1-propnol at 25°C.....	116
Table 9-33: Mixing reaction experimental results TEG-1-propnol at 40°C.....	117
Table 9-34: Mixing reaction experimental results TEG-1-propnol at 55°C.....	117
Table 9-35: Neutralization reaction experimental results at 25°C using stainless steel reactor plate with 6 Elements (M6E).....	118
Table 9-36: Neutralization reaction experimental results at 30°C using stainless steel reactor plate with 6 Elements (M6E).....	119

9 Appendix

9.1 Abbreviations and symbols

Table 9-1: List of Abbreviations.

3D	Three dimensional
A	Substrate stream A
B	Substrate stream B
C3E	Ceramic reactor plate with 3 segments (2 reaction segments)
cal	calculated
HPLC	High performance liquid chromatography
M3E	Stainless steel reactor plate with 3 segments (2 reaction segments)
M3Ebd	Stainless steel reactor plate with 3 segments (2 reaction segments) and bigger diameter of the channels
M3Ed	Stainless steel reactor plate with 3 segments (2 reaction segments) and double the reaction volume per segment
M6E	Stainless steel reactor plate with 6 segments (5 reaction segments)
o-R	Ortho-isomer of diazo coupling (Bourne Reaction)
out	Stream that leaves the reactor/device
p-R	Para-isomer of diazo coupling (Bourne Reaction)
pre	Preheating plate

r_1, r_2, r_3, r_4, r_5	Reaction segments in reactor plate
RTD	Residence time distribution
S	Biazo product of diazo coupling (Bourne Reaction)
SAR	Split-and-recombine
SE, pre	Preheating minus the entering values
SLM	Selective laser melting
SLA	Stereolithography
SOP	Standard operating procedure
UV-Vis	Ultraviolet-visible

Table 9-2: List of Symbols.

A	[-]	Absorption
Bo	[-]	Bodenstein number
c	[mol m ⁻³]	Concentration
C ₁ , C ₂ , C ₃	[-]	Calibration constants
C _p	[J mol ⁻¹ K ⁻¹]	Heat capacity
k _r	[(mol/m ³) ¹⁻ⁿ * s ⁻¹]	Reaction rate constant
d _h	[m]	Hydraulic diameter
Da _i	[-]	Damkoehler number i
D _{ax}	[m ² s ⁻¹]	Axial dispersion coefficient
ΔH _R	[J mol ⁻¹]	Reaction enthalpy
E	[s ⁻¹]	Exit age function

F	[-]	Cumulative age function
h	[J s]	Planck's constant
I	[W m ⁻²]	Intensity
l	[m]	Optical path length
l	[m]	Channel length
MB	[%]	Mass balance
n	[mol]	Amount of substance
\dot{n}	[mol s ⁻¹]	Molar flux
P	[W]	Power
\dot{Q}	[m ³ s ⁻¹]	Volumetric flow rate
Re	[-]	Reynolds number
t	[s]	Time
t _r	[s]	Reaction time
t _R	[s]	Retention time
t _{res}	[s]	Mean residence time
dT	[°C]	Temperature difference
T	[°C]	Temperature
u	[m s ⁻¹]	Flow velocity
U	[V]	Measured Voltage
V	[m ³]	Volume
x _i	[-]	Mole fraction
Y _S	[-]	Yield of S-product

Table 9-3: List of greek symbols.

ϵ_i	$[\text{m}^2 \text{mol}^{-1}]$	Molar extinction coefficient
ϵ_{diss}	$[\text{W kg}^{-1}]$	Energy dissipation rate
η	$[\text{Pa s}]$	Dynamic viscosity
θ	$[-]$	Dimensionless time
λ	$[\text{nm}]$	Wavelength
λ_f	$[-]$	Channel friction factor
ν	$[\text{s}^{-1}]$	Frequency
ν	$[\text{m}^2 \text{s}^{-1}]$	Kinematic viscosity
ρ	$[\text{kg m}^{-3}]$	Density
σ_t^2	$[\text{s}^2]$	Variance

9.2 List of chemicals

Table 9-4: List of chemicals.

Name	Company	Purity [%]
Tert-butyl nitrite	Sigma-Aldrich	90.0
Acetone	Sigma-Aldrich	99.9
Hydrochloric Acid	Roth	37.0
Acetic Acid	Sigma-Aldrich	99.8
Sodium Hydroxide	Sigma-Aldrich	98.0
Nitric Acid	Sigma-Aldrich	puriss. p.a., 65-67
Sulphuric Acid	Sigma-Aldrich	95.0-98.0
Phosphoric Acid	Sigma-Aldrich	85.0 wt. in H ₂ O
Ammonium Hydroxide	Sigma-Aldrich	28.0-30.0
Anti-pyruvic Aldehyde 1-oxime	Sigma-Aldrich	98.0
Ethanol	Sigma-Aldrich	96.0
Methanol	Lactan	99.8
Toluene	Chem-Lab	HPLC grade, 99.8+
Triethylene glycol (TEG)	Roth	≥98.0
1-Naphthol	Merck	≥ 99.0
Sulfanilic acid	Merck	≥ 99.0
Sodium nitrite	Roth	≥ 99.0

Sulfamic Acid	Roth	≥ 99.0
Sodium carbonate	Fluk	≥ 99.5
1-propanol	Roth	≥ 99.5
Sodium hydrogen carbonate	Roth	≥ 98.0

9.3 Reactor plates

Table 9-5: Different used reactor plates and their calculated overall volumes.

Name	Overall V including preheating element	Overall V of mixing elements (excluding preheating element)
	[μL]	[μL]
C3E	320	222
M3E	320	222
M3Ebd	499	346
M3Ed	438	340
M6E	1003	850

9.4 Calibration

9.4.1 SOP-calibration

1. Switch on the thermostat and set it to certain temperature (little bit higher than wanted temperature in the calorimeter).
2. Switch on the laptop.
3. Connect the USB cable from the calorimeter to the laptop and connect the white cable (power supply for calorimeter) to the power supply.
4. Start Teraterm software.
 - a. Choose the connection "Serial", then choose the COM Port which says Arduino and then press "OK".
 - b. A window should open which shows data every 2 seconds.
 - c. Choose "file", then "Log..." and after selecting a dataname press "Speichern".
 - d. Back at the main window press "Control" and afterwards "Broadcast command".
 - Deactivate "Realtime mode" and then select COM Port.
 - Pick "command" and in the dropdown menu search for "<1.25>", press "submit".
 - e. Wait for approximately 10 minutes.
 - f. Pick new command "<2,0,2>" the same way as before.
 - g. Wait for approximately 2 hours (± 15 minutes).
 - h. Pick new command "<4,0,0>" and then "<0,25>".
 - i. Close all, switch everything of (laptop and thermostat) and disconnect everything.

9.4.2 Calibration values for the Seebeck elements of the flow calorimeter

Calorimeter with 3 segments

Table 9-6: Calibration values for the Seebeck Elements for ceramic calorimeter with 3 segments (C3E). Temperature of calibration: 10°C; of thermostat: 13°C; of the room around: 23°C. Mean $R^2=0.9998$.

	pre	r1	r2
c1	0.0005	0.0070	-0.0015
c2	2.0503	1.7952	2.1170
c3	-0.3981	-0.1490	-0.4625

Table 9-7: Calibration values for the Seebeck Elements for ceramic calorimeter with 3 segments (C3E). Temperature of calibration: 18°C; of thermostat: 21°C; of the room around: 23°C. Mean $R^2=0.9999$.

	pre	r1	r2
c1	0.0647	0.0195	0.0496
c2	1.8834	1.7156	1.9536
c3	-0.1820	-0.0577	-0.2194

Table 9-8: Calibration values for the Seebeck Elements for ceramic calorimeter with 3 segments (C3E). Temperature of calibration: 25°C; of thermostat: 28°C; of the room around: 23°C. Mean $R^2=1$.

	pre	r1	r2
c1	0.04231	0.0134	0.0297
c2	1.8813	1.6846	1.9124
c3	0.0344	-0.0027	0.0394

Table 9-9: Calibration values for the Seebeck Elements for ceramic calorimeter with 3 segments (C3E). Temperature of calibration: 25°C; of thermostat: 28°C; of the room around: 28°C. Mean $R^2=1$.

	pre	r1	r2
c1	0.0158	-0.0049	0.0199
c2	1.8844	1.7172	1.9287
c3	-0.0498	-0.0478	-0.0629

Table 9-10: Calibration values for the Seebeck Elements for ceramic calorimeter with 3 segments (C3E). Temperature of calibration: 30°C; of thermostat: 33°C; of the room around: 25°C. Mean $R^2=0.9991$.

	pre	r1	r2
c1	-0.0101	0.0945	-0.0179
c2	1.9217	1.4660	1.9935
c3	0.1310	0.0933	0.1523

Table 9-11: Calibration values for the Seebeck Elements for ceramic calorimeter with 3 segments (C3E). Temperature of calibration: 40°C; of thermostat: 45°C; of the room around: 23°C. Mean $R^2=0.9997$.

	pre	r1	r2
c1	0.0510	0.0082	0.4944
c2	1.7645	1.6513	0.1681
c3	0.4944	1.8266	0.6115

Table 9-12: Calibration values for the Seebeck Elements for ceramic calorimeter with 3 segments (C3E). Temperature of calibration: 40°C; of thermostat: 45°C; of the room around: 23°C. Mean $R^2=1$.

	pre	r1	r2
c1	0.0105	0.0032	-0.0176
c2	1.8470	1.6473	1.9461
c3	0.4771	0.1549	0.5805

Table 9-13: Calibration values for the Seebeck Elements for ceramic calorimeter with 3 segments (C3E). Temperature of calibration: 40°C; of thermostat: 48°C; of the room around: 23°C. Mean $R^2=0.9996$.

	pre	r1	r2
c1	0.0597	-0.0018	0.0647
c2	1.7576	1.6343	1.7852
c3	0.4351	0.1923	0.5540

Table 9-14: Calibration values for the Seebeck Elements for ceramic calorimeter with 3 segments (C3E). Temperature of calibration: 50°C; of thermostat: 57°C; of the room around: 28°C. Mean $R^2=0.9999$.

	pre	r1	r2
c1	0.0392	0.014	0.0199
c2	1.7800	1.5912	1.8334
c3	0.6060	0.2522	0.8453

Table 9-15: Calibration values for the Seebeck Elements for ceramic calorimeter with 3 segments (C3E). Temperature of calibration: 55°C; of thermostat: 63°C; of the room around: 23°C. Mean $R^2=0.9998$.

	pre	r1	r2
c1	0.0356	0.0077	0.0601
c2	1.7195	1.5875	1.7471
c3	0.9546	0.3990	1.1268

Calorimeter with 6 segments

Table 9-16: Calibration values for the Seebeck Elements for stainless steel calorimeter with 6 segments (M6E). Temperature of calibration: 25°C; of thermostat: 28°C; of the room around: 22°C. Mean $R^2=0.9974$.

	pre	r1	r2	r3	r4	r5
c1	-0.3037	-0.4438	-0.4184	-0.4481	-0.4978	-0.4984
c2	1.909	1.9202	1.9828	1.9832	2.1603	2.0357
c3	0.1397	0.0466	0.0651	0.0841	0.0586	0.0977

Table 9-17: Calibration values for the Seebeck Elements for stainless steel calorimeter with 6 segments (M6E). Temperature of calibration: 30°C; of thermostat: 33°C; of the room around: 22°C. Mean $R^2=0.9964$.

	pre	r1	r2	r3	r4	r5
c1	-0.3791	-0.4355	-0.4858	-0.4356	-0.4943	-0.466
c2	1.8203	1.8280	1.9117	1.8756	2.0389	1.8862
c3	0.3624	0.1670	0.2020	0.2884	0.2154	0.3275

9.5 Residence time distribution (RTD)

9.5.1 SOP-RTD

The standard operating procedure used for the RTD experiments and reported here was retrieved from a previous work. [10]

As shown in the set-up two syringe pumps, 6-port injection valve, microfluidic device and Avantes flow cell are connected to each other. It is important to keep the distance between valve, microfluidic device and flow cell as short as possible to reduce falsification of results.

In AVASOFT the 'Integration Time' was set to 1.05ms and 'Averaging' was set to 500.

1. Turn on the Avantes station and the deuterium lamp (blue toggle switch) and let it warm up for 1h.
2. Flush the flow cell with the used solvent.
3. Turn on the shutter (red toggle switch) and start the measurement (start/stop button).
4. Take a light reference of the used solvent (white light bulb).
5. Turn off the shutter (red toggle switch) and take a dark reference (dark light bulb).
6. Turn on the shutter and stop the measurement (start/stop button).
7. Press the 'Time Series' button to add a continuous measurement. Add another 'Time Series' to perform a baseline correction.
8. Set the method of one tab as ansiole measurement with absorption measurement between 268nm and 274nm.
9. Set the method of the second tab as baseline correction with absorption measurement between 500nm and 506nm.
10. Set the time steps of the data export to EXCEL, depending on residence time of your device.
11. Start the measurement (start/stop button).
12. When the signal of the solvent is constant, switch the valve to "Inject" at a defined time to introduce the tracer. Write down the exact time of the switch and try to always switch fast.

13. When the signal of the tracer is constant switch the valve back to the “Load” position to perform a step-down signal. Write again the time of the step down.
14. Clean the flow cell with deionised water and ethanol and turn off the deuterium lamp (blue toggle switch).
15. Turn off the Avantes station after 15min. The exported data gives an EXCEL sheet with absorption data of the two wavelength ranges at specific times.

9.5.2 RTD experimental results

Table 9-18: Experimental results residence time distribution (RTD), Bodenstein number and Reynolds number depending on flow rate, measured on C3E.

Flow rate	t_{res}	t_{cal}	Bo	Re
[mL min ⁻¹]	[s]	[s]	[-]	[-]
0.295	277.01	65.08	4.43	10.48
1	103.56	19.20	3.98	35.51
2	44.77	9.60	4.38	71.02
4	31.70	4.80	5.89	142.04
6	26.92	3.20	5.83	213.06

Table 9-19: Experimental results residence time distribution (RTD), Bodenstein number and Reynolds number depending on flow rate, measured on M3E.

Flow rate	t_{res}	t_{cal}	Bo	Re
[mL min ⁻¹]	[s]	[s]	[-]	[-]
1	75.95	19.20	3.24	35.51
2	41.31	9.60	3.40	71.02
4	17.24	4.80	3.34	142.04
6	13.09	3.20	3.73	213.06

Table 9-20: Experimental results residence time distribution (RTD), Bodenstein number and Reynolds number depending on flow rate, measured on M3Ebd.

Flow rate	t_{res}	t_{cal}	Bo	Re
[mL min ⁻¹]	[s]	[s]	[-]	[-]
1	86.28	29.94	2.82	28.41
2	44.02	14.97	3.00	56.82
4	22.82	7.49	2.95	113.63
6	17.17	4.99	2.87	170.45

Table 9-21: Experimental results residence time distribution (RTD), Bodenstein number and Reynolds number depending on flow rate, measured on M3Ed.

Flow rate	t_{res}	t_{cal}	Bo	Re
[mL min ⁻¹]	[s]	[s]	[-]	[-]
1	129.45	26.28	4.51	35.51
2	76.89	9.60	6.53	71.02
4	45.56	4.80	6.61	142.04
6	5.11	3.20	1.49	213.06

Table 9-22: Experimental results residence time distribution (RTD), Bodenstein number and Reynolds number depending on flow rate, measured on M6E.

Flow rate	t_{res}	t_{cal}	Bo	Re
[mL min ⁻¹]	[s]	[s]	[-]	[-]
1	226.74	60.18	5.24	28.41
2	117.75	30.09	5.19	56.82
4	59.00	15.05	5.13	113.63
6	36.39	10.03	5.60	170.45

9.6 Bourne reaction

9.6.1 Preparation of reagents for Bourne reaction [10]

Buffer

222.2 mmol (23.551 g) of Na_2CO_3 and 222.2 mmol (18.667 g) of NaHCO_3 were dissolved in 1 L deionised water (HPLC gradient). The resulting solution should have a pH of 9.9 and an ionic strength of 888.8 mM. For spectrophotometric measurements the buffer stock was diluted in a 1:1 volumetric ratio with HPLC water, resulting in an ionic strength of 444.4 mM.

Reagent A - 1-Naphthol Solution

A 1.2 mM solution of 1-naphthol was prepared by dissolving 0.12 mmol (17.3 mg) 1-naphthol in 100 mL carbonate/bicarbonate buffer (each 222.2 mM) at room temperature, under intense stirring on a magnetic stirrer and exclusion of light. Dissolution took about 90 minutes. This solution was prepared fresh every morning before the experiments, stored cool and dark, thus minimizing any decomposition.

Reagent B - Diazotised Sulfanilic Acid

Diazotised sulfanilic acid was prepared as a 10 mM stock solution. For experiments, 10 mL of the stock solution were diluted with 90 mL of cold HPLC water, ensuring a 1 mM reaction solution B.

For the 10 mM stock, 0.5 mmol (53 mg) Na_2CO_3 were dissolved in 30 mL cold water. 1 mmol (173.2 mg) of sulfanilic acid was added and the solution was cooled in an ice bath. After dissolution, another 20 mL water were added to dissolve 1.05 mmol (74.2 mg) of sodium nitrite (NaNO_2). 2.08 mmol (2 mL) of 1 M hydrochloric acid were added dropwise over the course 15 minutes, while the solution was stirred and kept at a temperature below 5 °C. Excess of nitrite was destroyed by addition of 0.05 mmol (4.9 mg) sulphamic acid and the solution was stirred for 10 minutes. The mixture was filled up to a volume of 100 mL with cold water. This solution was prepared fresh every morning before the experiments, stored cool and dark, thus minimizing any decomposition.

9.6.2 Laboratory checklist for Bourne reaction

Bourne Reaction				
	needed amount	chemical	used amount	add. Info
Reagent A				
<input type="checkbox"/>	17.3 mg	1-naphthol	<input type="text"/>	room temperature sturring for 90 min
<input type="checkbox"/>	100 ml	undiluded Buffer		
Reagent B				
<input type="checkbox"/>	53 mg	Natriumcarbonat	<input type="text"/>	dissolve, cold
<input type="checkbox"/>	30 ml	Cold water		
<input type="checkbox"/>	173.2 mg	Sulfanilic Acid	<input type="text"/>	dissolve, ice bath cold
<input type="checkbox"/>	20 ml	Cold water		dissolve, cold
<input type="checkbox"/>	74.2 mg	Sodium nitrite	<input type="text"/>	
<input type="checkbox"/>	2 ml	Hydrochloric acid		dropwise 15 min sturring, ice bath
<input type="checkbox"/>	4.9 mg	Sulphamic acid	<input type="text"/>	afterwards 10 min sturring
<input type="checkbox"/>	until 100 ml	Cold water		
<input type="checkbox"/>	10 ml	solution diluded with 90 ml cold water		
Buffer				
<input type="checkbox"/>	50 ml	Undiluded Buffer		
<input type="checkbox"/>	50 ml	Water		

Figure 9-1: Laboratory checklist for Bourne reaction.

9.6.3 SOP-Bourne reaction

The standard operating procedure used for the mixing sensitive reaction experiments and reported here was retrieved from a previous work. [10]

After preparation of all solutions, connect the syringe pumps with the microfluidic device as illustrated in the set-up. After setting the desired flow rate on both pumps, start them at the same time and flush the microfluidic device for at least three residence times to reach a steady state. Afterwards 2mL is sampled and stored dark.

In AVASOFT the 'Integration Time' was set to 1.05ms and 'Averaging' was set to 100.

1. Turn on the Avantes station and the deuterium lamp (blue toggle switch) and let it warm up for 1h.
2. Set the data export wavelength between 390nm and 700nm in steps of 10nm.
3. Flush the flow cell with buffer solution (ionic strength 444.4mM).
4. Turn on the shutter (red toggle switch) and start the measurement (start/stop button).
5. Take a light reference of the buffer (white light bulb).
6. Turn off the shutter (red toggle switch) and take a dark reference (dark light bulb).
7. Turn on the shutter and stop the measurement (start/stop button).
8. Start the measurement (start/stop button) and switch to the absorption mode (A) in AVASOFT.
9. Suck the sample through the flow cell using a syringe.
10. Press 'file'-'export'-'ASCII' to store the data in a .txt-file.
11. If you have to measure more than one sample, flush the cell again with buffer and restart from point 5.
12. Once done analyzing the samples, clean the flow cell with deionised water and ethanol and turn off the deuterium lamp (blue toggle switch).
13. Turn off the Avantes station after 15min.

The exported .txt-files are adapted to be used with the MATLAB code:

- Remove the header and every blank space.
- Convert every comma into a dot (',' ' ').
- Convert every semicolon into blank space (';' ' ').

The MATLAB code and the .txt-files are saved in the same folder so MATLAB can import the files. The code used was adapted from [10] and is reported in the subchapter below.

9.6.4 MATLAB code for calculations Bourne reaction

```

clear all, clc
daten = dir('*.txt'); % loads all the .txt files from the folder
numfiles = numel(daten); %number of files loaded

flow=([0.295 1 2 3 4 5 6 7]); %flows QA+QB [mL/min]
c_B=10.00577*10/100/2 %concentration sulphanic acid for Mass Balance

%% calculation dilution before further dilution (change weights to actual
weights)
empty_weight=fliplr([9.8615 9.9471 9.9173 9.9799 9.9452 9.9565 9.9535 9.9567]);
% weight of the empty vials
buffer=fliplr([14.9160 14.9989 14.9954 14.9699 15.0136 15.0251 15.0070
15.0242]); %weight of the vials filled with buffer
sample_full=fliplr([15.6175 15.7042 15.7130 15.6879 15.7200 15.7310 15.7000
15.7134]); %weight of the vials filled with buffer and sample
buffersample= sample_full-empty_weight; %weight of only sample+buffer
sample_only=sample_full-buffer; %weight of only sample
f_dilution_und=buffersample./sample_only; %dilution factor for undiluted before
UV/VIS

%% calculation of further dilution
empty_weight12=fliplr([10.2718 8.9214 8.9945 8.9407 8.9550 8.9521 8.9474
8.9483]); % weight of the empty vials
buffer12=fliplr([12.2874 10.9400 11.0077 10.8363 10.9660 10.9677 10.9730
10.9669]); %weight of the vials filled with buffer
sample_full12=fliplr([13.2946 11.9529 12.0223 11.8454 11.9790 11.9813 11.9873
11.9798]); %weight of the vials filled with buffer and sample
buffersample12= sample_full12-empty_weight12; %weight of only sample+buffer
sample_only12=sample_full12-buffer12; %weight of only sample
f_dilution12=buffersample12./sample_only12; %dilution factor diluted 1:1 before
UV/VIS

%% dilution factor
f_dilution=f_dilution_und.*f_dilution12;

%%
absorption = nan((700-390)/10+1,numfiles); % generation of absorption matrix
Massenbilanz = nan(1, numfiles); % generation of the mass balance matrix
YS = nan(size(Massenbilanz)); %generation of the Xs vector

l=0.01; %optical path length [m]
ext_coeff=[277.6 400.6 654.7;411.2 395.5 761.3;588.7 463.6 972.2;794.2 576.6...
1246.9;1009.6 722.5 1544.1;1227.8 901.8 1830.4;1456.9 1110.6 2074.9;1717.1 ...
1345.8 2245.5;2025.7 1611.5 2318.7;2382.1 1892.3 2311.7;2728.4 2140.4 ...
2246.2;3009.6 2317.9 2157.5;3158.5 2381.6 2116.9;3140.3 2308.0 2175.0;2959.1
...
2108.3 2311.4;2618.4 1809.4 2467.4;2133.5 1431.3 2590.4;1583.6 1018.4 ...
2647.4;1057.6 638.6 2618.8;609.6 343.8 2486.1;302.7 166.1 2259.7;130.2 74.8 ...
1964.2;54.1 35.3 1618.4;23.2 15.7 1265.7;11.6 8.7 936.1;7.9 6.6 652.1;4.7 4.2
...
428.7;4.4 4.2 271.9;4.1 4.4 191.2;2.5 2.7 89.1;2.2 2.8 48.9;1.6 2.1 28.3].*1;
%epsilon[m^2/mol] * schichtdicke[m], letzte Zeile ist faktor fr summe von
konzentrationen

lb=[0;0;0]; %lower boundary for concentration
ub=[1;1;1]; %upper boundary for concentration
options=optimoptions('lsqlin','Algorithm','interior-
point','Display','iter');%optional

```

```

%% plot
figure
hold on
xlabel('Total Flow [mL/min]')
ylabel('YS')
for k=1:numfiles
    currentfile = daten(k); %loads each file after the other
    currentdata = load(currentfile.name); %loads all data in one file
    absorption(:, k) = currentdata(:, 5); % saves the data in the absorption
matrix
    d = currentdata(:, 5); %saves the data in the d vector
    c = f_dilution.*lsqlin(ext_coeff,d,[],[],[],[],lb,ub,[],options); %
calculates the concentration of o-R, p-R and S with the least square method
    Massenbilanz(k) = (c_B-c(1)-c(2)-2*c(3))/c_B*100; %massbalance (cB-cp-cO-
2*cS)/cB
    YS(k)=2*c(3)/(c(1)+c(2)+2*c(3)); % mixing performance, yield von S-product
    title('Results experiment on 31.07.2023 2nd measurement diluted 1:3');
    plot(flow, YS, '-.or') %plots the results for YS versus the flowrate
end
%% Show results
flow
YS
Massenbilanz

%% Save in excel
filename=['Ys_31.07.2023_2nd_measurement_diluted_1.3.xlsx'];
YSExcel=[flow',YS',Massenbilanz'];
xlswrite(filename,YSExcel);

```

9.6.5 Extinction coefficients for Bourne reaction

Table 9-23: Extinction coefficients for Bourne Reaction for para-isomer (p-P), ortho-isomer (o-R) and S-product. [4], [10]

Wavelength [nm]	Extinction coefficients [m ² mol ⁻¹]		
	para-isomer (p-R)	ortho-isomer (o-R)	S-product
390	277.6	400.6	465.7
400	411.2	395.5	761.3
410	588.7	463.6	972.2
420	794.2	576.6	1246.9
430	1009.6	722.5	1544.1
440	1227.8	901.8	1830.4
450	1456.9	1110.6	2074.9
460	1717.1	1345.8	2245.5
470	2025.7	1611.5	2318.7
480	2382.1	1892.3	2311.7
490	2728.4	2140.4	2246.2
500	3009.6	2317.9	2157.5
510	3158.5	2381.6	2116.9
520	3140.3	2308.0	2175.0
530	2959.1	2108.3	2311.4
540	2618.4	1809.4	2467.4
550	2133.5	1431.3	2590.4
560	1583.6	1018.4	2647.4
570	1057.6	638.6	2618.8
580	609.6	343.8	2486.1
590	302.7	166.1	2259.7
600	130.2	74.8	1964.2
610	54.1	35.3	1618.4
620	23.2	15.7	1265.7
630	11.6	8.7	936.1
640	7.9	6.6	652.1
650	4.7	4.2	428.7
660	4.4	4.2	271.9
670	4.1	4.4	161.2
680	2.5	2.7	89.1
690	2.2	2.8	48.9
700	1.6	2.1	28.3

9.7 Mixing enthalpy

9.7.1 Methanol-water experimental results

Table 9-24: Mixing reaction methanol-water experimental results at 18°C for volumetric ratio 1:1; different flow rates.

Total flow rate	ΔH_r
[mL min ⁻¹]	[kJ mol ⁻¹]
1.978	-0.6949
4.005	-0.8008
5.006	-0.8385
5.995	-0.8974
4.005	-0.8208
5.006	-0.8655
5.995	-0.9214
6.984	-0.9412
1.978	-0.6880
4.005	-0.7863
5.006	-0.8427
5.995	-0.8581
6.984	-0.9159
6.984	-0.9201
1.978	-0.6906

Table 9-25: Mixing reaction methanol-water experimental results at 25°C for volumetric ratio 1:1; different flow rates.

Total flow rate	ΔH_r
[mL min ⁻¹]	[kJ mol ⁻¹]
4.0	-0.7422
4.0	-0.7950
5.0	-0.8214
5.0.	-0.8149
6.0	-0.7318
6.0	-0.7833
7.0	-0.8258
7.0	-0.8269

9.7.2 methanol-water literature values

Table 9-26: Mixing reaction methanol-water literature values Tomasziewicz. [34]

X_{methanol}	X_{water}	Mixing enthalpy
[-]	[-]	[J mol⁻¹]
0.087	0.913	-510
0.131	0.869	-662
0.191	0.809	-782
0.25	0.75	-852
0.338	0.662	-870
0.357	0.643	-860
0.44	0.56	-825
0.525	0.475	-775
0.605	0.395	-702
0.672	0.328	-644
0.789	0.211	-465

Table 9-27: Mixing reaction methanol-water literature values Fenby. [36]

X_{methanol}	X_{water}	Mixing enthalpy
[-]	[-]	[J mol⁻¹]
0.087	0.913	-536
0.1095	0.8905	-619
0.2323	0.7677	-861
0.2924	0.7076	-890
0.325	0.675	-890
0.3372	0.6628	-884
0.5192	0.4808	-808
0.6279	0.3721	-696
0.7036	0.2964	-610
0.7852	0.2148	-494

Table 9-28: Mixing reaction methanol-water literature values Pineiro. [35]

X_{methanol}	X_{water}	Mixing enthalpy
[-]	[-]	[J mol⁻¹]
0.895	0.105	-283.8
0.717	0.283	-581.5
0.573	0.427	-737.7
0.454	0.546	-828.5
0.354	0.646	-882.8
0.268	0.732	-879.5
0.194	0.806	-811.8
0.101	0.899	-572.8
0.023	0.977	-161.8

9.7.3 TEG-water experimental results

Table 9-29: Mixing reaction experimental results TEG-water at 25°C.

Molar ratio [-]	n [-]	Measured reaction enthalpy [J mol ⁻¹]	Corrected reaction enthalpy [J mol ⁻¹]
0.9928	2	-0.0914	-0.1718
0.9812	1	-0.3420	-0.4224
0.9573	1	-0.7415	-0.8219
0.7870	1	-0.9314	-1.0119
0.6488	1	-0.8884	-0.9688
0.4249	1	-0.7173	-0.7978
0.2698	1	-0.5222	-0.6026

Table 9-30: Mixing reaction experimental results TEG-water at 40°C.

Molar ratio [-]	n [-]	Measured reaction enthalpy [J mol ⁻¹]	Corrected reaction enthalpy [J mol ⁻¹]
0.9568	3	-0.9300	-0.7514
0.8808	3	-1.5535	-1.3749
0.7870	3	-1.7449	-1.5663
0.6488	3	-2.4538	-2.2752
0.4249	2	-2.3237	-2.1451
0.2698	2	-2.5382	-2.3596

Table 9-31: Mixing reaction experimental results TEG-water at 55°C.

Molar ratio [-]	n [-]	Measured reaction enthalpy [J mol ⁻¹]	Corrected reaction enthalpy [J mol ⁻¹]
0.96	1	-1.4906	-0.7721
0.8808	1	-2.2100	-1.4915
0.7870	1	-2.6013	-1.8829
0.6488	1	-2.9363	-2.2178
0.4249	1	-2.9643	-2.2458
0.2698	1	-3.3149	-2.5964

9.7.4 TEG-1-propanol experimental results

Table 9-32: Mixing reaction experimental results TEG-1-propanol at 25°C.

Molar ratio [-]	Measured reaction enthalpy [J mol ⁻¹]	Corrected reaction enthalpy [J mol ⁻¹]
0.8443	0.8068	0.0434
0.6363	0.8405	0.0772
0.4666	0.9639	0.2007
0.3043	1.0878	0.3245
0.1489	1.0904	0.3271
0.0804	0.9434	0.1800

Table 9-33: Mixing reaction experimental results TEG-1-propanol at 40°C.

Molar ratio [-]	Measured reaction enthalpy [J mol ⁻¹]	Corrected reaction enthalpy [J mol ⁻¹]
0.8428	0.7375	0.0114
0.6412	0.2291	-0.4970
0.4718	-0.0537	-0.7798
0.3088	-0.2693	-0.9954
0.1516	-0.5873	-1.3134
0.0820	-0.7759	-1.5020

Table 9-34: Mixing reaction experimental results TEG-1-propanol at 55°C.

Molar ratio [-]	Measured reaction enthalpy [J mol ⁻¹]	Corrected reaction enthalpy [J mol ⁻¹]
0.0820	-3.2767	-4.3643
0.1516	-2.9774	-4.0650
0.3088	-1.8733	-2.9609
0.4718	-1.0959	-2.1836
0.6412	-0.1332	-1.2209
0.8428	0.8802	-0.2075

9.8 Neutralization reaction results

Table 9-35: Neutralization reaction experimental results at 25°C using stainless steel reactor plate with 6 Elements (M6E).

Total flow rate [mL min ⁻¹]	Average detected signal [W]	ΔH_r [kJ mol ⁻¹]	Deviation from literature [%]
0.2	-0.4395	-298.85	-421%
0.4	-0.5325	-181.04	-215%
1.0	-0.7985	-108.60	-89%
2.0	-1.1784	-80.02	-39%
3.0	-1.5293	-67.00	-17%
4.0	-1.8435	-61.06	-6%
5.0	-2.0749	-55.25	4%
6.0	-2.1953	-48.87	15%
7.0	-2.2794	-43.60	24%
8.0	-2.2773	-37.77	34%
9.0	-2.2841	-33.77	41%
10.0	-2.4190	-32.25	44%

Table 9-36: Neutralization reaction experimental results at 30°C using stainless steel reactor plate with 6 Elements (M6E).

Total flow rate [mL min ⁻¹]	Average detected signal [W]	ΔHr [kJ mol ⁻¹]	Deviation from literature [%]
0.2	-0.6045	-411.07	-616%
0.4	-0.7758	-263.79	-360%
1.0	-0.8662	-196.35	-242%
2.0	-1.2028	-81.79	-42%
3.0	-1.7296	-75.88	-32%
4.0	-2.1252	-70.50	-23%
5.0	-2.4250	-64.67	-13%
6.0	-2.8693	-63.97	-11%
7.0	-3.2754	-62.74	-9%
8.0	-3.6913	-61.22	-7%
9.0	-4.0995	-60.60	-6%
10.0	-4.5154	-60.21	-5%